THE APPLICATION OF ACTIVE LEARNING KRIGING IN DETERMINING THE RELIABILITY OF BRIDGE COMPONENTS

by

Courtney Elizabeth Buckley

Submitted in partial fulfillment of the requirements
for the degree of Master of Applied Science

at

Dalhousie University
Halifax, Nova Scotia
December 2022

Dalhousie University is located in Mi'kma'ki, the
ancestral and unceded territory of the Mi'kmaq.
We are all Treaty people.

DEDICATION PAGE

This thesis is dedicated to my loving husband and family. To my husband Jon, who has been a constant source of encouragement and support. To my mother Melissa and my father Cary, thank you for your understanding, patience, and constant faith in my abilities. To my siblings, Kaitlyn, Charles, and Dustyn thank you for your constant source of joy and love. To my grandmothers, Denice, and Elaine, thank you for always believing in me and for being a constant source of strength and perseverance. To my friends and family, without you, this would not have been possible.

TABLE OF CONTENTS

LIST OF TABLES

LIST OF FIGURES

ABSTRACT

The objective of this research was to develop a framework of analysis using Active Learning Kriging Monte Carlo Simulation (AK-MCS) to assess and optimize the reliability calculation of reinforced concrete bridges components. The methodology consisted of developing a computer code to perform AK-MCS analysis to calculate the reliability index of bridge girders and piers, verify the accuracy of the code by conducting a sensitivity analysis, and optimize AK-MCS analysis by balancing the accuracy and efficiency. The computer code was developed using MATLAB and its accuracy was verified by conducting 810 AK-MCS analyses (15 bridge girder and pier configuration x 54 unique AK configurations, where the latter refers to the set of correlation, regression, and learning functions). The verification analysis results indicted the sensitivity of the solution efficiency (run time and number of training points) to the choice of the AK configuration. The comprehensive metric system (CMS), developed elsewhere in literature, was utilized to propose optimum AK configurations for select girder and pier configurations by running 2160 AK-MCS analyses and ranking them according to CMS. The top 5 optimum AK configurations were then applied to a larger set of 40 girder configurations and 12 pier configurations to assess the accuracy and efficiency of the proposed optimum AK configurations. Analysis results indicted the accuracy of AK-MCS in predicting the reliability index of the considered girders and piers and the significant reduction in the computational time as compared with crude MCS (97.9%, reduction in time on average).

LIST OF ABBREVIATIONS AND SYMBOLS

AAE	Absolute Average Error
AASHTO	American Association of Sate Highway and Transportation Officials
ACI	American Concrete Institute
AK	Active Learning Kriging
AK-FORM	Active Learning Kriging First Order Reliability Method
AK-IS	Active Learning Kriging Importance Sampling
AK-MCS	Active Learning Kriging Monte Carlo Simulation
BC	Before Christ
CDF	Cumulative Distribution Function
CMS	Comprehensive Metric System
COV	Coefficient of Variation
CHBDC	Canadian Highway Bridge Design Code
DACE	Design and Analysis of Computer Experiments
DLA	Dynamic Load Allowance
DOC	Degree of Consistency
DoE	Design of Experiments
EFF	Effective Feasibility Function
EGRA	Efficient Global Reliability Analysis
FE	Finite Element
FORM	First Order Reliability Methods
ID	Identification Number
IS	Importance Sampling
KO	Kriging Occurrence
LRFD	Load and Resistance Factor Design
LS	Limit State
LSD	Limit State Design
LSF	Limit State Function
MCMC	Markov Chain Monte Carlo
MCS	Monte Carlo Simulation
MCS-IS	Monte Carlo Simulation with Importance Sampling

MSE	Mean Squared Error
NEBT	New England Bulb Tee
NS	Nova Scotia
OMC	Ordinary Monte Carlo
PDF	Probability Density Function
RC	Reinforced Concrete
REIF	Reliability-Based Improvement Function
RMSE	Root Mean Square Error
SAR	Structural Assessment and Retrofit
SORM	Second Order Reliability Methods
TTP	Total Training Points
ULS	Ultimate Limit State
A_{actual}	Area of Actual Cross-Sectional Geometry
A_g	Gross Cross-Sectional Area
A_{Ideal}	Area of Idealized Cross-Sectional Geometry
A_p	Cross-Sectional Area of Prestressed Steel
A_{s_i}	Area of Steel in the i^{th} Layer of Rebar
A_{st}	Total Area of Steel in the Cross-section
a	Equivalent Stress Block Depth
B	Width of the Section
C_r	Compressive Force
c	Depth to Neutral Axis
c_p	Center of Plastic (Geometric Center)
d_b	Diameter of Steel Bar Reinforcements
d_p	Depth to the Centroid of Prestressed Steel Reinforcement
d_i	Depth to i^{th} Layer of Rebar
$EFF(x)$	Effective Feasibility Learning Function
e	Axial Load Eccentricity with Respects to the Center of Plastic
$e_{cu,max}$	Maximum Strain in Concrete Compression Zone
e_{max}	Maximum Tolerable Error

e_{s_i}	Strain in the i^{th} Layer of Streel Reinforcing Bars
e^*	Axial Load Eccentricity with Respects to the Neutral Axis
F	Regression Realizations
F_x	Forces in the x Direction
f_{pr}	Factored Prestressed Reinforcement Strength
f_{pu}	Ultimate Strength of Prestressed Reinforcing Steel
f_y	Yield Strength of Steel
f_c'	Compressive Strength of Concrete
$f(x)$	Regression Evaluation of x
$G(x)$	Performance Function or Limit State Function
H	Height of the Cross-Section
$H(x)$	H Learning Function
$H_c(x)$	Corrected H Learning Function
I_{actual}	Second Moment of Inertia of Actual Cross-section
I_1	Transformed Root Mean Squared Error (RMSE)
I_2	Transformed Absolute Average Error (AAE)
I_3	Transformed Total Training Points (TTP)
I_4	Transformed Degree of Consistency (DoC)
I	Second Moment of Inertia
I_{ideal}	Second Moment of Inertia of Idealized Cross-section
$INDEX$	Vector that Details Which of the x Variables are Random
$KO(x)$	KO Learning Function
k_p	Stress-Strain Curve Factor for Prestressed Reinforcements
L	Correlation Length Vector
L^*	Optimum Correlation Length Vector
L_{effect}	Live Load Transfer Effect
$L(x)$	Load Model
M_c	Compressive Moment from Concrete Zone
$M_{D_{SW}}$	Dead Load Moment due to Self-Weight
$M_{D_{WS}}$	Dead Load Moment due to Wearing Surface

M_L	Live Load Moment
M_r	Moment Resistance
M_{s_i}	Tensile Moment Generated by the i^{th} Layer of Reinforcing Bars
M_x	Moment from the Integration Diagram
m	Number of Design Sites within Design of Experiments
M_{in}	Vector of Initial Inputs
M_{out}	Vector of Initial Outputs
N_{AK-MCS}	Number of Trials in the AK-MCS Analysis
N_{added}	Number of Added Training Points
N_{bl}	Number of Reinforcing Bar Layers within the Cross-section
N_{cs}	Number of Concrete Sections with Different Base Widths
N_{calls}	Summation Number of Initial and Added Training Points
N_f	Total Number of Failed Trials
N_I	Total Number of Identical Analyses
$N_{initial}$	Number of Initial Training Set
N_{MCS}	Total Number of Trials in a Monte Carlo Simulation
N_s	Number of Successful Reliability Analyses
N	Minimum Number of Trials
n	Number of Random Variables
P	Number of Initial Design Points Required to Generate Kriging Surrogate Model
P_c	Axial Force in Concrete Under Compression
PF	Professional Factor
P_f	Probability of Failure
$P_{f_{MCS}}$	Probability of Failure of Monte Carlo Simulation
$P_{f_{AK-MCS}}$	Probability of Failure of AK-MCS
$P_{f_{AK-MCS_i}}$	Probability of Failure of the i^{th} Identical AK Configuration
P_r	Axial Load Resistance
$P_{r_{max}}$	Maximum Allowable Axial Load
P_{ro}	Axial Load Resistance with an Eccentricity Value of Zero
P_{s_i}	Axial Force in the i^{th} Steel Rebar Under Tension

P_y	Axial Force from Interaction Diagram
$\hat{p}$	Expected Probability of Failure
q	Number of model outputs
$\hat{q}$	Expected Probability of Survival
R	Correlation Matrix
$REIF(x)$	Reliability Based Expected Improvement Learning Function
$R(x)$	Resistance Model
$r(x)$	Correlation Evaluation for x
S_i	Vector Containing the Inputs from all Design Sites
T_i	Tensile Force in the i^{th} Layer of Rebar
$U(x)$	U Learning Function
V	Coefficient of Variation
v_1	Linear Scale
v_2	Exponential Scale
v_3	Logarithmic Scale
X	Design Site
x	Vector made up of Randomly Generated Variables
$\bar{Y}$	Geometric Centroid
Y_{actual}	Depth to Centroid of Actual Cross-section
Y_i	Vector Containing the Outputs from all Design Sites
Y_{ideal}	Depth to Centroid of Idealized Cross-section
$y(x)$	Responses Generated by Original Model
$\hat{y}(x)$	Responses Generated by Kriging Surrogate Model
$\bar{y}(x)$	Mean Value of Kriging Prediction
Z_α	Z-value for Selected Confidence Level
α_1	Equivalent Whitney Stress Block Factor
β	Reliability Index
β_{AK-MCS}	Reliability Index for the AK-MCS for a Single Configuration and Geometry
β_{MCS}	Reliability Index for the MCS for a given Geometry
β_1	Equivalent Whitney Stress Block Factor

β_j	Matrix of Regression Coefficients
β^*	Kriging Shape Predictor Factor
γ^*	Kriging Shape Prediction Factor
δ	Step Measurement
$\epsilon(x)$	Error Measurements which Determine the Boarder of the Desired Range
λ	Bias
μ	Mean Value
$\mu_{\hat{G}}(x)$	Mean Value of the Kriging Predictor
ρ	Reinforcement Ratio
$\sigma_{\hat{G}}(x)$	Standard Deviation of the Kriging Predictor
$\Phi(.)$	Standard Normal Cumulative Distribution Function
$\Phi(.)^{-1}$	Inverse of the Standard Normal Cumulative Distribution Function
Φ_c	Resistance Factor of Concrete
Φ_s	Resistance Factor of Steel
Φ_p	Resistance Factor of Prestressed Steel
$\varphi(x)$	Variance of the Kriging Predictor
ω_{pu}	Prestressed Steel Ratio
$\mathcal{F}$	Regression Function
$\mathcal{Z}$	Stochastic Process

ACKNOWLEDGEMENTS

I would like to express my sincere gratitude and appreciation to my research supervisor Dr. Fadi Oudah for the opportunity to pursue graduate studies, for their support, guidance, and insight. I would like to personally thank post doctoral fellow Dr. Koosha Khorramian for their assistance, time, patience, and guidance in this project. To my peers, in the Assessment and Retrofit Research group thank you for the support and peer mentorships over the last two years, in particular David and Connor. To my friend and role model Raghad, thank you for your continual support. Lastly, I would like to thank the Natural Sciences and Engineering Research Council (NSERC) for funding this research and making this project possible.

CHAPTER 1 INTRODUCTION

1.1 BACKGROUND

In Nova Scotia (NS), there are approximately 4,100 bridges. The provincial five-year highway improvement plan for 2022-2023 includes a budget of $29.1 million dollars for the maintenance and repair of only 19 bridges within the province, that is less than 0.5% of the bridge inventory (Public Works, 2022b). One of the main obstacles of determining the priority of maintenance and repairs is budgetary restraints provided by the federal and provincial governments (Public Works, 2019a). It is imperative that both new infrastructure be developed for the growing population and the maintenance of existing infrastructure be balanced. One way of determining the priority of repairs and allocation of capital investment for bridge replacement and rehabilitation rests with the quantification of the risk of structural failures of the existing bridges. For a risk-based assessment approach, the probability of structural failure and the consequence of failure need to be quantified. The consequence of failure is typically determined in coordination with the authority having jurisdiction, while the probability of failure (P_f) can be quantified by structural engineers using reliability analysis.

1.2 RELIABILITY ANALYSIS FOR BRIDGE ASSESSMENT

Reliability analysis is utilized to quantify the probability of load effects (moment, shear, axial, strain, etc.) exceeding the structural resistance for a predefined limit state (LS). The method accounts for the inherent randomness in both the resistance of the structure and applied loads (Allen, 1991; Kaymaz, 2005). The probability of exceedance is typically referred to as P_f, while a LS implies the condition of the structure beyond which it no longer fulfil the relevant design

performance. A reliability index (β) is then calculated based on the quantified P_f and assumed distribution of the LS.

Reliability analysis has been utilized to calibrate the structural safety for limit state design (LSD) in bridge design codes such as the Canadian Highway Bridge Design Code (CSA S6, 2019) and the American Association of Sate Highway and Transportation Officials (AASHTO) load and resistance factor design (LRFD) manual (AASHTO LRFD Bridge Design Specifications, 2017). It has also been utilized for developing risk-based methods to manage existing bridge inventories since it provides a rational-based approach to quantify the likelihood of structural failures, and thus, bridge retrofit, and maintenance can be prioritized (Jiang et al., 1988; Estes and Frangopol, 2001; Lounis, 2000; Thompson et al., 1999; Khanzada, 2012).

Existing reliability-based bridge evaluation methods vary in functionality and robustness depending on the level of bridge complexity, required field data, and methods of reliability estimation (Ghosn et al., 2010; Jiang et al., 1988; Lounis, 2000). The choice of the reliability estimation method has been recognized as an important aspect of developing practical reliability-based bridge evaluation tools (Ghorbanpoor and Dudek, 2007). In the following paragraphs, the sources of uncertainty in a bridge reliability analysis and the existing reliability estimation methods are reviewed.

There are three general sources of uncertainties that can be potentially addressed in a reliability analysis. The first is the natural variability of physical properties which would include material strength, location of rebars, and manufacturing tolerances. The second is operating conditions which would encompasses the variability in loads, time-variant durability considerations and other environmental considerations. The third is the incomplete understanding or mathematical representation of the data (Moustapha et al., 2022), which can occur in instances where limited

non distructive tests are used to approximate the condition of a patially degraded or aged bridge. These uncertainties are quantified using random variables to represent the state of the engineering system (herein referred to as the system). This system is then evaluated using the ultimate limit state (ULS) which is expressed in Equation (1), as the resistance ($R(x)$) minus the load ($L(x)$), and failure occurs when loads surpass the resistance of the model, or when the performance function ($G(x)$) is less than or equal to zero (Zhaoyan et al., 2013). This concept of failure may not necessarily be a catastrophic failure but forms a technical failure, which occurs when technical requirements and capacities are inadequate (Melchers, 2006).

$$G(x) = R(x) - L(x) \leq 0 \tag{1}$$

The quantification of P_f and β enables a direct comparison amongst existing bridges for determining which structural repair takes priority. The concept of quantification of performance of the structure is not new and can be dated back to the earliest known building code in Mesopotamia roughly 1750 years before Christ (BC) (Nowak and Collins, 2013), where trial and error were the fundamental building blocks of reliability-based methods. If failure occurred, the builder would abandon or adjust the design depending on the consequence of failure.

There are two reasons that warranted the transition to modern probabilistic methods for structural analysis: i) the introduction of consistency in the decisions surrounding safety, and ii) the optimization to achieve structural economy (Melchers, 2006). As knowledge evolved, so did reliability methods, the capture of the inherent randomness of structural behaviour became possible with the development of computers and statistical reliability (Nowak and Collins, 2013). Over time, the typical limitations on the minimum factors of safety decreased, which is primarily attributed to the development of the profession's collective understanding, information about

material properties and their behaviours, and the increase detailing in load models (Melchers, 2006; Nowak and Collins, 2013). This progression has been instrumental in the development of the LSD approach to structural engineering codes and design guidelines (Melchers, 2006).

There are two primary categories of bridge reliability assessment, the first is code and policy-based assessments for proposed designs which are developed based on the guidelines and their provided code statistics. The second are deterioration models used to model ageing structures under environmental conditions and traffic loading which use inspection information to capture the degradation and in-situ conditions of the applied loads (Rakoczy and Nowak, 2013). Due to the variability of environmental conditions, weather patterns and accident-based damage, deterioration models are warranted in some situations to capture the true behaviour and response of the existing structure overtime.

Methods to determine β of structures (also called reliability estimation techniques) include approximate methods, simulation techniques, surrogate models, and surrogate model aided methods as summarized in Table 1 (Moustapha et al., 2022). There are two common approximate methods known as the first-order reliability methods (FORM) and second-order reliability methods (SORM). Approximate time-varying reliability method can be used as a degradation-based model for existing and ageing structures, which can include the consideration of alkali-silica, corrosion, sulfate attack, and freeze-thaw damage effects (Dey et al., 2019). The second is simulation techniques, which include Monte Carlo simulation (MCS), a well-known and commonly applied method of analysis that evaluates the LSF with a predefined number of trials in the MCS analysis (N_{MCS}), where P_f is calculated as the number of failed trails (N_f) divided by N_{MCS}. The MCS is a simple tool used frequently as it does not require the knowledge associated with the most probable point (Khorramian and Oudah, 2022a). In some non-linear LS, this method is inefficient due to the

magnitude of computational power or time required to run the analysis. The third class is the surrogate model methods, where the performance function is replaced with an equivalent or simplified model that is used in conjunction with the available reliability estimation techniques like FORM or MCS to evaluate P_f. An example of surrogate model is the Kriging method which uses regression and correlation functions to generate a surrogate model (Cressie, 1990). The fourth class is surrogate model aided methods, which utilize a form of simulation in conjunction with a surrogate model (Moustapha et al., 2022). Three examples of surrogate model aided methods include Active Learning Kriging Monte Carlo Simulation (AK-MCS), Monte Carlo Simulation with Importance Sampling (MCS-IS), and Active Learning Kriging First Order Reliability Method (AK-FORM).

Table 1. Reliability estimation techniques

Class	Definition	Example	Reference
Approximate Methods	Limit state function is linearized around a so-called design point, in a suitably transformed probabilistic design space.	- FORM - SORM	(Echard et al., 2011; Kaymaz, 2005; Moustapha et al., 2022; Rakoczy and Nowak, 2013)
Simulation Techniques	To numerically simulate some phenomenon and then observe the number of times an event of interest occurs.	- MCS	(Nowak and Collins, 2013; Moustapha, Marelli et al., 2022)
Surrogate Model	An alternative model typically used in place of the performance function to reduce computational demand.	- Kriging - Polynomial chaos	(Cressie, 1990; Echard et al., 2011)
Surrogate Model Aided Methods	A surrogate model that is augmented through the used of simulation and machine learning techniques.	- AK-MCS - AK-IS - AK-FORM	(Echard et al., 2011; Moustapha et al., 2022)

The choice of the reliability estimation technique to evaluate a particular LSF depends on balancing the accuracy and efficiency of the desired solution. The evolution of these methods is attributed to the limitations of each, firstly FORM and SORM methods work well in linear systems but when applied to non-linear LS they may perform poorly and become inconsistent (Kaymaz, 2005).

Literature indicates that the most credible and commonly applied simulation method of reliability analysis is MCS. MCS is perceived to yield the most accurate reliability estimation if an adequate number of trails is utilized to evaluate the performance function. MCS is proven to balance the efficiency and accuracy aspects when utilized to assess the reliability of design options or calibrate load and resistance factors because the resistance model in these applications is typically simple (closed-form solution or simple iterative solution). However, MCS can become computationally demanding when the P_f is low (large number of trails is required) or when the resistance model is computationally demanding (requires iterative solution or numerical simulation) such as the case of degrading existing bridges.

Existing structures degrade with time at different rates depending on the exposure condition and the deterioration state of the bridge (corrosion, freeze-thaw damage, etc.). Accurate closed-form solution or simple iterative solutions to assess the resistance model for degrading structures are often not feasible or yield inaccurate representation of the resistance. In fact, engineers often utilize numerical simulation techniques like nonlinear finite element (FE) analysis to evaluate the resistance of degrading elements by considering the spatial variability in the deterioration (Khorramian et al., 2022a; Khorramian et al., 2022b; Oudah and Alhashmi, 2022b; Petrie, 2022). Numerical simulation may take a considerable amount of time which makes the use of MCS cost prohibitive, especially for developing a risk-based computer tool to assess the reliability and

prioritize repairs for bridges in NS as previously discussed. The use of surrogate model aided methods (class 4 as discussed in Table 1) becomes appealing in such situations because it can significantly reduce the computational cost, where the computational cost refers to the number of times the performance function needs to be evaluated to arrive at an accurate reliability evaluation of the LSF (Moustapha, M., et al., 2022). Kriging, a type of surrogate model that has gained traction in the last few decades, can be utilized to solve reliability problems with complex resistance models. The efficiency of Kriging can be further optimized when augmented with learning functions, this collaboration is referred to as active learning Kriging (Echard et al., 2011; Al-Bittar et al., 2018). Surrogate model aided methods take the benefits of both surrogate methods and simulation methods to create an accurate representation of the LS with the least number of required training points.

1.3 Research Motivation and Context

A long-term research programme has been lunched at the structural assessment and retrofit (SAR) research group to develop computer tools to assess the risk of bridge structural failure in NS. To evaluate the reliability of bridges in different stages of their lifespan or condition, a *generic*, *accurate* and an *efficient* framework of reliability analysis is required, where *generic* means applicable to all possible LSF (ultimate, serviceability, fatigue, etc.) where the resistance model can be evaluated using simple closed-form equation or complex numerical simulation. *Efficient* means both within an acceptable amount of time and within standard computational specifications, and *accurate* means within reasonably low percentage of error.

AK-MCS, a form of surrogate model aided method, was utilized in the proposed framework of analysis as it can yield a *generic*, *accurate*, and an *efficient* method of analysis. This method uses a relatively small number of trials evaluated through the performance function (called original

performance) to train a surrogate model of the performance function. The surrogate model is updated by adding more trails evaluated through the original performance function, where the additional trials are selected based on a learning function and a stopping criterion (Khorramian and Oudah, 2022b). AK-MCS has been utilized in literature to evaluate the structural safety of various LS but was not utilized for bridge engineering applications (Moustapha et al., 2022). The scope of the present research is to develop a framework of reliability analysis using AK-MCS for typical multi-girder bridges in NS, validate the accuracy and efficiency of the framework for select design options, and further optimize the calculation process, with an ultimate goal of developing a generic computer software to assess the safety of existing bridges using AK-MCS.

There are four primary structural components of a multi-girder bridge, the bridge deck, the supporting girders, the piers, and the abutment as shown in Figure 1. The bridge deck is the portion of the bridge that carries the loads generated by the traffic (trains, vehicles, or pedestrians), the barriers, and it self-weight. The loads applied to the deck are then transferred to the supporting girders, which are longitudinal supports that transfer the load from the deck surface to the pier (in case of a multi-span bridge) and the end abutments. The piers and abutment transfer the loads to the ground through the foundation.

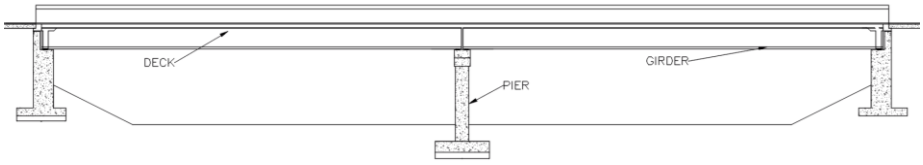

Figure 1. Schematic illustration of a multi-girder two-span bridge.

1.4 THESIS OBJECTIVES AND SCOPE

The objective of this research is to develop a functional framework and a computer code that evaluates the reliability of bridge components using AK-MCS as the method of analysis. The scope of work is as follows:

- Review key concepts of AK-MCS to provide contextual information surrounding the general procedure of reliability analysis, and the overview of existing and new methods.
- Develop a framework of analysis where a generalized procedure adaptable to different model types is developed and the simplified performance functions are created and tested.
- Validate the developed framework of analysis by conducting reliability analysis of bridge girders and piers and comparing with crude MCS.
- Optimize the analysis procedure by performing a sensitivity analysis to provide generic recommendations about the use of AK-MCS for assessing the reliability of bridge girders and piers. The sensitivity analysis considers the accuracy, efficiency, and consistency of the framework of analysis.

1.5 RESEARCH SIGNIFICANCE

An accurate reliability estimation of existing bridge components is hindered due to inefficiency concerns related to the high computational time required to perform advanced structural analysis like finite element (FE) to determine the structural resistance, where FE is used for complex bridge configurations or when deterioration is severe. Work is needed to explore efficient reliability analysis methods that utilize a smaller number of possible resistance realizations (i.e. scenarios). AK-MCS is proposed in this research as an efficient reliability technique that requires a substantially smaller number of resistance realizations as compared with conventional methods like crude MCS. In this work, the accuracy and efficiency of AK-MCS are evaluated and verified for bridge evaluation applications using simple resistance models for proof-of-concept purposes, while future research will utilize the verified AK-MCS method for FE analysis of existing bridges.

1.6 THESIS STRUCTURE

The thesis consists of six chapters, a bibliography, and appendices. The content and description of the chapters are given below:

Chapter 1. *Introduction*. It details the objective and scope of work and provides an overview of the thesis structure.

Chapter 2. *Literature Review*. It provides a contextual overview of relevant topics needed to understand the overall works presented. It reviews the definitions and provides a generalized background on relevant topics that pertain to the research topic. These topics include, reliability analysis, the Kriging method, active learning Kriging, and application to bridge reliability analysis.

Chapter 3. *Computer Code Development and Application*. It presents an overview of the AK-MCS analysis structure and breaks down the MATLAB® code structure.

Chapter 4. *Verification of AK-MCS Reliability for RC Bridges*. The functionality of the methodology and framework of analysis are verified for reinforced concrete bridge girders and piers through a limited parametric analysis.

Chapter 5. *Optimization of AK-MCS for Bridge Reliability Assessment*. The AK-MCS analysis procedure is optimized in this chapter to balance between the required efficiency and accuracy of the reliability solution. Recommendations for an optimized AK-MCS analysis for bridge applications are derived based on a sensitivity analysis and by utilizing a metric system developed elsewhere in literature.

Chapter 6. *Conclusions and Recommendations*. It reiterates the scope and methodology, lists the most significant findings, and details areas for further development.

CHAPTER 2 REVIEW OF KEY CONCEPTS FOR AK-MCS

2.1 INTRODUCTION

This chapter provides the required background information of the literature related to all aspects of the research topic. This includes a general introduction to the history of the Kriging method and its mathematical formulation, a general overview on MCS, basic procedural context to the AK method, formulation of learning functions used within the model verification in Chapter 4 and the sensitivity analysis in Chapter 5, and a summary of terminologies used throughout.

2.2 KRIGING

2.2.1 Origins and Historical Development

Kriging is a methodology that has been tailored to many different problems and types of analysis, including but not limited to geostatistics, reliability analysis, meteorology, forestry assessment, deterministic optimization, numerical optimization, design etc. The Kriging method was first developed in the 1950s by D.G. Krige (Cressie, 1990). Krige proposed a pure regression procedure to determine the best possible estimator of the mean grade of a block within the mining practice (Journel, 1977). In the 1960s it was formalized and generalized by Matheron at the University of France, and it was named 'Krigeage or Kriging' after the weighted moving-average methods initially developed by Krige (Journel, 1977). Dr. Krige was a mining specialist, who further developed the Kriging method based on his earlier works and Matheron research. In 1970, Watson Geoffrey used the Universal Kriging method, a method for estimating and contouring in trend surface analysis (Watson, 1970). This application of the Kriging method was applied to the quantification of geological variables and was presented at the international symposium on techniques for decision making in the mineral industry. In 1975, Kriging was utilized for

cartography of the sea floor (Chiles and Chauvet, 1997). In 1977, the use of Kriging for the evaluation of empirical data sets in geology was further researched (Whiten, 1977). In the 1980s, Kriging was tailored to computer experimental fields and in the 1990s to deterministic optimization problems (Kaymaz, 2005). It was not until the early 2000s that it was used for analytical functions and structural reliability.

The term Kriging encompasses many different estimation and regression procedures, various terms have been used within literature, such as universal Kriging, linear Kriging, log-normal Kriging, ordinary Kriging, etc. The term Kriging has also become synonymous to that of 'optimal predictor' as Kriging methods involve the use of interpolators to predict the behavior between points of data (Cressie, 1990); where the data can be adapted to the scope of interest. The term Kriging was retained because linear and nonlinear methods all shared the same common principle of minimizing the variance (Journel, 1977). Of the various terms used to describe the Kriging method, the Kriging process is the most accurate in describing the method of analysis presented in this works. Kriging is a nonlinear stochastic regression method (Kaymaz, 2005). Its primary role is to define a predictor frequently referred to as a surrogate model, based on two things, the first is the regression function and the second is the stochastic process. There are three common regression functions in literature including constant, linear, and quadratic (Lophaven et al., 2002). The primary difference between Kriging and conventional regression methods is related to how the error function is selected. In standard regression models, the error is a deterministic value, while for Kriging the error is represented as a stochastic process (Khorramian and Oudah, 2022b). In the stochastic process, there are two components considered, the mean value (μ) which is set to be zero, and the covariance which is the process variance times the correlation function. There are six standard correlation functions commonly used in literature including exponential, Gaussian, linear,

spherical, cubic, and spline (Lophaven et al., 2002). The mathematical formulation of the regression and correlation functions are presented in Section 3.3.2 and 3.3.3.

2.2.2 Formulation

To train the Kriging surrogate model there are two formulation considerations, the regression evaluation, and the stochastic process. The regression function relates the design of elements (DoE) data and fits it with a polynomial function (typically of degree zero, one or two), where the error is the distance between the fitted curve and the known point of data. The stochastic process treats the response for each design site and unknown site as a random variable. The correlation function is used to relate the random variables within the stochastic process. The estimated response of the system by the Kriging predictor is denoted by $\hat{y}(X)$ for a new design site (X). This estimation is then used in place of the response generated by the original model ($y(X)$). The number of input sites from the original model is denoted by S_i, and the output is also known as a response (Y_i) as shown in Equations (2) and (3), respectively, where n is the number of random variables considered and q is the number of model outputs.

$$S_i = [S_{i1}, S_{i2}, \dots, S_{in}] \tag{2}$$

$$Y_i = [Y_{i1}, Y_{i2}, \dots, Y_{iq}] \tag{3}$$

The DoE is a set of two matrices shown in Equations (4) and (5). They are formulated based on the number of design sites (m) and their number of responses (m).

$$S = \begin{bmatrix} S_{11} & \cdots & S_{1n} \\ \vdots & \ddots & \vdots \\ S_{m1} & \dots & S_{mn} \end{bmatrix} \tag{4}$$

$$Y = \begin{bmatrix} Y_{11} & \cdots & Y_{1q} \\ \vdots & \ddots & \vdots \\ Y_{m1} & \dots & Y_{mq} \end{bmatrix} \tag{5}$$

Equation (6) represents the Kriging predictor ($\hat{y}(X)$) where $\mathcal{F}$ is the regression function, z is the stochastic process and β_j is a matrix of regression coefficients to be determined through the optimization of the mean squared error (MSE) of the predictor (Khorramian and Oudah, 2022b).

$$\hat{y}_j(X) = \mathcal{F}(\beta_j, X) + z_j(X); \tag{6}$$

A regression function can be selected and the corresponding regression realizations for design sites (F) can be built as shown in Equation (7) and (8).

$$F = \begin{bmatrix} f(S_1)^T \\ \vdots \\ f(S_m)^T \end{bmatrix} = \begin{bmatrix} f_1(S_1) & \cdots & f_p(S_1) \\ \vdots & \ddots & \vdots \\ f_1(S_m) & \cdots & f_p(S_m) \end{bmatrix} = \begin{bmatrix} F_{11} & \cdots & F_{1p} \\ \vdots & \ddots & \vdots \\ F_{m1} & \dots & F_{mp} \end{bmatrix} \tag{7}$$

$$F_{ij} = f_j(S_i); i = 1, \dots, m; j = 1, \dots, p \tag{8}$$

The next stage is the selection of the correlation function. The correlation length vector (L) can be assumed and the correlation matrix (R) is subsequently built as shown in Equation (9).

$$R = \begin{bmatrix} R_{11} & \cdots & R_{1m} \\ \vdots & \ddots & \vdots \\ R_{m1} & \cdots & R_{mm} \end{bmatrix}; R_{ij} = R(L, S_i, S_j) \tag{9}$$

Now that the (R) and (F) matrices are built, an iterative procedure is used to calculate the optimum correlation length (L^*) and the Kriging shape predictor factor (β^*) as expressed in Equations (10) and (11), respectively. Khorramian and Oudah (2022b) uses a Gaussian formulation as an example to find L^*, however, there are a total of six correlation functions all with there own correlation length equations.

$$\beta^* = (F^T R^{-1} F)^{-1} F^T R^{-1} Y \tag{10}$$

$$L^* = \min_L \left\{ |R| \frac{1}{m} \sigma_k^2 \right\}; \sigma_k^2 = \frac{1}{m} (Y - F\beta^*)^T F^{-1} (Y - F\beta^*) \tag{11}$$

Once the optimum is determined, the remaining parameters can be found, this is completed by applying Equation (12) to (13), where the regression evaluation for X is f and the correlation evaluation for X is equal to r.

$$f = f(X) = \begin{bmatrix} f_1 \\ \vdots \\ f_p \end{bmatrix}; f_i = f_i(X) \tag{12}$$

$$r = r(L, X, S) = \begin{bmatrix} r_1 \\ \vdots \\ r_m \end{bmatrix} = \begin{bmatrix} R(L, X, S_1) \\ \vdots \\ R(L, X, S_m) \end{bmatrix}; r_i = R(L, X, S_i) \tag{13}$$

The Kriging predictor is related to the DoE through both Kriging shape predictor factors β^* and γ^*, as articulated in Equations (10) and (14). An additional calculation is shown in Equation (14), where the generalized least square approach was used to calculate Equation (15).

$$\gamma^* = R^{-1}(Y - F\beta^*) \tag{14}$$

$$\sigma_k^2 = \frac{1}{m} (Y - F\beta^*)^T R^{-1} (Y - F\beta^*) \tag{15}$$

The mean value of the Kriging predictor (surrogate model) ($\bar{y}(X)$) and the variance of the Kriging predictor ($\varphi(X)$) are expressed in Equations (16) and (17), respectively.

$$\bar{y}(x) = f(X)^T \beta^* + r(X)^T \gamma^* \tag{16}$$

$$\varphi(X) = \sigma_k^2 (1 + u^T (F^T R^{-1} F)^{-1} u - r^T R^{-1} r) \tag{17}$$

$$u = F^T R^{-1} r - f \tag{18}$$

Figure 2 depicts the overall mathematical framework of the Kriging method and how the different equations relate to each other (Khorramian and Oudah, 2022b).

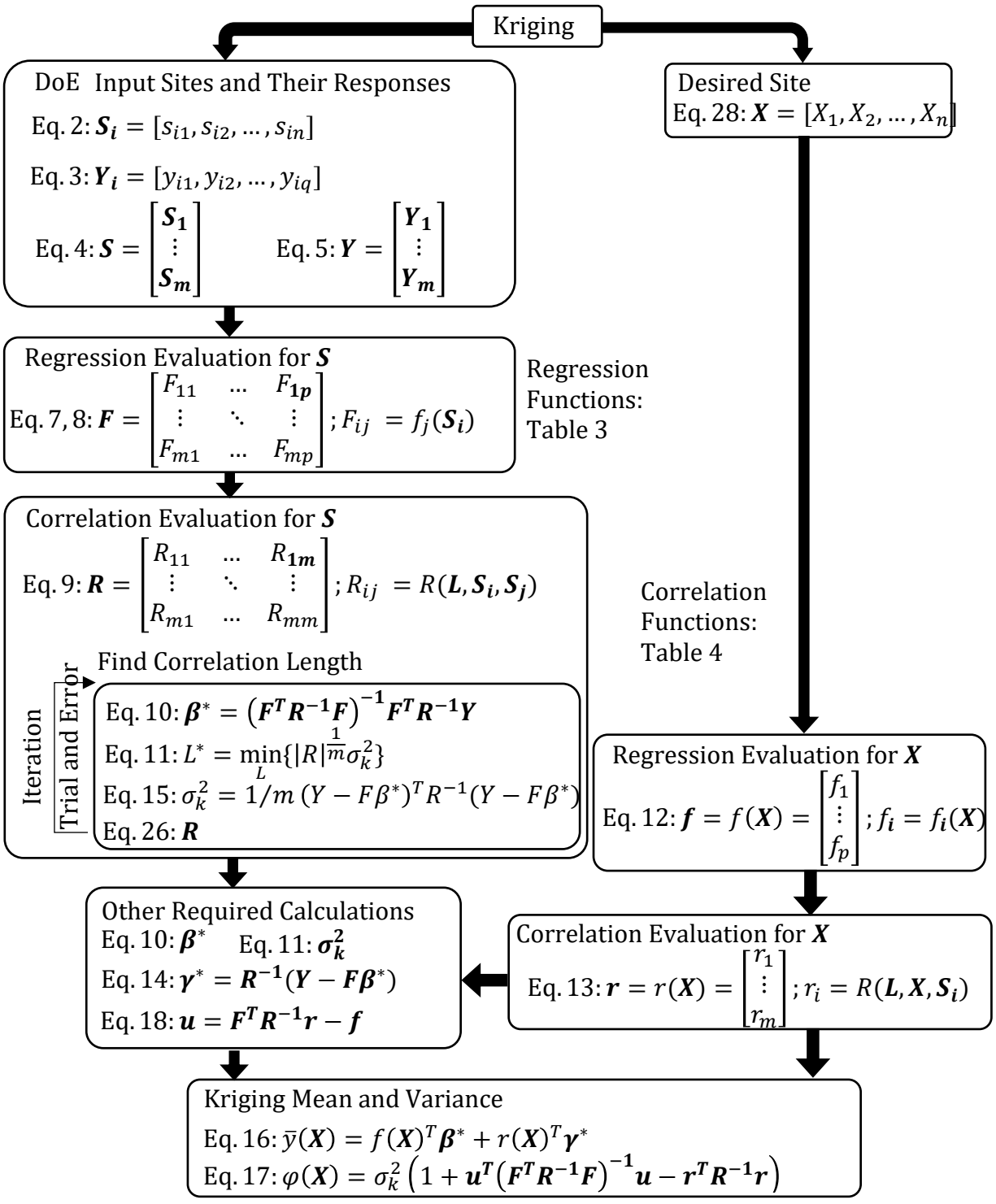

Figure 2. Summary of Kriging procedure (Khorramian and Oudah, 2022b).

2.3 MONTE CARLO SIMULATION (MCS)

The name 'Monte Carlo' started out as a name representing the casino at Monte Carlo that operated in the 1950s. Due to the fact that gambling was illegal and also random, the name Monte Carlo Simulation (MCS) was adopted soon after as the technical term for the simulation of random processes (Brooks et al., 2011). The MCS development is rooted in Los Alamos Scientific Laboratory during the second world war, as scientists engaged in building the first atomic bomb. The first modeling application of the MCS was modeling the diffusion process in fissionable material, where the goal was to estimate the neutron multiplication rate (Assad and Gass, 2005). The development of the method was not possible without the development of scientific computers. As such, the method did not attain momentum in statistical analysis until after the 1990s and is the basis of the method used in the 21st century (Assad and Gass, 2005).

The MCS is sometimes referred to as brute MCS or crude MCS in studies that have conventional MCS models alongside augmented hybrids models, for example AK-MCS. The fundamental concept of the MCS is the evaluation of a LSF based on a predetermined failure criterion for a large number of trials. In other words, to numerically simulate some phenomenon and then observe some event of interest (Nowak and Collins, 2013). Using the statistical data from previous observations to represent the uncertainties (or randomness) of the system to represent (or predict) the behaviour of the systems response. MCS allows engineers and researchers the ability to generate results of interest without conducting large numbers of physical testing. The MCS can be applied to linear and non-linear LS, however depending on the complexity of the system it can be computationally demanding to simulate. MCS has been used to assess β because of its accuracy and ability to capture multimodal and highly nonlinear LSF as compared with gradient-based methods such as FORM and variance reduction methods. However, MCS has an efficiency-related

issue if a large number of trials is required for problems where the expected β is relatively high and if the cost of the computational model is high. These challenges are often encountered in bridge engineering where the expected β is typically greater than 4.0 and the LSF is often assessed using numerical nonlinear FE analysis, especially when the soil-structure interaction is considered or when spatially distributed degradation is present (Khorramian et al., 2022; Oudah and Alhashmi, 2022).

The stopping criterion of the MCS are associated with the targeted error and thresholds for certainty. The number of trails in MCS (N_{MCS}) is determined based on the desired confidence level and the maximum tolerable error (e_{max}) (Huang et al., 2012). These components are related to each other as defined in Equation (19), where (Z_α) is the Z-value for the selected confidence level, $\hat{p}$ is the expected probability of failure, and $\hat{q}$ is the probability of survival expected. For example, the number of MCS trials required to achieve 95% confidence with a 5% error for a target β of 4.0 is 49 million, which makes MCS less efficient if nonlinear FE is required to assess the LSF.

$$N_{MCS} = \frac{Z_\alpha^2 \hat{p}\hat{q}}{e^2} \tag{19}$$

The probability of failure (P_f), calculation is expressed in Equation (20), where N_f is the total number of failures (refer to Section 1.2 for more details).

$$P_f = \frac{N_f}{N_{MCS}} \tag{20}$$

The reliability index (β), is expressed in Equation (21), where Φ is the cumulative distribution function (CDF) and Φ^{-1} is the inverse CDF.

$$\beta = \Phi^{-1}(1 - P_f) \tag{21}$$

2.4 ACTIVE LEARNING KRIGING MONTE CARLO SIMULATION (AK-MCS)

2.4.1 General Concept

The fundamental concept of active-learning Kriging (AK) reliability is the reduction of simulation cost by introducing a surrogate model as an inexpensive representation of a complex LSF. AK uses the Kriging predictor as a surrogate model of the performance function, combining it with any reliability estimation method like MCS. The DoE are then used to train the surrogate model in a stepwise manner. There are numerous learning functions in the literature for the AK method, where the primary role of the learning function is to determine what additional points are selected to be added to the DoE. The term AK configuration refers to the selection of the regression, correlation and learning functions required to perform AK analysis. The AK configuration of the analysis needs to be optimized to reap any of the benefits of the AK method.

There are four main sections to the AK analysis, the initial DoE, Kriging, active learning, and reliability assessment. Within the DoE, n denotes the number of random variables, that are used to generate the initial inputs for the original model which is represented as the LSF expressed in Equation (1). The initial DoE is comprised of the initial inputs and the initial outputs, where the outputs are the results of the LSF. This DoE is then submitted to Kriging. Kriging is used to generate a surrogate predictor using prescribed regression and correlation functions, where the number of required initial training points (P) varies depending on the regression function. Once the surrogate predictor is trained using the initial DoE, the learning process commences, where additional DoE are selectively submitted to the Kriging to form an updated Kriging predictor. In the learning process, the mean and variance values are fed into a learning function. The learning function will then determine the next DoE candidate while a stopping criterion is established and

used to determine the desired level of accuracy for updating the Kriging predictor. If the stopping criterion is not met, an additional candidate will be selected and put through the original model to gain the output, where this new input and output would be one added design site to the DoE. The analysis will then restart with the new DoE until such time as the stopping criterion is met. Once it is met, the analysis moves to the fourth and final stage, the reliability assessment. In the reliability assessment all trials will be fed through the surrogate predictor to predict the performance function, and hence determining the P_f. The reliability assessment method of choice in this research is MCS.

2.4.2 Learning Functions

There are multiple learning functions in literature. Five learning functions were reviewed and considered in this research: U, H, EFF, REIF, and KO. The learning functions are reviewed in the following subsections, where $\mu_{\hat{G}}(x)$ is the mean value of the Kriging predictor and $\sigma_{\hat{G}}(\boldsymbol{x})$ is the standard deviation of the Kriging predictor:

2.4.2.1 U Learning Function

The U learning function $U(x)$, was developed based on the concept that when performing MCS, only the sign of the performance function is relevant (Echard et al., 2011). A positive value would indicate a pass, whereas a negative would indicate a failure. Based on this, the occurrences with the highest potential of crossing from positive to negative ($G(x) = 0$) must be evaluated by the performance function. The U learning function represents the risk of making a mistake on the sign of the performance function and is expressed in Equation (22). The learning criterion is the minimization of $U(x)$, and the stopping criterion is defined as ($U(x)_{min} \geq 2$).

$$U(x) = \frac{|\mu_{\hat{G}}(x)|}{\sigma_{\hat{G}}(\boldsymbol{x})} \tag{22}$$

2.4.2.2 H Learning Function

The H learning function $H(x)$, as expressed in Equation (23), was derived based on information entropy theory, which describes the disorder degree or uncertainty of the prediction (Shi et al., 2020). The learning criterion is the maximization of $H(x)$ and the stopping criterion is defined as $H(x)_{max} \leq 0.5$ (Zhaoyan et al., 2013).

$$H(x) = \left| \ln\left(\sqrt{2\pi}\sigma_{\hat{G}}(x) + \frac{1}{2}\right)\left[\Phi\left(\frac{2\sigma_{\hat{G}}(\boldsymbol{x}) - \mu_{\hat{G}}(x)}{\sigma_{\hat{G}}(\boldsymbol{x})}\right) - \Phi\left(\frac{-2\sigma_{\hat{G}}(\boldsymbol{x}) - \mu_{\hat{G}}(x)}{\sigma_{\hat{G}}(\boldsymbol{x})}\right)\right]\right.$$
$$- \left[\left(\frac{2\sigma_{\hat{G}}(\boldsymbol{x}) - \mu_{\hat{G}}(x)}{2}\right)\phi\left(\frac{2\sigma_{\hat{G}}(\boldsymbol{x}) - \mu_{\hat{G}}(x)}{\sigma_{\hat{G}}(\boldsymbol{x})}\right)\right. \tag{23}$$
$$\left.\left. + \left(\frac{2\sigma_{\hat{G}}(\boldsymbol{x}) + \mu_{\hat{G}}(x)}{2}\right)\phi\left(\frac{-2\sigma_{\hat{G}}(\boldsymbol{x}) - \mu_{\hat{G}}(x)}{\sigma_{\hat{G}}(\boldsymbol{x})}\right)\right]\right|$$

Upon investigation, it was found that there was a discrepancy in the formulation of the H learning function, the corrected version of the H learning function is shown in Equation (24) and the changes are noted in red. The detailed derivation of the corrected version of the $H(x)$ function (donated $H_c(x)$ thereafter) is included in Khorramian and Oudah (2022b). Both H and H_c were utilized in this research.

$$H_C(x) = \left| \left(\ln\left(\sqrt{2\pi}\sigma_{\hat{G}}(x)\right) + \frac{1}{2}\right)\left[\Phi\left(\frac{2\sigma_{\hat{G}}(\boldsymbol{x}) - \mu_{\hat{G}}(x)}{\sigma_{\hat{G}}(\boldsymbol{x})}\right) - \Phi\left(\frac{-2\sigma_{\hat{G}}(\boldsymbol{x}) - \mu_{\hat{G}}(x)}{\sigma_{\hat{G}}(\boldsymbol{x})}\right)\right]\right.$$
$$- \left[\left(\frac{2\sigma_{\hat{G}}(\boldsymbol{x}) - \mu_{\hat{G}}(x)}{2\sigma_{\hat{G}}(\boldsymbol{x})}\right)\phi\left(\frac{2\sigma_{\hat{G}}(\boldsymbol{x}) - \mu_{\hat{G}}(x)}{\sigma_{\hat{G}}(\boldsymbol{x})}\right)\right. \tag{24}$$
$$\left.\left. + \left(\frac{2\sigma_{\hat{G}}(\boldsymbol{x}) + \mu_{\hat{G}}(x)}{2\sigma_{\hat{G}}(\boldsymbol{x})}\right)\phi\left(\frac{-2\sigma_{\hat{G}}(\boldsymbol{x}) - \mu_{\hat{G}}(x)}{\sigma_{\hat{G}}(\boldsymbol{x})}\right)\right]\right|$$

2.4.2.3 Effective Feasibility Function

The effective feasibility function (EFF) was inspired by contour estimation work and is derived from the efficient global reliability analysis (EGRA) method (Echard et al., 2011). It provides an indication of how much less the true value of the response at a point can be expected to be compared to the current best solution. Points with large uncertainty will also have large expected feasibility values. The function is depicted in Equation (25), where $G^{+}(\mathrm{x}) = \bar{G}(\mathrm{x}) + \varepsilon(x)$ and $G^{-}(\mathrm{x}) = \bar{G}(\mathrm{x}) - \varepsilon(x)$, where $\epsilon(x)$ is the measure of error which determines the borders of the desired range. The learning criterion is the maximization of $EFF(x)$ and the stopping criteria is $EFF(x)_{max} \leq 0.001$.

$$
\begin{aligned}
EFF(x) = \left(\mu_{\hat{G}}(\boldsymbol{X}) - \bar{G}(\boldsymbol{X})\right)\left[2\Phi\left(\frac{\bar{G}(\boldsymbol{X}) - \mu_{\hat{G}}(\boldsymbol{X})}{\sigma_{\hat{G}}(\boldsymbol{X})}\right) - \Phi\left(\frac{G^{+}(\boldsymbol{X}) - \mu_{\hat{G}}(\boldsymbol{X})}{\sigma_{\hat{G}}(\boldsymbol{X})}\right) - \Phi\left(\frac{G^{-}(\boldsymbol{X}) - \mu_{\hat{G}}(\boldsymbol{X})}{\sigma_{\hat{G}}(\boldsymbol{X})}\right)\right] \\
- \sigma_{\hat{G}}(\boldsymbol{X})\left[2\phi\left(\frac{\bar{G}(\boldsymbol{X}) - \mu_{\hat{G}}(\boldsymbol{X})}{\sigma_{\hat{G}}(\boldsymbol{X})}\right) - \phi\left(\frac{G^{+}(\boldsymbol{X}) - \mu_{\hat{G}}(\boldsymbol{X})}{\sigma_{\hat{G}}(\boldsymbol{X})}\right) - \phi\left(\frac{G^{-}(\boldsymbol{X}) - \mu_{\hat{G}}(\boldsymbol{X})}{\sigma_{\hat{G}}(\boldsymbol{X})}\right)\right] \\
+ \varepsilon\left[\Phi\left(\frac{G^{+}(\boldsymbol{X}) - \mu_{\hat{G}}(\boldsymbol{X})}{\sigma_{\hat{G}}(\boldsymbol{X})}\right) - \Phi\left(\frac{G^{-}(\boldsymbol{X}) - \mu_{\hat{G}}(\boldsymbol{X})}{\sigma_{\hat{G}}(\boldsymbol{X})}\right)\right]
\end{aligned}
\tag{25}
$$

2.4.2.4 Reliability-Based Expected Improvement Function

The reliability-based expected improvement function (REIF), as shown in Equation (26), was derived based on the folded-normal distribution for structural reliability analysis (Zhang et al., 2019). The learning criterion is the minimization of $REIF(x)$, and the stopping criterion is defined as $(REIF(x)_{min} \leq 0)$.

$$
REIF(x) = \mu_{\hat{G}}(\boldsymbol{x})\left[1 - 2\Phi\left(\frac{\mu_{\hat{G}}(\boldsymbol{x})}{\sigma_{\hat{G}}(\boldsymbol{x})}\right)\right] + \sigma_{\hat{G}}(\boldsymbol{x})\left[2 - \sqrt{\frac{2}{\pi}}exp\left(-\frac{1}{2}\left(\frac{\mu_{\hat{G}}(\boldsymbol{x})}{\sigma_{\hat{G}}(\boldsymbol{x})}\right)^{2}\right)\right] \tag{26}
$$

2.4.2.5 Kriging Occurrence Learning Function

The Kriging Occurrence (KO) learning function was developed by Khorramian and Oudah (2022a). Theoretically, the KO learning function is the probability that the response of point *x* occurs in the desired area, within the vicinity of the LSF, where the desired area is within the range of $G(x) - \epsilon(x)$ to , $G(x) + \epsilon(x)$. Mathematically, the KO learning function is the area under the probability density function (PDF) of a point x, that overlaps with the desired area (Khorramian and Oudah, 2022a). The KO function is expressed in Equation (27).

$$KO(x) = \Phi\left(\frac{\bar{G}(x) + \epsilon(x) - \mu_{\hat{G}}(x)}{\sigma_{\hat{G}}(x)}\right) - \Phi\left(\frac{\bar{G}(x) - \epsilon(x) - \mu_{\hat{G}}(x)}{\sigma_{\hat{G}}(x)}\right) \quad (27)$$

The measure of error which determines the borders of the desired range, $\epsilon(x)$, is recommended to be two or five standard deviations of the Kriging predictor ($\sigma_{\hat{G}}(x)$). The selection criterion for the addition of a training point, is the maximization of the learning function. This means that the point selected is the point with the highest probability of occurrence and is expected to give the lowest error. Alternatively, it could be defined as the selection of the new training point that reduces the error of the surrogate model the most (Khorramian and Oudah, 2022a). The stopping criterion is defined based on the level of accuracy required for the model, where the stopping criterion is equal to $KO(x) < 0.05$ for 95% accuracy or $KO(x) < 0.005$ for 99.5% accuracy (Khorramian and Oudah, 2022a). Four variations of the KO function were considered, $\mathrm{KO}_{05(2)}$, $\mathrm{KO}_{005(2)}$, $\mathrm{KO}_{05(5)}$, and $\mathrm{KO}_{005(5)}$, where the naming convention is based on the accuracy and the $\epsilon(x)$ values considered. If the learning function had 95% accuracy and an $\epsilon(x) = 2\sigma_{\hat{G}}(x)$, the name of the function is $\mathrm{KO}_{05(2)}$, and if the function had an accuracy of 99.5% and $\epsilon(x) = 5\sigma_{\hat{G}}(x)$, the name of the function is $\mathrm{KO}_{005(5)}$.

2.4.3 Application in Structural Safety

The applicability of AK-MCS to assess the reliability of engineering systems has been investigated in literature through a series of examples. Echard (2011) investigated four examples that covered a wide variety of LS, including high non-linearity, non-convex domains of failure, and moderate and high dimensional problems. These examples included a series system with four branches (dimension 2), a non-linear analytical function with moderate dimension called the modified Rastrigin function, the dynamic response of a non-linear oscillator, and a high dimensional example.

Peijuan et al., (2017) applied the AK-MCS method to problems with a connected domain of failure (not involving several scattered gaps of failure), in effort to improve the speed of convergence. Three academic examples including the two-dimensional example and non-linear oscillator example from B. Echard (2017) and Kaymaz (2005) were also examined. Peijuan et al. (2017) also investigated a three-unequal-span continuous girder with an implicit performance function to verify the accuracy and validity of the methodology (Peijuan et al, 2017). Al-Bittar et al. (2018) applied the AK-MCS method to the reliability analysis of strip footings resting on spatially varying soils. Focusing on the probabilistic analysis of the ULS of the shallow footing, where the soil cohesion and angle of internal friction are considered as random fields. AK-MCS was also utilized to assess the safety of group piles interacting with soil where the spatial distributions of the soil and pile properties were considered (Khorramian et al., 2022a; Khorramian et al., 2022b).

One of the primary findings in works related to the AK-MCS methodology is the ineffectiveness of the method in applications where the P_f is small (10^{-5} to 10^{-9}) as compared with other reliability estimations techniques are used as AK importance sampling (AK-IS). In 2020,

Razaaly and Congedo proposed a variation the AK-MCS method called the extreme AK-MCS (eAK-MCS). Several examples where considered, including, a four branch 2D series, deviation of a cantilever beam 2D, response of a nonlinear oscillator 6D, and borehole-function 8D (Razaaly and Congedo, 2020). AK-MCS has also been applied in nuclear passive safety systems (Puppo et al., 2021), where the safety performance is evaluated through a computationally expensive thermal-hydraulic simulations models.

Structural reliability-based problems are used for both design and for assessment at some point in the structures service life, where service life refers to the period of time the structure is designed to fulfill its intended function. When considering a point in time during the service life, time-dependant durability questions arise. AK-MCS has been considered for use in time-dependant reliability analysis for similar reasons as its applicability and benefits to general reliability-based problems. Time dependant reliability analysis has gained a lot of attention due to its connection with performance degradation, lifetime cost estimation, maintenance, lifetime testing and system resilience (Hu and Mahadevan, 2016). Shi et al. (2019) explored the application of time-dependant reliability analysis in structural assessment. An example of a stone arch under hurricane loading, roof truss structure, and a bean under stochastic loads were assessed. A FE model was used along with a single loop Kriging and a multiple loop Kriging and found that the double loop method was the most optimal as it required the least number of calls to the FE model. In time-dependent analysis, the resistance of the model would be replaced with a degradation model of sorts. A prime example would be FE analysis that reflects the in-situ conditions based on non-invasive material testing.

2.5 SUMMARY OF TERMINOLOGIES

Table 2 describes the definitions of common terminologies relevant to the reliability analysis performed in this research. They are defined in sections of the text but have been dictated in table format for easy reference.

Table 2. Definitions of reliability-related terms utilized in this research.

Terms	Definition	Reference
Crude Monte Carlo Simulation (MCS)	A form of simulation model that runs a predefined number of randomly generated trials through the original performance function and not a surrogate performance function.	(Nowak and Collins, 2013; Zhang et al., 2020)
Kriging	It is a nonlinear regression method that utilises a regression function where the error is represented as a stochastic process.	(Echard et al., 2011; Khorramian and Oudah, 2022b)
Active Learning Kriging Monte Carlo Simulation (AK-MCS)	It is a surrogate-based model, augmented through the use of MCS trails and learning function to optimize and train the surrogate model.	(Echard et al., 2011)
Active Learning Kriging Configuration (AK-Configuration)	Refers to the selection and combination of regression, correlation and learning functions used within an AK analysis.	(Buckley, et al., 2021)
Structural Service Life	It is the duration of time the structure in question was designed to fulfill its function.	(Hu and Mahadevan, 2016)

CHAPTER 3 COMPUTER CODE DEVELOPMENT AND APPLICATION

3.1 INTRODUCTION

This chapter covers the development of the AK reliability analysis framework and details the methodology that was implemented to develop a MATLAB® code to perform the analysis. Two code structures including crude MCS and AK-MCS were developed. The former was used to calculate a benchmark β to assess the accuracy of the AK-MCS method through the comparison of results. Section 3.2 and 3.3 detail the code structure for each, respectively. The term "crude" is utilized in this context to highlight the use of MCS as a reliability estimation technique that utilizes the original performance function to evaluate all trails, as opposed to when MCS is used in combination with AK to estimate the reliability using a surrogate performance function.

3.2 MATLAB® CODE: CRUDE MCS

The main script of the crude MCS *(Main_Crude_MCS_Script*) is where the primary analysis is completed. This script calls, processes and stores all the analysis data, by calling other scripts and functions while loading the required inputs. The main script calls the (*X_MCS_Creator*) script which consolidates the input statistics, geometric input, and calculates the mean loads based on the resistance function. This information is then fed into the (*Random_Generator*) script which generates an x vector, containing the randomly generated and constant variables. The x vector is then loaded into the performance function for girders (*Performance_NEBT_Girder*) or piers (*Performance_Square_Pier*) that calculates the resistance of the section based on the respective resistance function, for girders (*Resistance_NEBT_Girder*) or piers (*Resistance_Square_Pier*). The mean total loads are calculated based on the resistance model and applicable load/resistance factors. The loads are then randomly generated for each trial, and failure occurs when the load

surpasses the resistance of the section. The P_f and β are calculated in the main MCS script as per Equations (20) and (21).

3.3 MATLAB® CODE: AK-MCS

3.3.1 AK-MCS Code Flowchart

AK-MCS method has four distinctive steps of analysis as indicated in Figure 3. The initial DoE is the design space represented by the random variables. Kriging is the second step that uses regression and correlation functions to evaluate a small number of the predetermined scenarios to develop a surrogate model. In the third step, the model is evaluated with a learning function and a stopping criterion, which determine if another trial is required to decrease the error associated with the surrogate model. If the stopping criterion is not met and another trial is added to the DoE, the new trial is selected by the learning function selection criterion. Once a new trial is added, the first three steps are repeated. This continues until a suitable surrogate model is developed, where suitable means the learning function stopping criterion is met (typically a form of error minimization requirements). This surrogate model is then used to evaluate all the pre-generated randoms variables sets and the AK-MCS probability of failure ($P_{f_{AK-MCS}}$) and AK-MCS reliability index (β_{AK-MCS}) are calculated based on the number of failed (or negative valued) trials and the total number of trials.

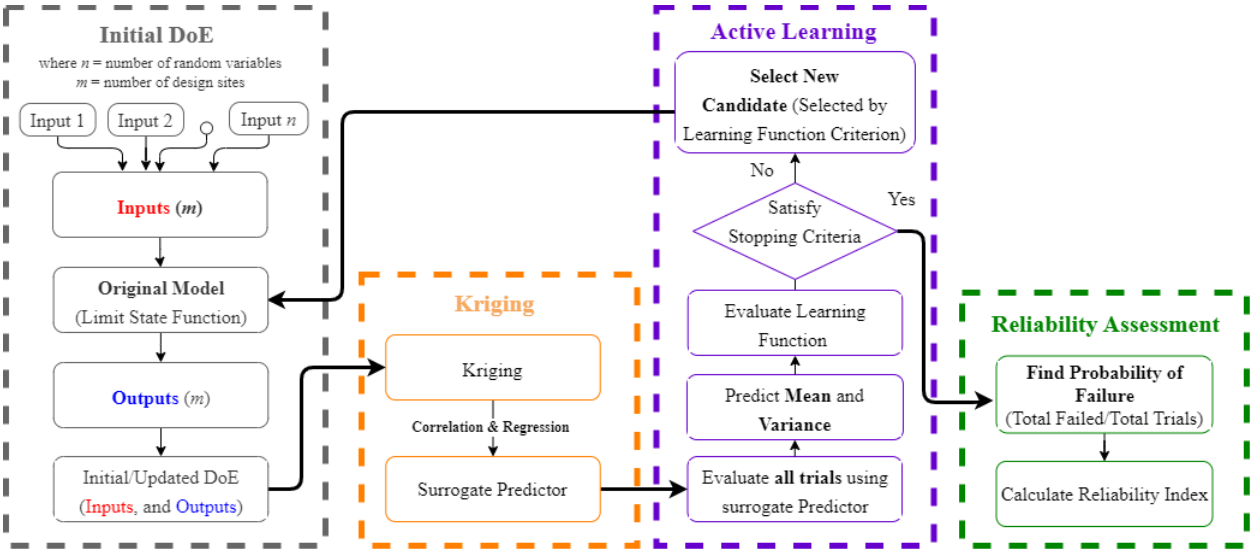

Figure 3. AK-MCS a flowchart for the MATLAB® Code.

The input parameters to the AK-MCS code are similar to the MCS code with the addition of input of the parametric definition. The parametric definition are the vectors that contain the AK-configuration information (regression, correlation, and learnings functions). The mathematical formulations of the used regression, correlation, and learning functions are outlined the following sections.

The mean load, statistical, parametric, and input data are stored in the AK-MCS script, where the *Parametric_set_up* is called and outlines the number of trials run through the final predictor and defines the AK configurations considered based on a set range that can include some or all functions in the parametric input. The *Index_input* script takes the defined AK configurations and indexes them accordingly, which stores the number associated with the regression, correlation and learning functions respectively. The *Initial_Analysis* script takes the defined input parameters and feeds them into the random generator function, creating a vector of inputs based on the statistics and mean value for each individual trial considered. This set of trails is the data set in which the analysis pulls from when training the surrogate model, and the trials that will be fed through the final surrogate predictor to calculate the P_f and β at the end of the AK-MCS procedure.

The script called *AK_Fn_Fast* is the script that preforms the AK procedure, which encompasses the Kriging and active learning as detailed in Figure 3. The Kriging portion generates the surrogate model using the design and analysis of computer experiments (DACE) toolbox (Lophaven et al, 2002). *AK_Fn_Fast* calls the *Active_Learning* function to implement the selection and stopping criterion of the learning function used to augment the Kriging predictor. The final surrogate model is determined based on the stopping criterion of the learning function in question. This predictor is then used to evaluate all the trials noted in the *Parametric_set_up.* The P_f and β are calculated based on the number of failed trials and the total number of trials.

3.3.2 Regression Functions

Three regression functions were used in the AK-MCS analysis as summarized in Table 3.

Table 3. Regression functions considered in the AK-MCS analysis.

Type	**Required number of design sites to initiate the analysis, *P***	**Functions**
Constant	$P = 1$	$f_1(x) = 1$
Linear	$P = n + 1$	$f_1(x) = 1\,, f_2(x) = x_1\,, \dots, f_{n+1}(x) = x_n$
Quadratic	$P = \frac{1}{2}(n+1)(n+2)$	$f_1(x) = 1\,, f_2(x) = x_1\,, \dots, f_{n+1}(x) = x_n\,,$ $f_{n+2}(x) = {x_1}^2\,, \dots, f_{2n+1}(x) = x_1\,x_n\,,$ $f_{2n+2}(x) = {x_2}^2\,, \dots, f_{3n}(x) = x_2\,x_n\,,$ $\dots\,, \dots, \dots, f_p(x) = {x_n}^2$

Note: P = required size of initial training set and number of regression terms; n = number of input random variables

3.3.3 Correlation Functions

Six correlation functions were coded within this research to perform the AK-MCS analysis as summarized in Table 4.

Table 4. Correlation functions considered in the AK-MCS analysis.

Correlation Function	**Function:** $\boldsymbol{R(\theta, w, x) = \prod_{j=1}^{n} R_j(\theta, d_j)\ , d_j = w_j - x_j}$
Gaussian	$R_j(\theta, d_j) = \exp(-\theta_j {d_j}^2)$
Cubic	$R_j(\theta, d_j) = 1 - 3{\xi_j}^2 + 2{\xi_j}^3, \quad \xi_j = min\{1, \theta_j \lvert d_j \rvert\}$
Exponential	$R_j(\theta, d_j) = \exp(-\theta_j \lvert d_j \rvert)$
Linear	$R_j(\theta, d_j) = \max\{0, 1 - \theta_j \lvert d_j \rvert\}$
Spherical	$R_j(\theta, d_j) = 1 - 1.5\xi_j + 0.5{\xi_j}^3, \quad \xi_j = min\{1, \theta_j \lvert d_j \rvert\}$
Spline	$R_j(\theta, d_j) = \varsigma(\xi_j), \quad \xi_j = \theta_j \lvert d_j \rvert$ $\varsigma(\xi_j) = \begin{cases} 1 - 15\xi_j + 30{\xi_j}^3 & if \quad 0 \le \xi_j \le 0.2 \\ 1.25(1 - \xi_j)^3 & if \quad 0.2 < \xi_j < 1 \\ 0 & if \quad 1 \le \xi_j \end{cases}$

Note: n = number of input random variables for Kriging and reliability analysis.

3.3.4 Learning Functions

The primary objectives of the learning function are to evaluate the accuracy of the surrogate model, determine if it meets the predefined stopping criterion and if not, select the next training point to be added to the DoE. The three key parameters associated with each learning function are the function, the stopping criterion, and the selection criterion. Each individual learning functions has their own unique set of parameters and are based on different methodologies as detailed in Section 2.4.2. The learning functions coded in the MATLAB® script are summarized in Table 5, while the associated selection and stopping criteria are summarized in Table 6.

Table 5. Learning functions considered in the AK-MCS analysis.

Learning Function	**Ref.**	**Functions**
U	(Echard et al., 2011)	$U(\boldsymbol{x}) = \dfrac{\lvert \hat{G}(\boldsymbol{x}) \rvert}{\sigma_{\hat{G}}(\boldsymbol{x})}$
H	(Zhaoyan et al., 2015)	$H(x) = \left\lvert \ln\left(\sqrt{2\pi}\sigma_{\hat{G}}(x) + \dfrac{1}{2}\right)\left[\Phi\left(\dfrac{2\sigma_{\hat{G}}(\boldsymbol{x}) - \mu_{\hat{G}}(x)}{\sigma_{\hat{G}}(\boldsymbol{x})}\right) - \Phi\left(\dfrac{-2\sigma_{\hat{G}}(\boldsymbol{x}) - \mu_{\hat{G}}(x)}{\sigma_{\hat{G}}(\boldsymbol{x})}\right)\right] - \left[\left(\dfrac{2\sigma_{\hat{G}}(\boldsymbol{x}) - \mu_{\hat{G}}(x)}{2}\right)\phi\left(\dfrac{2\sigma_{\hat{G}}(\boldsymbol{x}) - \mu_{\hat{G}}(x)}{\sigma_{\hat{G}}(\boldsymbol{x})}\right) + \left(\dfrac{2\sigma_{\hat{G}}(\boldsymbol{x}) + \mu_{\hat{G}}(x)}{2}\right)\phi\left(\dfrac{-2\sigma_{\hat{G}}(\boldsymbol{x}) - \mu_{\hat{G}}(x)}{\sigma_{\hat{G}}(\boldsymbol{x})}\right)\right] \right\rvert$

Learning Function	Ref.	Functions
H_c	(Khorramian and Oudah, 2022a)	$H_C(x) = \left\lvert \left(\ln\left(\sqrt{2\pi}\sigma_{\hat{G}}(x)\right) + \frac{1}{2}\right)\left[\Phi\left(\frac{2\sigma_{\hat{G}}(x) - \mu_{\hat{G}}(x)}{\sigma_{\hat{G}}(x)}\right) - \Phi\left(\frac{-2\sigma_{\hat{G}}(x) - \mu_{\hat{G}}(x)}{\sigma_{\hat{G}}(x)}\right)\right] - \left[\left(\frac{2\sigma_{\hat{G}}(x) - \mu_{\hat{G}}(x)}{2\sigma_{\hat{G}}(x)}\right)\phi\left(\frac{2\sigma_{\hat{G}}(x) - \mu_{\hat{G}}(x)}{\sigma_{\hat{G}}(x)}\right) + \left(\frac{2\sigma_{\hat{G}}(x) + \mu_{\hat{G}}(x)}{2\sigma_{\hat{G}}(x)}\right)\phi\left(\frac{-2\sigma_{\hat{G}}(x) - \mu_{\hat{G}}(x)}{\sigma_{\hat{G}}(x)}\right)\right]\right\rvert$
EFF	(Bichon et al., 2008)	$EFF(x) = \left(\mu_{\hat{G}}(X) - \bar{G}(X)\right)\left[2\Phi\left(\frac{\bar{G}(X) - \mu_{\hat{G}}(X)}{\sigma_{\hat{G}}(X)}\right) - \Phi\left(\frac{G^{+}(X) - \mu_{\hat{G}}(X)}{\sigma_{\hat{G}}(X)}\right) - \Phi\left(\frac{G^{-}(X) - \mu_{\hat{G}}(X)}{\sigma_{\hat{G}}(X)}\right)\right] - \sigma_{\hat{G}}(X)\left[2\phi\left(\frac{\bar{G}(X) - \mu_{\hat{G}}(X)}{\sigma_{\hat{G}}(X)}\right) - \phi\left(\frac{G^{+}(X) - \mu_{\hat{G}}(X)}{\sigma_{\hat{G}}(X)}\right) - \phi\left(\frac{G^{-}(X) - \mu_{\hat{G}}(X)}{\sigma_{\hat{G}}(X)}\right)\right] + \varepsilon\left[\Phi\left(\frac{G^{+}(X) - \mu_{\hat{G}}(X)}{\sigma_{\hat{G}}(X)}\right) - \Phi\left(\frac{G^{-}(X) - \mu_{\hat{G}}(X)}{\sigma_{\hat{G}}(X)}\right)\right]$
REIF	(Zhaoyan et al., 2013)	$REIF\left(\hat{G}(\boldsymbol{x})\right) = \mu_{\hat{G}}(\boldsymbol{x})\left[1 - 2\Phi\left(\frac{\mu_{\hat{G}}(\boldsymbol{x})}{\sigma_{\hat{G}}(\boldsymbol{x})}\right)\right] + \sigma_{\hat{G}}(\boldsymbol{x})\left[2 - \sqrt{\frac{2}{\pi}}exp\left(-\frac{1}{2}\left(\frac{\mu_{\hat{G}}(\boldsymbol{x})}{\sigma_{\hat{G}}(\boldsymbol{x})}\right)^2\right)\right]$
KO	(Khorramian and Oudah, 2022a)	$KO(x) = \Phi\left(\frac{\bar{G}(x) + \epsilon(x) - \mu_{\hat{G}}(x)}{\sigma_{\hat{G}}(x)}\right) - \Phi\left(\frac{\bar{G}(x) - \epsilon(x) - \mu_{\hat{G}}(x)}{\sigma_{\hat{G}}(x)}\right)$

Note: Reference = Ref.; Φ and ϕ are CDF and PDF operators for a standard normal distribution.

Table 6. Selection and stopping criterion of the learning functions.

Learning Function	Reference	Selection Criterion	Stopping Criteria
U	(Echard et al., 2011)	$min\{U(x)\}$	$min\{U(x)\} > 2$
H	(Zhaoyan et al., 2013)	$max\{H(x)\}$	$max\{H(x)\} < 0.5$
H	(Khorramian and Oudah, 2022a)	$max\{H(x)\}$	$max\{H(x)\} < 0.5$
EFF	(Bichon et al., 2008)	$max\{EFF(x)\}$	$max\{EFF(x)\} < 0.001$
REIF	(Zhaoyan et al., 2013)	$max\{REIF(x)\}$	$max\{REIF(x)\} \leq 0$
KO	(Khorramian and Oudah, 2022a)	$max\{KO(x)\}$	$max\{KO(x)\} < 0.05\ or\ 0.01$

CHAPTER 4 VERIFICATION OF AK-MCS RELIABILTY FOR RC BRIDGES

4.1 INTRODUCTION

The objectives of this chapter are to i) verify the accuracy of the coded AK-MCS reliability analysis for predicting the reliability of steel reinforced concrete (RC) new England bulb tee (NEBT) bridge girders and square RC piers; and ii) evaluate the efficiency of the analysis method. The MATLAB® codes detailed in Section 3.2 and 3.3 were utilized to perform the analysis. The findings of this verification exercise will be utilized in Chapter 5 to recommend specific AK configurations to meet predefined desired accuracy and efficiency levels (sets of learning, regression, and correlation functions). The load and resistance models utilized in the analysis are described first, followed by presenting the procedure for conducting the reliability analysis, and concludes with analysis results and recommendations.

4.2 CONSIDERED GEOMETRIC CONFIGURATIONS

The AK-MCS reliability was verified by assessing the reliability of nine prestressed NEBT girders as summarized in Table 7 and six square steel RC bridge piers as summarized in Table 8. The selections of pier configuration were based on typical cross-sections found in practice. There were three variables considered in the geometric cases, the height of the section (H), the bar sizes, and distribution of the rebar, which represented the reinforcement ratios (ρ) implicitly. The depth to rebar (d_i) was governed by the section H as concrete cover and spacing between bar layers were kept constant at 50 mm, and 100 mm, respectively. The detailing of both the cross-section geometry and the reinforcing are found in Table 7. The selection of pier configuration was based on typical cross-sections found in practice. There were three variables considered in the geometric

cases, the height of the section (H), the bar sizes, and distribution of the rebar. By varying these properties, the reinforcement ratio of the section was considered implicitly. The depth to rebar (d_i) was governed by the section H as concrete cover and spacing between bar layers were kept constant at 50 mm, and 100 mm, respectively. The detailing of both the cross-section geometry and the reinforcing are found in Table 7 and was designed as per the Canadian Highway Bridge Design Code (CHBDC) (CSA S6, 2019). The selection of the girder geometry and configuration was based on the three typical configurations for NEBT girders and three standard pre-stressed reinforcing strands. A single configuration or "layout" of the steel reinforcing bars was considered (it defines the concrete cover, spacing between rebar layers and the number of rebars per layer). The varied parameters within the cross-sections were the overall section height, and the diameter of the rebars (d_b). By varying these two geometric parameters, the reinforcement ratios of the sections were considered implicitly. The depth to the reinforcing layers varies with the height of the section. However, the concrete cover and spacing between bars remains constant. Table A.1 of Appendix A includes the cross-section geometry of the idealized NEBT concrete girders. Table 7 details the reinforcements within the designated cross-section, where the section identification (ID) numbers, d_b, the cross-sectional area of all the rebar in the section (A_{st}), the bar configuration (A_s^*), depth to each layer (d_s^*) and the actual reinforcement ratio (ρ) are noted.

Table 7. Details of girders considered in the analysis.

Section ID	NEBT ID	d_b (mm)	A_{st} (mm^2)	A_s* (mm^2)	d_s* (mm)	ρ (%)
GIRD 01	NEBT 3	9.5	994	A_b[2,2,2,4,4]	[1100,1200,1300,1400,1500]	0.1950
GIRD 02	NEBT 2	9.5	994	A_b[2,2,2,4,4]	[900,1000,1100,1200,1300]	0.1822
GIRD 03	NEBT 1	9.5	994	A_b[2,2,2,4,4]	[700,800,900,1000,1100]	0.1709
GIRD 04	NEBT 3	11	1,330	A_b[2,2,2,4,4]	[1100,1200,1300,1400,1500]	0.2609
GIRD 05	NEBT 2	11	1,330	A_b[2,2,2,4,4]	[900,1000,1100,1200,1300]	0.2437
GIRD 06	NEBT 1	11	1,330	A_b[2,2,2,4,4]	[700,800,900,1000,1100]	0.2286
GIRD 07	NEBT 3	12.5	1,717	A_b[2,2,2,4,4]	[1100,1200,1300,1400,1500]	0.3369
GIRD 08	NEBT 2	12.5	1,717	A_b[2,2,2,4,4]	[900,1000,1100,1200,1300]	0.3146
GIRD 09	NEBT 1	12.5	1,717	A_b[2,2,2,4,4]	[700,800,900,1000,1100]	0.2952

Note: Values presented for the five layers of reinforcement [Layer 1, Layer 2, Layer 3, Layer 4, Layer 5]

The selections of pier configuration were based on typical cross-sections found in practice. There were three variables considered in the geometric cases, the height of the section (H), the bar sizes and configuration, which represented the reinforcement ratios (ρ) implicitly. The depth to rebar (d_i) was governed by the section H as concrete cover and spacing between bar layers were kept constant at 50 mm, and 100 mm, respectively. The detailing of both the cross-section geometry and the reinforcing are found in Table 8.

Table 8. Details of piers considered in the analysis.

Section ID	H (mm)	Bar Size	A_{st} (mm^2)	A_{si} (mm^2)	d_i (mm)	ρ (%)
PIER 01	500	25M	3000	25M*[2,2,2]	[50,250,450]	1.20
PIER 02	500	25M	5000	25M*[4,2,4]	[50,250,450]	2.00
PIER 05	750	30M	4200	30M*[2,2,2]	[50,375,700]	1.12
PIER 06	750	30M	8400	30M*[5,2,5]	[50,375,700]	2.24
PIER 09	1000	35M	6000	35M*[2,2,2]	[50,500,950]	1.20
PIER 10	1000	35M	10000	35M*[4,2,4]	[50,500,950]	2.00

Note: Values presented for the three layers of reinforcement [Layer 1, Layer 2, Layer 3]

4.3 ULTIMATE LIMIT STATE

The reliability of the select bridge girders and piers described in Section 4.2 was evaluated for the ULS Combination 1 in Table 3.1 and Table 3.2 in *cl. 3.5.1* of the CHBDC (CSA S6, 2019). ULS combination 1 is expressed in Equation (28), where M_L, $M_{D_{SW}}$, $M_{D_{WS}}$, and DLA, are the live load moment, dead load moment due to girder weight, dead load moment due to wearing surface weight,

and the dynamic load allowance (accounts for vibratory effects of the moving vehicle and the bridge), respectively.

$$M_r \geq 1.2MD_{sw} + 1.5MD_{ws} + 1.7M_L(1 + DLA) \quad (28)$$

4.4 LOAD MODEL

Five random variables were considered for the load model including MD_{SW}, MD_{WS}, M_L, DLA, and live load effect (L_{effect}). Table 9 details the distribution type, λ, coefficient of variation (COV) and the corresponding reference. The live load distribution type was considered Gumbel, while the dead loads, DLA, and live load effect were considered normal (CSA S6.1, 2019; Kennedy, 1992). The statistical parameters of the load model generally align with the values utilized in the calibration of the CHBDC and are based on field measurements in Canada. Note M_L was multiplied by L_{effect} to account for the transformation of the live load applied on the girder to a moment, excluding the dynamic effect which is accounted for in DLA factor. Refer to the Section 4.7 for the steps followed to determine the mean values of the load effects.

Table 9. Input statistical properties of the load random variables.

Variable	Definition	Distrib.	λ	V	Reference
M_L	Live load moment	Gumbel	1.1680	0.0686	(CSA S6.1, 2019)
L_{effect}	Live Load Effect	Normal	1.0200	0.0900	(CSA S6.1, 2019)
$M_{D_{SW}}$	Dead load generated by self-weight	Normal	1.0436	0.0359	(Kennedy, 1992)
$M_{D_{WS}}$	Dead load generated by wearing surface	Normal	1.4370	0.5316	(Kennedy, 1992)
DLA	Dynamic load allowance	Normal	1.0110	0.3010	(Kennedy, 1992)

4.5 RESISTANCE MODEL

4.5.1 Girder Resistance Model

The resistance model for girders corresponds to the nominal bending resistance of bridge girder calculated based on CHBDC and the Concrete Design Handbook (CSA A23.3, 2014; CSA S6, 2019). The standard geometry of the girder was idealized into an I-shaped cross-section as

summarized in Table 10. When idealizing the cross section, a series of design checks were put in place, where the gross cross-sectional area, second moment of inertia, and centroids were compared between the original cross section and the idealized cross section as detailed in Appendix A: Girder Section Idealization.

Table 10. Idealized girder cross-sectional dimensions considered in the analysis.

NEBT ID	H (mm)	H_1 (mm)	H_2 (mm)	H_3 (mm)	B_1 (mm)	B_2 (mm)	B_3 (mm)	A_c (mm^2)
NEBT 1	1200	130	270	800	1200	810	180	518,700
NEBT 2	1400	130	270	1000	1200	810	180	554,700
NEBT 3	1600	130	270	1200	1200	810	180	589,000

The equivalent stress block methodology was used for determining the resistance of the section. Figure 4 details the sum of the forces in the *x* direction and a singular option for the location of the neutral axis. The equivalent stress block factors (α_1 and β_1) are expressed in Equations (29) and (30), where, f_c' is the concrete compressive strength (Brzev and Pao, 2016a; CSA A23.3, 2014). The material resistance factors for concrete (Φ_c) was taken as 0.75 and steel (Φ_s) was considered 0.95 for pre-stressed steel tendons in the girders as per CSA S6 (2019). The material resistance factors were set to unity for the reliability analysis.

$$\beta_1 = 0.97 - 0.0025 f_c' \leq 0.67 \tag{29}$$

$$\alpha_1 = 0.85 - 0.0015 f_c' \leq 0.67 \tag{30}$$

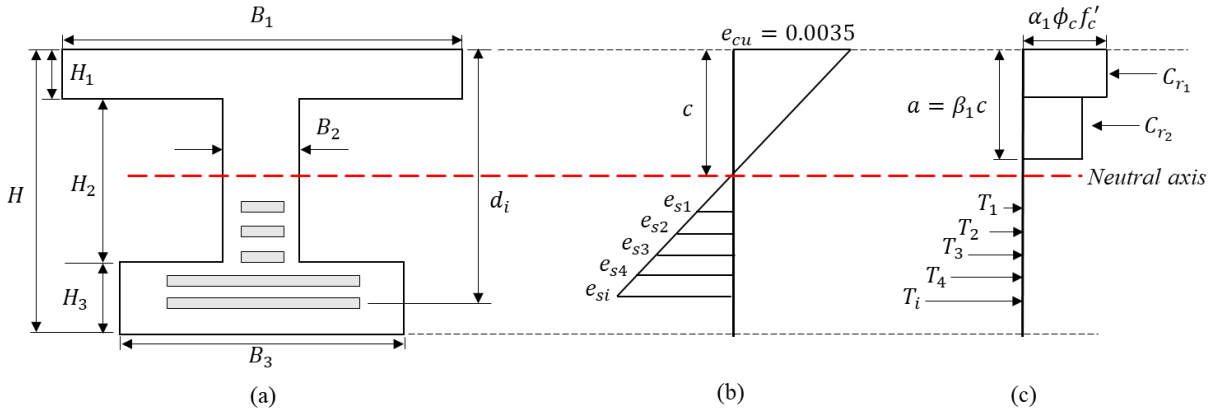

Figure 4. Girder diagram: (a) geometric cross-section, (b) strain diagram, and (c) stress diagram.

The geometric measurements of the section are articulated in Figure 4. H, is the height of the section, B is the base widths of the section, and d_i is the depth to the individual layers of reinforcing bars. The sum of forces in the x direction (F_x) and the sum of moments (M) are set equal to zero. The sum of forces is used to solve for the depth to the neutral axis (c) as detailed in Equation (31), where T_i and C_r refer to a tension force at layer i and the compression force, respectively. Note N_{cs} is the number of concrete sections with different base dimensions within a singular cross-section, and N_{bl} is the number of reinforcing bar layers within the cross-section. The moment capacity of the section is calculated as per Equation (32). Φ_s is only utilized when determining the mean loads applied on the cross-section, while it is set to unity in the reliability analysis (refer to Section 4.7 for explanation).

$$\sum F_x = 0, \qquad \sum C_r = \sum_{i=1}^{N_{bl}} T_i = \sum_{i=1}^{N_{bl}} \Phi_s f_s A_{s_i} \tag{31}$$

$$\sum M = 0, \quad M_r = \sum_{j=1}^{N_{cs}} M_{C_j} - \sum_{i=1}^{N_{bl}} T_i \, (c - d_i \,) \tag{32}$$

4.5.1.1 Concrete Compression Force and Moment

There are three possible locations for the neutral axis in the I-shaped girder (upper flange, web, lower flange). Equations (31) and (32) are expanded in Table 11 for the case of I-shaped girder. The code developed was validated against a series of textbook examples (Brzev and Pao, 2016b).

Table 11. Concrete force and moment calculation for an I-shaped girder.

Location of a	Force and moment
$a < H_1$	$C_{r_1} = \alpha_1 \Phi_c f_c' (B_1 a)$ $M_{c_1} = \alpha_1 \Phi_c f_c' \left(B_1 a \left(c - \frac{a}{2} \right) \right)$
$H_1 < a \leq H_1 + H_2$	$C_{r_2} = \alpha_1 \Phi_c f_c' \left(B_1 H_1 + B_2 (a - H_1) \right)$ $M_{c_2} = M_{r_1} + \alpha_1 \Phi_c f_c' \left(B_2 (a - H_1) \left(c - H_1 - \frac{a - H_1}{2} \right) \right)$
$H_2 < a \leq H_1 + H_2 + H_3$	$C_{r_3} = \alpha_1 \Phi_c f_c' \left(B_1 H_1 + B_2 H_2 + B_3 \left(a - (H_1 + H_2) \right) \right)$ $M_{c_3} = M_{c_2} + \alpha_1 \Phi_c f_c' \left(B_3 \left(a - (H_1 + H_2) \right) \left(c - H_1 - H_2 - \left(\frac{a - H_1 - H_2}{2} \right) \right) \right)$

4.5.1.2 Steel Tension Force and Moment

Prestress steel tendons or bars are used when i) self weight of the structures is large and serviceability LS are difficult to meet, ii) the length of the beam/girder is very long and/or iii) where additional resistance is required when the section is limited in size (CPCI Design Manual, 2017). This form of reinforcement can be used in conjunction with standard steel reinforcement (partially prestressed sections) or as the sole form of reinforcing (fully prestressed section). The shape of the stress-strain curve for the different types of conditions of prestressed reinforcements are represented by k_p. k_p is a constant value equal to 0.28 for low relaxation strand, 0.38 for plain prestressing bars, and 0.48 for deformed prestressing bars (CPCI Design Manual, 2017). The steel tendons considered are plain prestressed reinforcing bars with a tensile strength (f_{pu}) of 1860 MPa. The approximate method can be used to determine the stress in the prestressed reinforcement at factored resistance (f_{pr}). The f_{pr} value can then be used in the stress strain analysis in the MATLAB® code. There are two checks required to implement the approximate method. The first is that the compressive section must be idealized as a square, meaning that the depth to the neutral axis must be less than the height of the top flange as detailed in Equations (33). The second is the ratio between the depth of the neutral axis (c) and the depth to the centroid of the rebar layers (d_p)

must be less then 0.5 as shown in Equation (34). Both checks ensure that the approximation of the effective stress is within the allowable error outlined by the CSA A23.3 (2014) code. If both conditions outlined are met, Equation (35) is used to calculate the reduced f_{pr}, where A_p is the area of the prestressed reinforcing bars, ω_{pu} is the prestressed steel ratio and the resistance factor for the prestressed bars (Φ_p) is 0.95.

$$a = \frac{\phi_p d_p \omega_{pu}}{\alpha_1 \phi_c \left(1 + k_p \frac{\phi_p \omega_{pu}}{\alpha_1 \phi_c \beta_1}\right)} < H_1 \tag{33}$$

$$\frac{c}{d_p} = \frac{1}{\left(\frac{\alpha_1 \phi_c \beta_1}{\phi_p \omega_{pu}} + k_p\right)} < 0.5 \tag{34}$$

$$f_{pr} = f_{pu}\left(1 - \frac{k_p c}{d_p}\right) \tag{35}$$

4.5.2 Pier Resistance Model

There are three general sections to the resistance model for the pier geometry; the first is the generation of the interaction diagram based on geometric properties and incrementing c from zero to $10H$, where an interaction diagram is a diagram that relates the axial load and moment combination. The second is the generation of the eccentricity line, where each line represents a singular c value. The third section is to determine the intersection point between the interaction diagram and the eccentricity line to determine the section capacity. Φ_c was taken as 0.75 and Φ_s was considered 0.9 for standard reinforcement rebars in the piers as per CSA S6 (2019).

4.5.2.1 Interaction Diagram

The maximum axial force ($P_{r,max}$), which is a function of the factored axial load resistance at zero eccentricity (P_{ro}) is described in Equation (36) from *cl. 10.10.4* (CSA A23.3, 2014).

$$P_{ro} = \alpha_1 \Phi_c f_c' \left(A_g - A_{st} - A_t - A_p\right) + \Phi_s f_y A_{st} + \phi_a f_y A_t - f_{pr} A_p \tag{36}$$

$P_{r,max}$ as defined by concrete handbook *cl. 10.10.4* (CSA A23.3, 2014). For circular piers the reinforcement type is spiral, $P_{r,max}$ is noted in Equation (37), and if the pier is square the reinforcement type is tied, $P_{r,max}$ is noted in Equation (38) governs.

$$P_{r,max} = 0.9 P_{ro} \tag{37}$$

$$P_{r,max} = (0.2 + 0.002h) P_{ro} \leq 0.8 P_{ro} \tag{38}$$

4.5.2.2 Generation of Interaction Diagram

The interaction diagram is parabolic in shape and is generated within this works based on incrementing the c value from zero to $10H$ for a singular geometric configuration. Each point on the generated line is associated with an eccentricity value, where the eccentricity is measured as the distance from the geometric center of the structural member and the applied load. The first step would be to calculate the axial force for the specified c value. The procedure is summarized in Figure 5, and expressed in Equation (39) to (43).

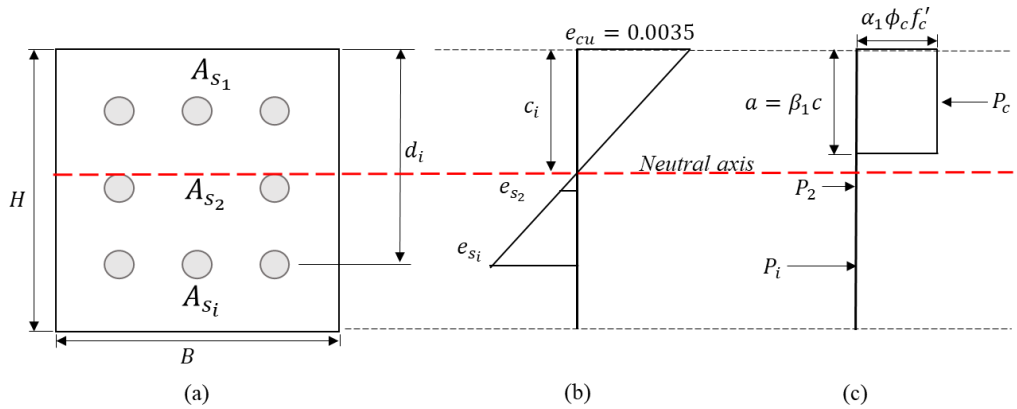

Figure 5. Pier diagram (a) cross-sectional geometry, (b) strain diagram, and (c) stress diagram.

There are two components to the axial force resistance of the section, the concrete under compression (P_c) and the steel rebar under tension (P_{s_i}). P_c is calculated as shown in Equation (39) (CSA A23.3, 2014).

$$P_c = \alpha_1 \Phi_c f_c' B(\beta_1 c) \tag{39}$$

The calculation of P_s is described in Equations (40) to (42), where e_{s_i} is the tensile strain in the i^{th} layer of rebar and $e_{cu,max}$ is the maximum compressive strain in the concrete compression zone.

$$e_{s_i} = e_{cu,max}\left(1 - \frac{d_i}{c}\right) \tag{40}$$

$$f_{y_i} = E\mathrm{e_{s_i}} \tag{41}$$

$$P_s = \Phi_s f_{y1} A_{s1} \tag{42}$$

The steel rebars below the neutral axis are under tension and therefore are subtracted P_c as shown in Equation (43) to calculate the axial force (P_y).

$$P_y = P_c - \sum_{i=1}^{N_{bl}} P_s \tag{43}$$

Once the axial force (P_y) is calculated, the second step is calculating the moment (M_x) based on the section properties and c value based on Figure 6 and Equations (44) to (45), where M_c is the moment generated by the compressive zone and M_{s_i} is the tensile moment generated by the i^{th} layer of reinforcing bars. The code developed to generate the interaction diagram was validated against a series of textbook examples (Brzev and Pao, 2016b). If the interaction point (moment and axial) of a given cross-section falls outside the boundaries of the interaction diagram, the section would be considered inadequate (failure).

$$M_x = \mathrm{M_c} \pm \sum_{i=1}^{N_{bl}} M_{S_i} \tag{44}$$

$$M_x = P_c\left(c - \frac{a}{2}\right) \pm \sum_{i=1}^{N_{bl}} P_{S_i}(c - d_s) \tag{45}$$

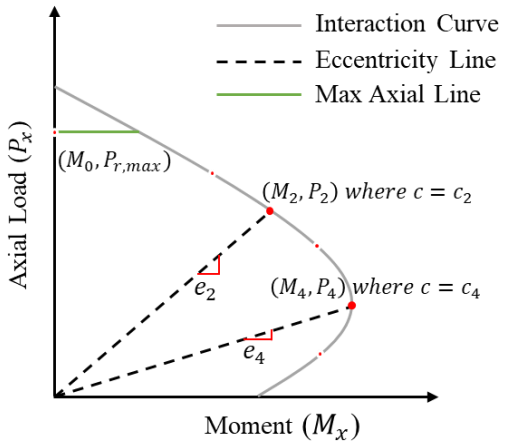

Figure 6. Schematic illustration of an interaction diagram pier resistance prediction.

4.5.2.3 Generation of Eccentricity Line

The eccentricity line is a linear representation between the eccentricity (e) of the applied load and a location on the interaction cure. This point of the curve is indicative of a singular c value and is related to the e as shown in Equation (46), where c_p is known as center of plastic equal to half the cross-sectional height, e^* is the axial load eccentricity with respects to the neutral axis, M_x is the moment from the interaction diagram with respects to the neutral axis, and P_y is the axial load from the interaction diagram with respects to the neutral axis.

$$e_* = \frac{M_x}{P_y}, \qquad e = e_* - c + c_p \tag{46}$$

The eccentricity line is a straight line, the slope of the line is e^{-1} and the intercept is zero. The equation of eccentricity is shown in Equation (47), where x is the axial force and y is the moment.

$$y = mx + b = \frac{1}{e}x \tag{47}$$

When generating the eccentricity line, the moment values from the interaction diagram were substituted into the equation of the eccentricity line, meaning the points on each line share an x coordinate with a point on the opposing line. This simplifies the determination of the point of intersection between the eccentricity line and interaction diagram.

4.5.2.4 Intersection of Eccentricity Line and Interaction Diagram

The location where the interaction diagram and the eccentricity line intersect is the capacity for both axial and moment of the specified section. The resistance function outputs the axial force and moment of each point along the interaction diagram to determine the intersection point. The moment value is substituted for *x* in the eccentricity line of Equation (47) as seen in Equation (48).

$$y = \frac{1}{e}x = \frac{1}{e}M \tag{48}$$

The intersection point occurs when the sign of the difference changes from positive to negative. The last positive difference is set to equal (X_1, Y_1) and the first negative difference is set to (X_2, Y_2). As each point on the eccentricity line share an *x* coordinate with the interaction diagram, points 1 and 3 share the same moment, and points 2 and 4 share the same moment, as shown in Figure 7. This further simplifies the interpolation between the four known points to obtain the intersection point. This intersection is characterized by Equations (49) and (50) for axial force and moment, respectively.

$$P_r = Y_{intersect} = \left(\frac{(X_1Y_2 - Y_1X_2)(Y_3 - Y_4) - (X_3Y_4 - Y_3X_4)(Y_1 - Y_2)}{(X_1 - X_2)(Y_3 - Y_4) - (Y_1 - Y_2)(X_3 - X_4)} \right) \tag{49}$$

$$M_r = X_{intersect} = \left(\frac{(X_1Y_2 - Y_1X_2)(X_3 - X_4) - (X_3Y_4 - Y_3X_4)(X_1 - X_2)}{(X_1 - X_2)(Y_3 - Y_4) - (Y_1 - Y_2)(X_3 - X_4)} \right) \tag{50}$$

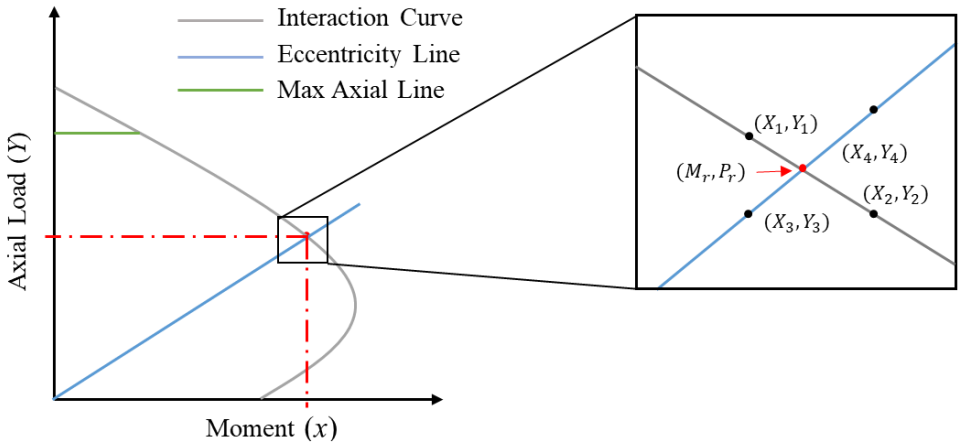

Figure 7. Schematic illustration of the intersection points in a pier interaction diagram.

4.5.3 Statistics for Resistance

There are a total of five base random variables considered in the resistance model, the professional factor (PF), $f_c^{'}$, f_y, d_{s_i}, and the area of steel in each rebar layer (A_{S_i}) as summarized in Table 12. $f_c^{'}$, f_y, and A_{s_i} account for the material variability, while d_{s_i} accounts for the variabilities in installation and PF accounts for the uncertainty in the structural analysis of the specific sections (Nowak and Szerzen, 2003). There are two distribution types considered in the resistance model: normal and truncated normal (Kennedy et al., 1992). Equation (51) denotes the equation used to calculate λ for the $f_c^{'}$ random variable as it varies with the target compressive strength.

$$\lambda = -2.4713\text{x}10^{-5} f_c'^{3} + 0.003174 f_c'^{2} - 0.135436 f_c' + 3.064 \qquad (51)$$

It is noted that material properties are often modeled using lognormal distribution to avoid realizations of negative values (a material strength cannot be negative). However, it is unlikely for that to happen in the considered analysis since the mean values are relatively high, the biases are relatively low, and the coefficient of variation (V) is relatively small. This approach has been taken

by research utilized to calibrate the member reduction factors for the American Concrete Institute (ACI) 318 code (Nowak and Szerzen, 2003).

Table 12. Input statistical properties of the resistance random variables (Nowak et al., 2003)

Variable	Definition	Distrib.	λ	V
PF_{pier}	Professional factor (tied rein.)	Normal	1.0000	0.0800
PF_{Girder}	Professional factor	Normal	1.0200	0.0600
f_c'	Concrete compressive strength	Normal	Eq. (51)	0.1000
$f_{y\,(9.5mm)}$	Yield strength of prestressed steel	Normal	1.0600	0.0300
$f_{y\,(11mm)}$	Yield strength of prestressed steel	Normal	1.0700	0.0100
$f_{y\,(12.5mm)}$	Yield strength of prestressed steel	Normal	1.0400	0.0025
$f_{y\,(25M)}$	Yield strength of steel	Normal	1.1450	0.0500
$f_{y\,(30M)}$	Yield strength of steel	Normal	1.1400	0.0400
$f_{y\,(35M)}$	Yield strength of steel	Normal	1.1450	0.0350
A_{s_i}	Area of still in i^{th} layer	Normal	1.0000	0.0150
d_{s_i}	Depth to i^{th} rebar layer	Truncated Normal	1.0000	0.0250

4.6 CONSIDERED AK CONFIGURATIONS

The AK Configurations (defined in Section 2.4.1) corresponds to the choice of the regression, correlation, and learning functions. The number of unique AK configurations considered in the analysis of the girders and piers is 54 (each girder and pier configuration described in Table 7 and Table 8 was evaluated using 54 AK configurations). The 54 AK configurations are made up of three regression functions (constant, linear and quadratic), six correlation functions (Gaussian, cubic, exponential, linear, spherical and spline), and three learning functions (EFF, U, H for the girders and EFF, U, REIF for the peris). The formulation of the regression, correlation, and learning functions are detailed in Sections 3.3.2, 3.3.3, and 3.3.4, respectively. The AK configuration IDs are provided in Table B.1 for girder and Table B.2 for piers in Appendix B: AK Configurations.

4.7 STEPS OF THE RELIABILITY ANALYSIS

The reliability analysis was conducted in three steps per each of the bridge and pier configurations described in Section 4.2 as follows:

Step 1. Determine the mean load effect for the load model detailed in Section 4.4. The nominal value of M_L was calculated using Equation (52) by setting M_r equal to the factored applied moment (M_f), where the latter equals the summation of the factored load effects in Equation (30) (i.e., utilization ratio of unity – ratio of demand to capacity equals one), MD_{sw}/M_L ratio of 0.5213, and MD_{ws}/M_L ratio of 0.0887. The values for MD_{sw}/M_L and MD_{ws}/M_L were obtained based on field measurements in Alberta (Kennedy et al., 1992). The bridge girder and pier factored resistance M_r was calculated by utilizing the material resistance factor in CSA S6 (2019): 0.75 for concrete (Φ_c), 0.95 for pre-stressed steel tendons in the girders (Φ_s), and 0.9 for the non-prestressed steel reinforcement in the piers. According to *cl. 3.8.4.5.3* of the CHBDC, where there are three or more axles of the CL-W truck or more than one axle unit of a special truck(s), the DLA for a concrete girder and pier is equal to 0.25 (CSA S6, 2019; CSA S6.1, 2019).

$$M_L = \frac{M_r}{1.2(MD_{sw}/M_L) + 1.5(MD_{ws}/M_L) + 1.7(1 + DLA)} \tag{52}$$

Step 2. Conduct AK-MCS using the select AK Configurations. The reliability for each bridge girder and pier configuration described in Section 4.2 was evaluated using 54 AK configurations (described in Section 4.6) using the developed MATLAB® code for AK-MCS described in Section 3.3.

Step 3. Conduct crude MCS for comparison purposes. The reliability for each bridge girder and pier configuration described in Section 4.2 was evaluated using the developed MATLAB® code for crude MCS described in Section 3.2.

4.8 AK-MCS Reliability Analysis Results and Discussion

A total of 486 AK-MCS analyses were conducted for the girder application (9 girder configurations x 54 AK configuration) and 324 AK-MCS analyses were conducted for the pier application (6 pier configurations x 54 AK configuration). The analysis results were compared with crude MCS for verification. The number of AK-MCS (N_{AK-MCS}) trials was determined to be 1×10^6 and 5×10^7 for the crude MCS analyses with a confidence interval of 95% and a margin of error of 1.8% and 15% as per Equation (19) for β of 3.5 and 4.5, respectively. The AK-MCS analysis was conducted using the SAR research group server: a windows-based server with dual Intel Xeon Gold 5220R 2.20GHz processors (48 cores), a NVIDIA Quadro P620 graphics card, and 128 Gb of available RAM. The analysis results are evaluated based on accuracy (error in predicting the reliability index relative to the crude MCS) and efficiency (number of points required to train the surrogate Kriging model).

4.8.1 Accuracy of Results

For the accuracy evaluation, the analysis results are summarized in Table 13 and Table 14 for the girder and pier analysis, respectively. Only the top 10 AK-MCS analyses ranked based on the lowest error in predicting the β as compared with crude MCS are shown in the tables, while the reader is referred to Appendix C: Reliability Indexes Chapter 4 for the complete list of analysis results (54 AK-MCS analyses per girder and pier configuration). The error was calculated by comparing the β_{AK-MCS} against the β_{MCS} as expressed in Equation (53) (Buckley et al., 2021). The analysis results for the 54 AK configurations for the girder and pier applications are shown schematically in Figure 8 and Figure 9, respectively.

$$Error = \sqrt{\sum_{j=1}^{ID}\left(\frac{\sum_{i=1}^{AK\ Config.}\beta_{AK-MCS}(i) - \beta_{MCS}(j)}{N_s(j)}\right)^2} \tag{53}$$

Table 13. Comparison of reliability indexes for MCS versus AK-MCS for girders – Analysis results ranked based on accuracy.

Analysis Type	AK ID	Error	GIRD ID								
			1	2	3	4	5	6	7	8	9
Crude MCS	-	-	4.1700	4.2073	4.1897	4.4627	4.4790	4.4920	4.2276	4.2609	4.3197
AK-MCS	32	1.9E-04	4.1318	4.1449	4.2059	4.5264	4.5264	4.4652	4.1892	4.2649	4.3439
AK-MCS	54	2.0E-04	4.1735	4.1193	4.2436	4.4652	4.4652	4.5264	4.2436	4.3145	4.2436
AK-MCS	53	2.1E-04	4.1449	4.1449	4.1892	4.3776	4.5264	4.5264	4.1892	4.3776	4.3439
AK-MCS	36	2.5E-04	4.1587	4.2649	4.2436	4.5264	4.4172	4.4172	4.1449	4.3439	4.2884
AK-MCS	46	2.6E-04	4.2649	4.2059	4.1587	4.3776	4.3776	4.4652	4.1735	4.3439	4.3145
AK-MCS	42	2.8E-04	4.2240	4.3439	4.2240	4.5264	4.5264	4.5264	4.2649	4.2436	4.3439
AK-MCS	18	2.9E-04	4.0962	4.2436	4.3145	4.3439	4.4652	4.5264	4.2059	4.3145	4.3439
AK-MCS	45	3.0E-04	4.1587	4.2059	4.1892	4.6114	4.4172	4.4172	4.2059	4.2240	4.3145
AK-MCS	24	3.0E-04	4.1735	4.2240	4.1587	4.4652	4.4652	4.3439	4.1449	4.2240	4.3145
AK-MCS	43	3.2E-04	4.1193	4.1735	4.2059	4.4652	4.6114	4.4172	4.3439	4.2649	4.3439
AK-MCS	32	1.9E-04	4.1318	4.1449	4.2059	4.5264	4.5264	4.4652	4.1892	4.2649	4.3439

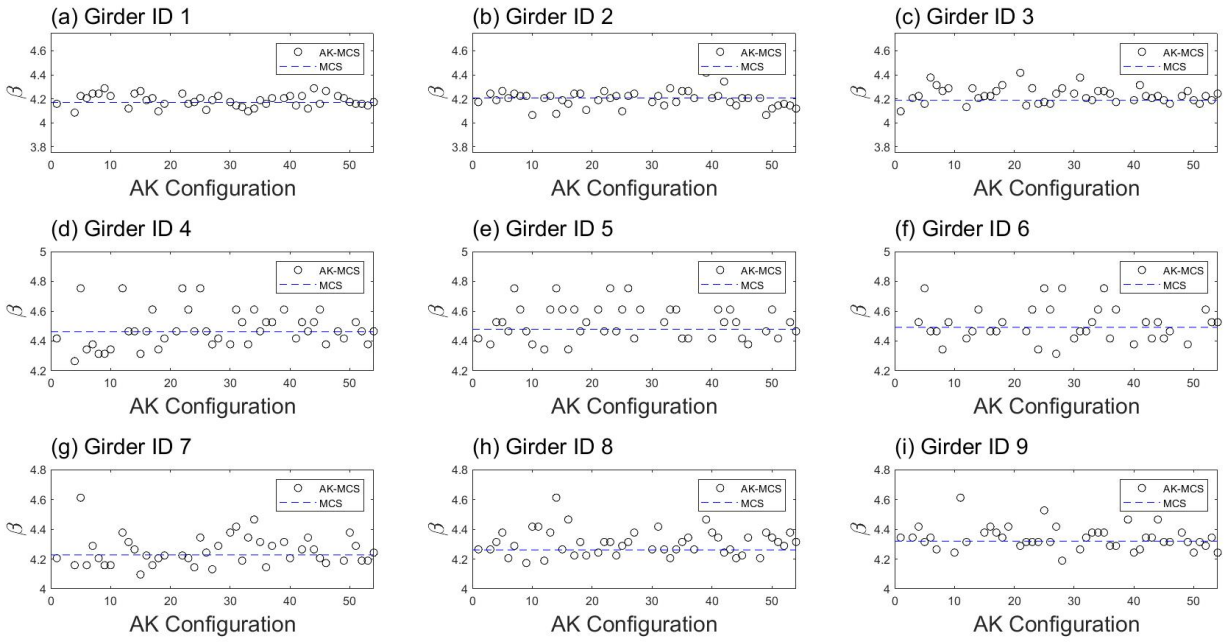

Figure 8. Reliability indexes versus the AK configurations with 10^6 trials: (a) Girder ID 1, (b) Girder ID 2, (c) Girder ID 3, (d) Girder ID 4, (e) Girder ID 5, (f) Girder ID 6, (g) Girder ID 7, (h) Girder ID 8, and (i) Girder ID 9.

Table 14. Comparison of reliability indexes for MCS versus AK-MCS for Piers – Analysis results ranked based on accuracy.

Analysis Type	AK ID	Error	PIER ID					
			1	2	5	6	9	10
Crude MCS	-	-	4.5658	4.6667	4.5714	4.6351	4.5758	4.6404
AK-MCS	36	4.0E-04	4.5264	4.6114	4.6114	4.5264	4.734	4.5264
AK-MCS	9	4.1E-04	4.4652	4.4652	4.6114	4.6114	4.4652	4.6114
AK-MCS	22	4.2E-04	4.6114	4.4651	4.6114	4.6114	4.4651	4.7534
AK-MCS	43	4.3E-04	4.5264	4.6114	4.6114	4.4651	4.3776	4.6114
AK-MCS	54	4.4E-04	4.6114	4.6114	4.4652	4.4652	4.4652	4.5264
AK-MCS	32	4.6E-04	4.4652	4.6114	4.6114	4.5264	4.5264	4.4172
AK-MCS	44	4.6E-04	4.5264	4.7534	4.4172	4.5264	4.4172	4.5264
AK-MCS	13	4.8E-04	4.4652	4.6114	4.5264	4.4652	4.7534	4.7534
AK-MCS	34	5.0E-04	4.5264	4.4172	4.5264	4.6114	4.5264	4.4652
AK-MCS	42	5.8E-04	4.4652	4.4172	4.4652	4.4652	4.4652	4.5264

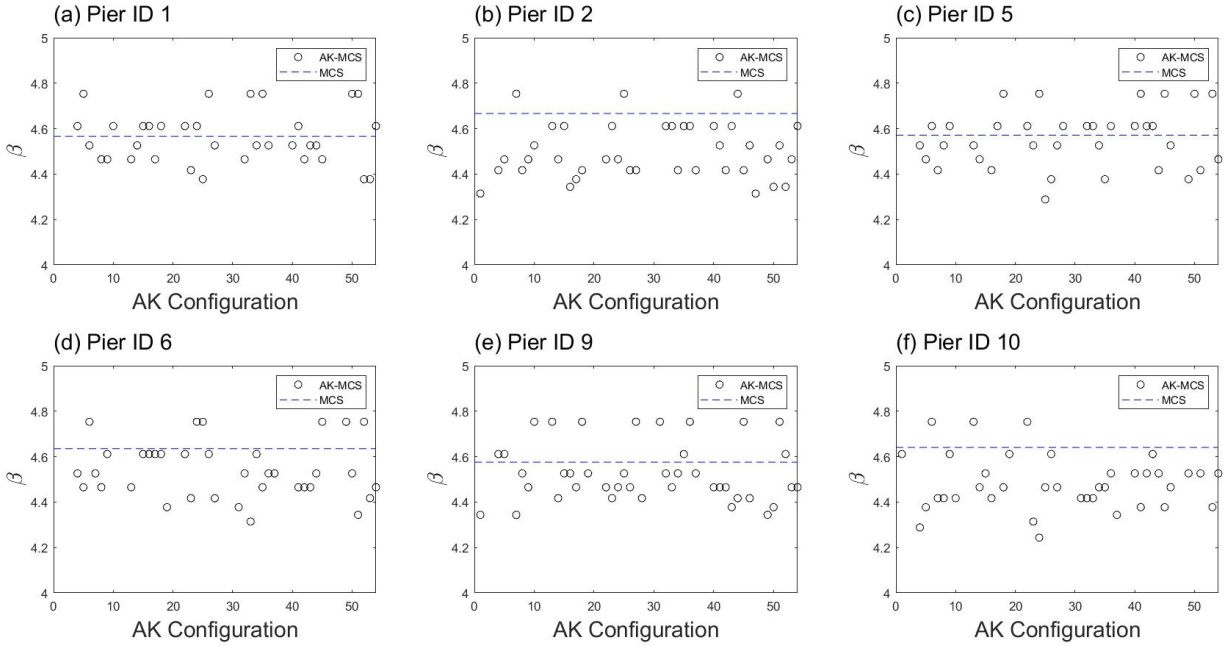

Figure 9. Reliability indexes versus the AK configurations with 10^6 trials: (a) Pier ID 1, (b) Pier ID 2, (c) Pier ID 5, (d) Pier ID 6, (e) Pier ID 9, and (f) Pier ID 10.

The β_{MCS} are aligned with target values used in calibrating bridge design codes including the CHBDC and AASHTO LRFD, which confirms the accuracy of the crude MCS analysis (LS, load model, resistance model, and statistical parameters). Typical range of reliability indexes for bridge

components designed per CHBDC is 3.5 to 4.5 (CSA S6, 2019). The following observations can be made regarding the accuracy evaluation of the AK-MCS analysis:

- The analysis results confirm that the developed MATLAB® script of the AK-MCS is functional as it was able to predict β for the considered bridge girders and piers within a tolerable margin of error (less then 5%).
- The accuracy of prediction depends on the choice of the AK configuration (regression, correlation, and learning functions) utilized in the AK-MCS analysis.
- The mean error of the β_{AK-MCS} of all 54 AK configurations is 0.0225 ± 0.0307. It was also observed that the target β_{MCS} seems to impact the spread of results. As the β_{MCS} increases, the larger is the variability in the results plotted in Figure 8. The β_{MCS} for GIRD ID 1, 2, and 3 is 4.2. The dispersion of the β_{AK-MCS} around the β_{MCS} is the least for GIRD ID 1, 2, and 3 as compared to the other girders. GIRD ID 7, 8, 9 have a β_{MCS} of 4.35 with a slightly larger spread of β_{AK-MCS}, and GIRD ID's 4, 5, and 6 has a β_{MCS} of 4.5 with the largest variation in β_{AK-MCS} results. In other words, when the target β_{MCS} increases, the variability in the performance of the AK configurations increases. This can be attributed to the number of trials needed to achieve an accurate presentation of β as the target β_{MCS} increase.
- The mean error of the AK-MCS of all 54 pier configurations is 0.3601 ± 0.01089. The mean errors for piers with a ρ of 1% (Pier 1, Pier 5, and Pier 9) and 2% (Pier 2, Pier 6, and Pier 10) are 0.0792 ± 0.02636 and 0.0453 ± 0.0258, respectively, where positive indicates overprediction and negative indicates underprediction.
- The girder analysis sees a larger number of overpredictions, whereas the pier analysis generates mostly under predictions. This is likely attributed to the lower probability of

failure of the piers as compared with the girders. Should the number of trails of the AK-MCS analysis of the piers increase, more overpredictions may occur.

- The choice of the optimal AK configuration may be influenced by the complexity of the considered LS and the number of considered random variables. This observation is the primary motive for conducting the optimization exercise of the AK-MCS analysis presented in Chapter 5.
- A single or multiple AK configurations may exist to optimize the accuracy prediction of the AK-MCS per design problem.

4.8.2 Efficiency of Method

For the efficiency evaluation, the analysis results are summarized in Table 15. The total number of points (N_{calls}) required to train the surrogate model for the respective AK-MCS analysis was a secondary consideration for ranking the performance of the AK configurations after the error. N_{calls} is equal to the summation of the initial training points (N_{inital}) and the added training points (N_{added}), as expressed in Equation (54). The minimum value of N_{inital} is a function of the regression function used in the AK-configuration as detailed in Table 3. N_{inital} for the girder application using the quadratic, linear, and constant functions were 6, 18, and 110, respectively. N_{inital} for the pier application using the quadratic, linear, and constant functions were 6, 19, and 125, respectively.

$$N_{calls} = N_{inital} + N_{added} \tag{54}$$

Table 15. AK-MCS analyses ranked based on accuracy for predicting β for girders.

Analysis Type	AK-Conf.	$N_{initial}$	N_{added}	N_{calls}	Regression Function	Correlation Function	Learning Function	Error
AK-MCS	32	18	30	48	Linear	Linear	U	1.9E-04
AK-MCS	54	110	2	112	Quadratic	Spline	H_I	2.0E-04
AK-MCS	53	110	3	113	Quadratic	Spline	U	2.1E-04
AK-MCS	36	110	2	112	Quadratic	Linear	U	2.5E-04
AK-MCS	46	6	55	61	Constant	Spline	EFF	2.6E-04
AK-MCS	42	18	68	86	Linear	Spherical	H_I	2.8E-04
AK-MCS	18	110	4	114	Quadratic	Cubic	H_I	2.9E-04
AK-MCS	45	110	3	113	Quadratic	Spherical	H_I	3.0E-04
AK-MCS	24	18	52	70	Linear	Exponential	H_I	3.0E-04
AK-MCS	43	110	4	114	Quadratic	Spherical	EFF	3.2E-04

Table 16. AK-MCS analyses ranked based on accuracy for predicting β for piers.

Analysis Type	AK-Conf.	$N_{initial}$	N_{added}	N_{calls}	Regression Function	Correlation Function	Learning Function	Error
AK-MCS	36	125	0	125	Quadratic	Linear	REIF	4.0E-04
AK-MCS	9	125	2	127	Quadratic	Gaussian	REIF	4.1E-04
AK-MCS	22	19	29	48	Linear	Exponential	EFF	4.2E-04
AK-MCS	43	125	4	129	Quadratic	Spherical	EFF	4.3E-04
AK-MCS	54	125	1	126	Quadratic	Spline	REIF	4.4E-04
AK-MCS	32	19	15	34	Linear	Linear	U	4.6E-04
AK-MCS	44	125	1	126	Quadratic	Spherical	U	4.6E-04
AK-MCS	13	19	41	60	Linear	Cubic	EFF	4.8E-04
AK-MCS	34	125	2	127	Quadratic	Linear	EFF	5.0E-04
AK-MCS	42	19	14	33	Linear	Linear	REIF	5.8E-04

Figure 10 displays sample relationships between the reliability index and how it changes as the number of added points (N_{added}) increase for six of the AK configurations run for the GIRD ID 4: 23, 24, 32, 36, 53 and 54. As the number of training points increase, the β value converges. In configurations 36, 53 and 54, it is clear that the number of initial training points ($N_{initial}$) represents the data well as the convergence has largely happened prior to the addition of new points. In other instances, like configurations 23, 24, and 32, it can be seen that as the new points are added to the DoE, the value of β converges and significant improvement of the accuracy of the surrogate model is made. This occurs when $N_{initial}$ is low and the N_{added} is high.

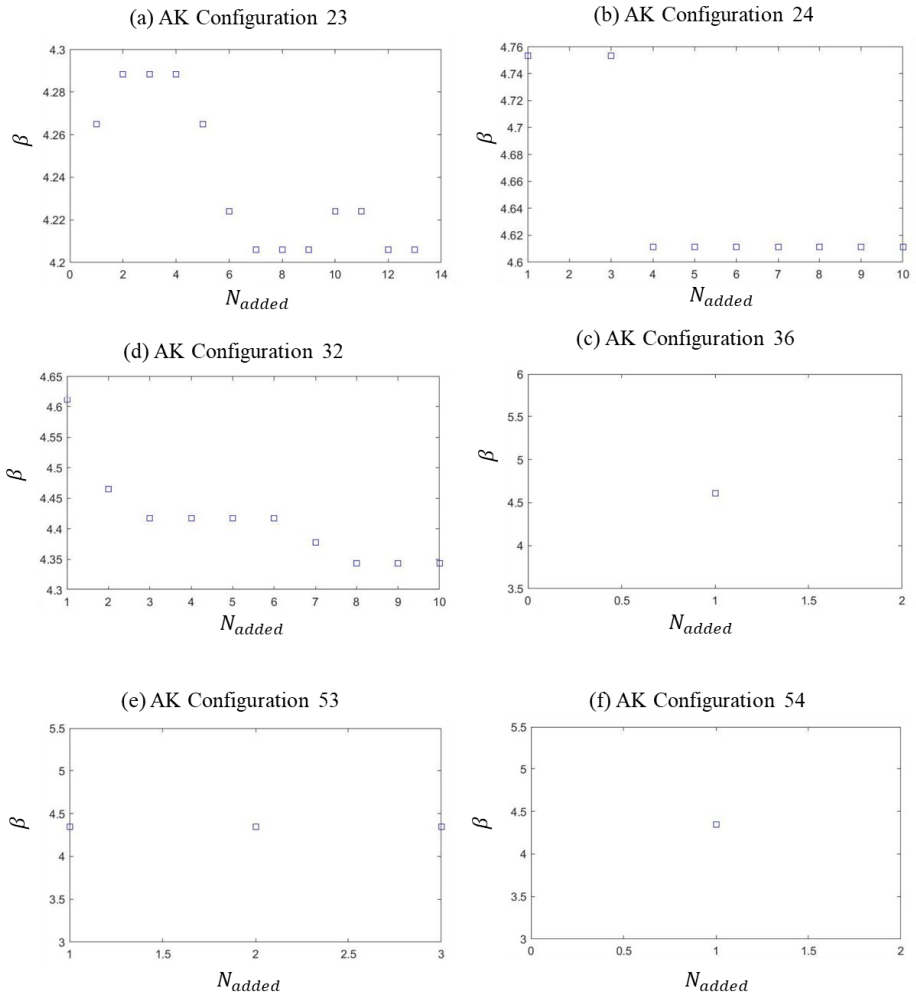

Figure 10. Reliability index versus the number of added points for AK-MCS GIRD ID 4: (a) Configuration 23, (b) Configuration 24, (c) Configuration 32, (d) Configuration 36, (e) Configuration 53, and (f) Configuration 54.

For the constant regression function trails, the majority of improvement of the Kriging surrogate predictor happens within the first 150 added training points. Figure 10(e) displays configuration 53 (quadratic regression, spline correlation and U learning functions). Due to the large number of $N_{initial}$ required, the N_{added} are low and make very little improvement on the surrogate model in general. It can be concluded that in the case of the quadratic regression function, the final Kriging predictor suffices for the reliability prediction as opposed to conducting the active learning

component. Since there are little to no added points, the learning function may not be utilized and therefore deemed ineffective.

4.9 CHAPTER SUMMARY

Overall, the functionality of the framework of analysis indicates consistent results from the AK-MCS analyses. The reliability indexes from the crude MCS, used as a reference (or benchmark) solutions, are within typical ranges for standard bridge components. Analysis results indicate the following concerns about AK-MCS analysis: i) the impact of the bias associated with the random generator, and the question of consistency of the model based on this bias, and ii) its sensitivity to assess multiple types of girders and piers. To address the concerns of consistency, it is recommended that the same analysis is run multiple times to remove the bias associated with the randomly generated input variables, and create a ranking structure to consider the error, the number of training points and the consistency of the outputs. These concerns are addressed in Chapter 5.

CHAPTER 5 OPTIMIZATION OF AK-MCS FOR BRIDGE RELIABILITY ASSESSMENT

5.1 INTRODUCTION

The accuracy and efficiency of the AK-MCS analysis are sensitive to the choice of the AK configuration as concluded in Chapter 4. Therefore, optimization is required to determine optimal AK configurations to meet prescribed performance objectives of the AK-MCS analysis (prioritize accuracy, or efficiency or balance both). A new metric system called the comprehensive metric system (CMS) has been introduced in literature by Khorramian and Oudah (2022c) to propose the optimal AK configuration for AK analyses by considering both the accuracy and efficiency aspects of the reliability analysis. In the CMS, the accuracy is assessed using root mean squared error (RSME), absolute average error (AAE), degree of consistency (DOC), and the efficiency is assessed using the total number of required initial and added points and is represented by the total training points (TTP) required to generate the surrogate model. The objective of this chapter is to apply the CMS metric to determine optimal AK configurations for select girder and pier configurations considered in Chapter 4 (GIRD ID 1, and PIER ID 5) and utilize the derived optimal AK configurations to assess the reliability of a larger set of girder and pier configurations using AK-MCS reliability analysis.

The formulation of the CMS metric is reviewed first in the following subsection, followed by presenting the results of the optimal AK configurations for the select girder and pier configurations. Finally, the results of the AK-MCS reliability analysis for the parametric analysis is presented.

5.2 METRIC BREAKDOWN

There are four parameters considered in the CMS, the RMSE, the AAE, the TTP, and DoC (Khorramian and Oudah, 2022c) and are detailed in Equations (55) to (58). The RMSE and AAE are computed with relation to the difference between the AK-MCS analysis output, probability of failure of the i^{th} identical AK configuration run ($P_{f_{Ak-MCS_i}}$) and $P_{f_{MCS}}$ from the crude MCS.

$$RMSE = \sqrt{\frac{\sum_{i=1}^{N_s}\left(P_{f_{AK-R_i}} - P_{f_{MCS}}\right)^2}{N_s}} \tag{55}$$

$$AAE = \frac{\sum_{i=1}^{N_s}\left|\frac{P_{f_{AK-R_i}} - P_{f_{MCS}}}{P_{f_{MCS}}}\right|}{N_s} \tag{56}$$

The DoC is an indicator of the consistency of the applied method and is expressed in Equation (57). The rational for the DoC parameter is as follows. As the initial training set of DoE is randomly generated, the bias associated with different initial training sets can be mitigated by running the same analysis multiple times for the same AK configuration, each with a different randomly generated training point. Thus, DoC is simply defined as the number of successful analyses (N_s) divided by the total number of identical analyses (N_I), where the term successful analysis refers to a numerical reliability index output of the AK-MCS.

$$DoC = \frac{N_s}{N_I} \tag{57}$$

The TTP is the summation of the initial and added points of each identical analysis divided by the total number of successful analyses as noted in Equation (58).

$$TTP = \frac{\sum_{i=1}^{N_s}(N_{initial} + N_{added_i})}{N_s} \tag{58}$$

To identify the optimal AK configurations, the four discussed parameters need to be transformed, scaled, and ranked (Khorramian and Oudah, 2022c). This is due to the similarities in data or values being too close to distinguish from each other. This separation between data points needs to be present to rank the data, and this separation is the scaling of the parameters considered.

The most accurate and consistent AK configuration should be considered, which implies the minimization of the error measures (RMSE and AAE) and the TTP, while maximizing the DoC. The transformation of each parameter to a value between zero and one is shown in Equations (59) to (62). Transformed RMSE is represented by I_1, transformed AAE is represented by I_2, transformed DoC is represented by I_3 and transformed TTP is represented by I_4.

$$I_1 = 1 - \left(\frac{RMSE - RMSE_{min}}{RMSE_{max} - RMSE_{min}}\right) \tag{59}$$

$$I_2 = 1 - \left(\frac{AAE - AAE_{min}}{AAE_{max} - AAE_{min}}\right) \tag{60}$$

$$I_3 = \left(\frac{DoC - DoC_{min}}{DoC_{max} - DoC_{min}}\right) \tag{61}$$

$$I_4 = 1 - \left(\frac{TTP - TTP_{min}}{TTP_{max} - TTP_{min}}\right) \tag{62}$$

Once the data is transformed, the next step is to scale the data to ensure there is variability in the distribution of the parameter points (Khorramian and Oudah, 2022c). There are three possible scales as shown in Equations (63) to (65) that can be used including variation 1 (v_1) linear, variation 2 (v_2) exponential or variation 3 (v_3) logarithmic. Depending on the data in question, the

selection of the scale varies, and the recommended scale for structural applications is logarithmic which aligns with the findings in Section 5.3.3 (Khorramian and Oudah, 2022c).

$$I_{liner} = I_i \tag{63}$$

$$I_{exponential} = \exp\{I_i\} \tag{64}$$

$$I_{logorithmic} = \log\{I_i\} \tag{65}$$

Once the scaling is complete, the final step is to rank the data. Since the goal is to find the cases that yield highest values in all four parameters simultaneously, a step-based ranking is completed. Figure 11 shows the four parameters number 1 through 4. The steps are articulated by the letter, step one (δ) for all four parameters is represented by (a) and step two (2δ) is represented by (b). If all parameters are within the first step, then that AK configuration would be ranked first. The step will continue to be increased until all the AK configurations have been ranked.

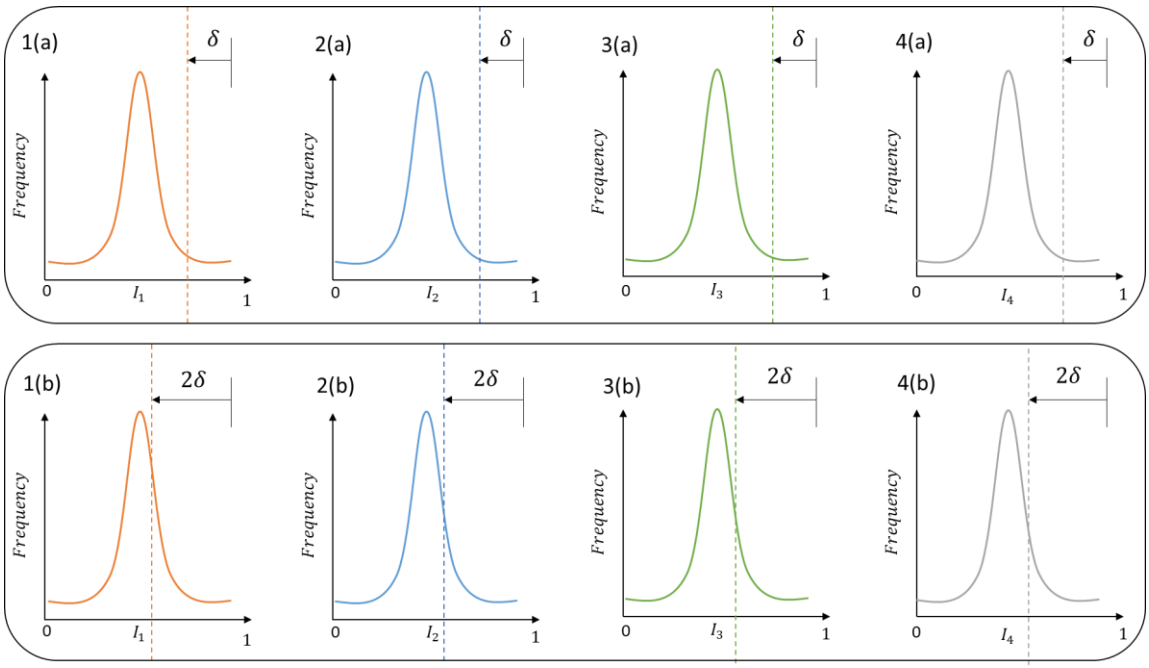

Figure 11. Illustration of ranking increments of the metric parameters.

5.3 GIRDER ANALYSIS

5.3.1 General

The metric analysis was performed on GIRD ID 1, as detailed in Table 7 within Section 4.2., to determine the top five ranked optimum AK configurations. The top five optimum AK configurations are then applied to 41 additional analysis, GIRD ID 2 through 21 at 45 MPa and GIRD ID 1 through 21 at 55 MPa. The results are then compared to the β_{MCS} to assess the performance of the optimal AK configurations in yielding accurate results for the considered girder and pier configurations.

5.3.2 Input Parameters

Figure 12 details the geometric parameters including cross-sectional and reinforcing geometry of GIRD ID 1. The statistical data from Chapter 4 was applied to this analysis (refer to Table 11 and Table 12). The six correlation functions detailed in Table 4 were considered, while only the constant and linear regression functions shown in Table 3 were considered. The quadratic regression function was excluded due to the large number of initial training points required. Nine learning functions were selected including EFF, U, H_c, H, REIF and four variations of the KO function, $KO_{05(2)}$, $KO_{005(2)}$, $KO_{05(5)}$, and $KO_{005(5)}$ (refer to Section 2.4.2 for the detailed formulation of the learning functions). The variation residing with the change of the stopping criterion and accuracy.

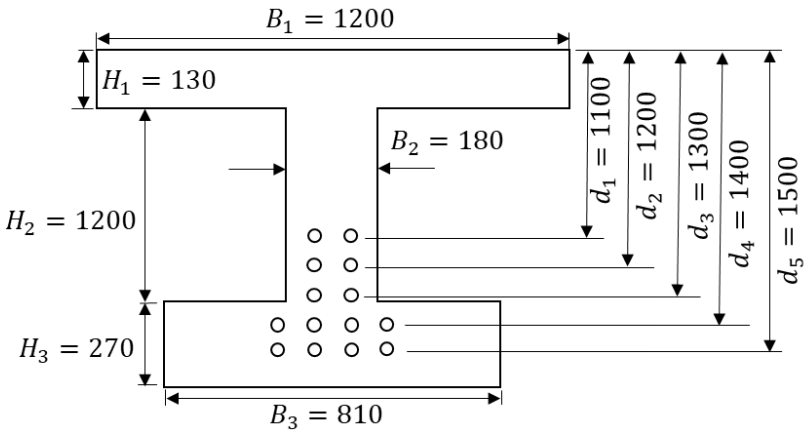

Figure 12. Geometry of GIRD ID 1.

5.3.3 Summary of Results

For section GIRD ID 1, the MCS reliability index (β_{MCS}) and $P_{f_{MCS}}$ were determined to be 4.1675 and $1.5400x10^{-5}$, respectively, based on crude MCS with 5x10^6 trials. The three forms of scaling presented in Section 5.2 were initially investigated. As shown in Figure 13, the logarithmic scale shows an approximately normal distribution for parameters I_1 and I_2. Additionally, the variations captured by the scaling models for I_3 and I_4 are better represented by the logarithmic scale. The recommended scale for the proposed analysis is therefore the logarithmic scale, which will also be applied to the pier configurations in Section 5.4.

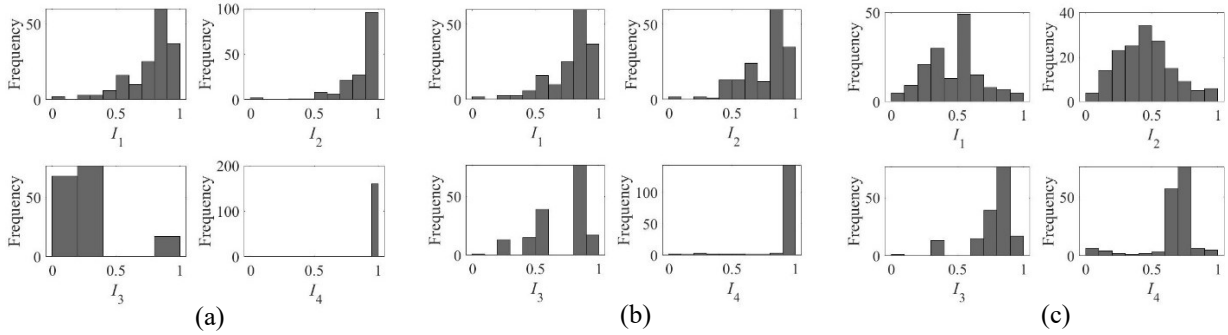

Figure 13. Scaling options for metric application: (a) linear scale, (b) exponential scale, and (c) logarithmic scale.

The summary findings of the CMS are detailed in Table 17. It is evident that the linear regression function relates the data more accurately when considering all four parameters simultaneously, however, it provides poor prediction when considering the four parameters separately. The REIF learning function only appears when all four parameters are considered. The correlation function results do not indicate an optimal function when considering all four parameters of interest individually or simultaneously (RMSE, AAE, DoC and TTP). The two correlation functions that reoccur the most frequently are Gaussian and cubic. As displayed in Table 17, the spherical correlation function for Opt (AK-MCS) analysis reoccurs the most when considering all four parameters but does not when considering individual evaluation parameters. The reliability index was not found to be significantly influenced by the choice of the correlation function.

Using the SAR research groups server, the 108 AK configurations took about 7 days with the majority of cases needing about 30 minutes to run, while 18 AK configurations took 5-8 hours each (37, 38, 39, 40, 41, 55, 56, 57, 58, 59, 73, 74, 75, 76, 77, 78, 79, 80). In comparison to the MCS analysis, which took a total of eight hours for each geometric configuration considered, the AK-MCS analysis has a time saving roughly between 37.5% and 93.75%.

Table 17. Metric AK configuration ranking for girder.

Ranking Method	Rank	Regression function	Correlation function	Learning function	I_1	I_2	I_3	I_4
Best I_1 (RMSE)	1	Constant	Spline	H_c	1.0000	1.0000	0.0000	0.9483
	2	Constant	Spline	$KO_{005(5)}$	0.6854	0.7564	0.6132	0.6099
	3	Constant	Gaussian	$KO_{05(5)}$	0.6757	0.7013	0.7737	0.6154
	4	Linear	Gaussian	EFF	0.6505	0.7129	0.8982	0.4771
	5	Constant	Cubic	$KO_{05(5)}$	0.6354	0.6733	0.8982	0.4985
Best I_2 (AAE)	1	Constant	Spline	U	1.0000	1.0000	0.0000	0.9483
	2	Constant	Spline	U	0.6854	0.7564	0.6132	0.6099
	3	Linear	Gaussian	$KO_{05(2)}$	0.6505	0.7129	0.8982	0.4771
	4	Constant	Gaussian	$KO_{05(2)}$	0.6757	0.7013	0.7737	0.6154
	5	Constant	Cubic	$KO_{005(2)}$	0.6354	0.6733	0.8982	0.4985
Best I_3 (DoC)	1	Constant	Gaussian	$KO_{005(5)}$	0.0000	0.0357	1.0000	0.5339
	2	Constant	Gaussian	H_I	0.1248	0.1287	1.0000	0.5070
	3	Linear	Gaussian	1	0.0851	0.0664	1.0000	0.5424
	4	Linear	Gaussian	2	0.1766	0.2546	1.0000	0.5079
	5	Linear	Gaussian	3	0.1736	0.1946	1.0000	0.4711
Best I_4 (TTP)	1	Constant	Cubic	U	0.5839	0.5742	0.3869	1.0000
	2	Constant	Cubic	U	0.3601	0.3453	0.0000	1.0000
	3	Constant	Spline	H_c	0.0995	0.0786	0.3869	0.9483
	4	Constant	Spline	H_c	1.0000	1.0000	0.0000	0.9483
	5	Constant	Gaussian	H_c	0.2488	0.2373	0.6132	0.8443
Opt (AK-MCS)	1	Linear	Spherical	REIF	0.4364	0.4395	0.8982	0.6266
	2	Linear	Spherical	U	0.3931	0.4173	0.8982	0.6369
	3	Linear	Cubic	H_c	0.4161	0.4528	0.8982	0.5695
	4	Linear	Linear	REIF	0.3828	0.4100	0.8982	0.6196
	5	Linear	Spline	H_c	0.4480	0.4406	0.8982	0.5659

5.3.4 Parametric Analysis of Multiple Girder Design Configurations

Four girder cross-sectional sizes were considered in this analysis, three of which were covered in Chapter 4. The idealized geometries are included in Table 18. A total of 21 unique girder configurations (size and bar distribution) have been considered as include in Table 19.

Table 18. Idealized girder cross-sectional section IDs.

NEBT ID	H (mm)	H_1 (mm)	H_2 (mm)	H_3 (mm)	B_1 (mm)	B_2 (mm)	B_3 (mm)	A_c (mm^2)
NEBT 1	1200	115	280	805	1200	810	180	509,700
NEBT 2	1400	115	280	1005	1200	810	180	545,700
NEBT 3	1600	115	280	1205	1200	810	180	581,700
NEBT 4	1800	115	280	1405	1200	810	180	617,700

Table 19. Details of additional girders considered.

Section ID	NEBT ID	d_b (mm)	A_s (mm^2)	A_{si} (mm^2)	d_s (mm)	ρ_{act} (%)
GIRD 01	NEBT 3	9.5	994	A_b [2,2,2,4,4]	[1100,1200,1300,1400,1500]	0.1950
GIRD 02	NEBT 2	9.5	994	A_b [2,2,2,4,4]	[900,1000,1100,1200,1300]	0.1822
GIRD 03	NEBT 1	9.5	994	A_b [2,2,2,4,4]	[700,800,900,1000,1100]	0.1709
GIRD 04	NEBT 3	11	1,330	A_b [2,2,2,4,4]	[1100,1200,1300,1400,1500]	0.2609
GIRD 05	NEBT 2	11	1,330	A_b [2,2,2,4,4]	[900,1000,1100,1200,1300]	0.2437
GIRD 06	NEBT 1	11	1,330	A_b [2,2,2,4,4]	[700,800,900,1000,1100]	0.2286
GIRD 07	NEBT 3	12.5	1,717	A_b [2,2,2,4,4]	[1100,1200,1300,1400,1500]	0.3369
GIRD 08	NEBT 2	12.5	1,717	A_b [2,2,2,4,4]	[900,1000,1100,1200,1300]	0.3146
GIRD 09	NEBT 1	12.5	1,717	A_b [2,2,2,4,4]	[700,800,900,1000,1100]	0.2952
GIRD 10	NEBT 1	9.5	1134.12	A_b [2,2,2,4,6]	[891,955,1017,1080,1143]	0.2225
GIRD 11	NEBT 2	9.5	1134.12	A_b [2,2,2,4,6]	[1091,115,1217,1280,1343]	0.2708
GIRD 12	NEBT 3	9.5	1134.12	A_b [2,2,2,4,6]	[1291,1355,1417,1480,1543]	0.1950
GIRD 10	NEBT 1	9.5	1134.12	A_b [2,2,2,4,6]	[891,955,1017,1080,1143]	0.2225
GIRD 11	NEBT 2	9.5	1134.12	A_b [2,2,2,4,6]	[1091,115,1217,1280,1343]	0.2708
GIRD 12	NEBT 3	9.5	1134.12	A_b [2,2,2,4,6]	[1291,1355,1417,1480,1543]	0.1950
GIRD 13	NEBT 4	9.5	1134.12	A_b [2,2,2,4,6]	[1491,1555,1617,1680,1743]	0.1836
GIRD 14	NEBT 1	11	1520.53	A_b [2,2,2,4,6]	[891,955,1017,1080,1143]	0.2983
GIRD 15	NEBT 2	11	1520.53	A_b [2,2,2,4,6]	[1091,115,1217,1280,1343]	0.2786
GIRD 16	NEBT 3	11	1520.53	A_b [2,2,2,4,6]	[1291,1355,1417,1480,1543]	0.2614
GIRD 17	NEBT 4	11	1520.53	A_b [2,2,2,4,6]	[1491,1555,1617,1680,1743]	0.2462
GIRD 18	NEBT 1	12.5	1963.50	A_b [2,2,2,4,6]	[891,955,1017,1080,1143]	0.3852
GIRD 19	NEBT 2	12.5	1963.50	Ab [2,2,2,4,6]	[1091,115,1217,1280,1343]	0.3598
GIRD 20	NEBT 3	12.5	1963.50	Ab [2,2,2,4,6]	[1291,1355,1417,1480,1543]	0.3375
GIRD 21	NEBT 4	12.5	1963.50	Ab [2,2,2,4,6]	[1491,1555,1617,1680,1743]	0.3179

*Values presented for the five layers of reinforcement [Layer 1, Layer 2, Layer 3, Layer 4, Layer 5], where Layer 5 is the lowermost layer

Table 20 and Table 21 list the summary findings of the top 5 optimum AK configurations based on a concrete compressive strength of 45 MPa and 55 MPa. The top 5 optimum AK configurations were determined based on the CMS and are summarised in Table 17. Two error calculations were considered, the error as per Equation (66) and the AAE as per Equation (56), where, negative indicates underprediction and positive represents over predication.

$$Error = \frac{\sum_{i=1}^{AK\ Config.} \left(\frac{\beta_{AK-MCS}(i) - \beta_{MCS}}{\beta_{MCS}} \right)}{5} \tag{66}$$

The error calculation identifies and distinguishes cases where over and under prediction occur. This identifies the geometric cases where the surrogate model is conservative in nature

(underpredict). The number of underpredicted cases increase from 5/21 cases to 8/21 as the $f_c^{'}$ was changed from 45 MPa to 55 MPa, respectively. The AAE identifies the consistency of the AK configuration based on the absolute differences in the results, which results in a larger error value. When both the error and AAE are equal, the results are all a form of overprediction, if the AAE is larger then the error, there are some cases where the β_{AK-MCS} is less then the β_{MCS}, and there are no cases where the error can be larger then the AAE.

When utilizing the top 5 optimum AK configurations on the assorted geometric configurations, the number of added points ranged from 0 to 36, with the mean value of 13.3 and the mode value of 1 and initial points of 18. This range is small in comparison to the results from the Chapter 4 analysis that had a range of initial points between 6 and 110, and the number of added points between 0 and 300, with the mean value of 31 and the mode value of 0. The reasoning for the mode of zero in the Chapter 4 analysis results is due to the use of the quadratic regression function, most times 0 added points were needed as the number of initial training points were very high (over 100), where as the Chapter 5 Chapter 5. results cover only linear and constant regression functions meaning the number of initial training points was lower and the number of added higher.

Each analysis took approximately 5-10 minutes to run, reducing the computational demand by 97% compared to the crude MCS method. The computationally demanding portion of the AK-MCS method is the training of the surrogate model, same is true for more complex LSF represented by complex and demanding resistance and load models. If an optimum configuration can be determined, the cost savings of a more complex system can be exponentially higher, as the total time the model would have taken with MCS is exponentially longer then the current simplified LSF being assessed in this works.

Table 20. Optimum AK-MCS configuration for alternate girder configurations at 45 MPa.

GIRD ID	β_{MCS}	β_{AK-MCS} Values for Optimum AK Config.					Min Error	Max Error	Average Error	AAE
		1	2	3	4	5				
02	4.2073	4.1318	4.2240	4.2240	4.2649	4.1449	-0.0180	0.0137	- 0.0220	0.0109
03	4.1897	4.3145	4.2884	4.2059	4.1193	4.2059	-0.0168	0.0298	0.0089	0.0156
04	4.4627	4.3439	4.2884	4.4172	4.4172	4.4172	-0.0390	-0.0102	- 0.0193	0.0193
05	4.4790	4.4652	4.4652	4.7534	4.7534	4.2436	-0.0526	0.0613	0.0128	0.0363
06	4.4920	4.5264	4.6114	4.7534	4.7534	4.3439	-0.0329	0.0582	0.0235	0.0367
07	4.2276	4.1735	4.2436	4.3439	4.2884	4.2649	-0.0128	0.0275	0.0083	0.0135
08	4.2609	4.3145	4.2059	4.2884	4.3776	4.5264	-0.0129	0.0623	0.0192	0.0243
09	4.3197	4.3439	4.4172	4.3439	4.3776	4.2240	-0.0222	0.0226	0.0050	0.0139
10	4.2092	4.2059	4.2059	4.1587	4.1735	4.3439	-0.0120	0.0320	0.0020	0.0108
11	4.2079	4.2240	4.2884	4.4172	4.2059	4.1449	-0.0150	0.0497	0.0114	0.0176
12	4.1699	4.1735	4.2240	4.1449	4.2436	4.1449	-0.0060	0.0177	0.0039	0.0087
13	4.1658	4.1892	4.1193	4.2240	4.4172	4.2884	-0.0112	0.0604	0.0196	0.0241
14	4.5184	4.4652	4.5264	4.4172	4.4652	4.4652	-0.0224	0.0018	- 0.0112	0.0119
15	4.4766	4.7534	4.4172	4.7534	4.4172	4.5264	-0.0133	0.0618	0.0217	0.0323
16	4.4434	4.3145	4.4652	4.4172	4.4652	4.3439	-0.0290	0.0049	- 0.0095	0.0134
17	4.4255	4.3439	4.5264	4.4652	4.5264	4.4652	-0.0184	0.0228	0.0090	0.0164
18	4.3248	4.3439	4.5264	4.3439	4.5264	4.3439	0.0044	0.0466	0.0213	0.0213
19	4.2898	4.2884	4.4172	4.1075	4.4172	4.6114	-0.0425	0.0750	0.0183	0.0354
20	4.2251	4.2649	4.2884	4.2436	4.3439	4.2240	-0.0003	0.0281	0.0113	0.0114
21	4.2361	4.2649	4.1892	4.2436	4.2059	4.2240	-0.0111	0.0068	- 0.0025	0.0059

Table 21. Optimum AK-MCS configuration for alternate girder configurations at 55 MPa.

GIRD ID	β_{MCS}	β_{AK-MCS} Values for Optimum AK Config.					Min Error	Max Error	Average Error	AAE
		1	Min	Min	4	5				
02	4.1844	4.1735	4.1587	4.1318	4.1318	4.2436	- 0.0126	0.0141	- 0.0039	0.0096
03	4.1788	4.3439	4.1587	4.1449	4.2059	4.2649	- 0.0081	0.0395	0.0107	0.0159
04	4.4128	4.7534	4.3145	4.3439	4.4172	4.4652	- 0.0223	0.0772	0.0104	0.0256
05	4.4230	4.4172	4.4652	4.3776	4.2884	4.4652	- 0.0304	0.0095	- 0.0046	0.0122
06	4.4213	4.4172	4.6114	4.4172	4.4652	4.4652	- 0.0009	0.0430	0.0122	0.0129
07	4.1960	4.2649	4.1193	4.1193	4.1587	4.2649	- 0.0183	0.0164	- 0.0025	0.0157
08	4.2303	4.3145	4.2884	4.4652	4.2436	4.2884	0.0031	0.0555	0.0212	0.0212
09	4.2622	4.4172	4.2884	4.1735	4.3145	4.3439	- 0.0208	0.0364	0.0106	0.0190
10	4.1784	4.1587	4.1075	4.1892	4.2240	4.1587	- 0.0170	0.0109	- 0.0026	0.0080
11	4.1685	4.2884	4.1587	4.2240	4.1318	4.1318	- 0.0088	0.0288	0.0044	0.0124
12	4.1620	4.0291	4.1193	4.1193	4.2649	4.1735	- 0.0319	0.0247	- 0.0050	0.0160
13	4.1947	4.1587	4.1193	4.1449	4.2240	4.0854	- 0.0261	0.0070	- 0.0115	0.0143
14	4.4485	4.4652	4.4652	4.6114	4.6114	4.4652	0.0038	0.0366	0.0169	0.0169
15	4.4299	4.3776	4.4652	4.4172	4.6114	4.5264	- 0.0118	0.0410	0.0112	0.0171
16	4.3947	4.4652	4.7534	4.7534	4.3145	4.7534	- 0.0182	0.0816	0.0485	0.0558
17	4.3810	4.6114	4.3776	4.3439	4.2884	4.3146	- 0.0211	0.0526	0.0014	0.0196
18	4.2657	4.4172	4.4652	4.2649	4.4172	4.3145	- 0.0002	0.0468	0.0258	0.0259
19	4.2415	4.2436	4.1449	4.2240	4.2649	4.2436	- 0.0228	0.0055	- 0.0041	0.0067
20	4.2128	4.1735	4.2240	4.2059	4.1735	4.1735	- 0.0093	0.0027	- 0.0054	0.0065
21	4.1705	4.2059	4.3439	4.2436	4.2240	4.2059	0.0085	0.0416	0.0178	0.0178

5.4 PIER ANALYSIS

5.4.1 General

The configuration of the pier that was selected to undergo five identical comprehensive AK configuration runs (5 x 108 AK configurations) was PIER ID 5 as detailed in Table 8 within Section 4.2. The top five AK configurations were then applied to assess the reliability of six additional pier configurations as detailed in the parametric analysis subsection.

5.4.2 Input Parameters

There are three types of input parameters, the geometric considerations, the statistical random variables, and the AK configurations. The geometric case that is considered is section PIER ID 5, as shown in Figure 14. The statistical parameters for the random variables and load case have been maintained from Chapter 4 and include five load and five resistance based random variables. Where the $f_c^{'}$ is 45 MPa, Φ_c is 0.75, Φ_s is 0.9 and the reinforcing bars are tied and not prestressed. The total number of AK configurations considered are 108, all six correlation functions (exponential, Gaussian, linear, spherical, cubic, and spline), only two regression functions were considered (constant and linear). Quadratic regression was not considered as the number of points required for training the initial Kriging predictor is large enough that no additional added points are required for training. A total of nine learning functions were considered including EFF, U, H_c, H, REIF, $KO_{05(2)}$, $KO_{005(2)}$, $KO_{05(5)}$, and $KO_{005(5)}$.

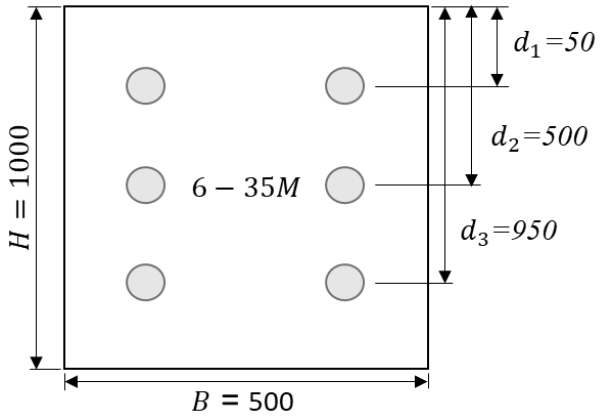

Figure 14. Geometry of PIER ID 5.

5.4.3 Summary of Results

The MCS with $5x10^7$ trials was considered as the exact solution when comparing to the AK-MCS results. For PIER ID 5, the target β_{MCS} and P_f were determined to be 4.5714 and $2.44x10^{-6}$, respectively. Table 22 details the summary of outputs based on five ranking criteria detailed in Section 5.2. The first two are I_1 and I_2 which are based on the RMSE and the AAE, respectively. The third is I_3 which details the DoC and the fourth is I_1 which defines the TTP. Lasty the optimum configuration satisfying all four methods of criterion simultaneously. Using the SAR research groups server the 108 AK configurations took about 24 hours each run averaging between 10-15 minutes. The MCS analysis took six hours per analysis, meaning that the AK-MCS method provided a time savings between 95.8% and 97.2% of the total MCS analysis duration.

Table 22. Metric AK configuration ranking for piers.

Ranking Method	Rank	Regression function	Correlation function	Learning function	I_1	I_2	I_3	I_4
Best I_1 (RMSE)	1	Constant	Gaussian	H_c	1.0000	1.0000	0.0000	1.0000
	2	Constant	Gaussian	$KO_{05(2)}$	0.6614	0.6561	0.6131	0.7819
	3	Constant	Spline	$KO_{005(2)}$	0.5538	0.5660	0.6131	0.7338
	4	Constant	Gaussian	H_c	0.5498	0.5387	0.3869	1.0000
	5	Constant	Cubic	H_c	0.5262	0.5163	0.7737	0.8124
Best I_2 (AAE)	1	Constant	Gaussian	H_c	1.0000	1.0000	0.0000	1.0000
	2	Constant	Gaussian	$KO_{05(2)}$	0.6614	0.6561	0.6131	0.7819
	3	Linear	Gaussian	H_c	0.5255	0.6169	0.8982	0.6451
	4	Constant	Spline	$KO_{005(2)}$	0.5538	0.5660	0.6131	0.7338
	5	Constant	Gaussian	H_c	0.5498	0.5387	0.3869	1.0000
Best I_3 (DoC)	1	Constant	Gaussian	H	0.1554	0.1815	1.0000	0.5281
	2	Linear	Gaussian	$KO_{05(2)}$	0.5100	0.4997	1.0000	0.6076
	3	Linear	Gaussian	$KO_{005(2)}$	0.2994	0.3054	1.0000	0.5444
	4	Linear	Gaussian	$KO_{05(5)}$	0.2912	0.2943	1.0000	0.4829
	5	Linear	Gaussian	$KO_{005(5)}$	0.3991	0.4147	1.0000	0.4646
Best I_4 (TTP)	1	Constant	Gaussian	H	0.5498	0.5387	0.3869	1.0000
	2	Constant	Gaussian	H	1.0000	1.0000	0.0000	1.0000
	3	Constant	Spline	H	0.2516	0.2332	0.3869	0.9765
	4	Constant	Spline	H	0.3294	0.3129	0.0000	0.9765
	5	Constant	Cubic	H	0.5262	0.5163	0.7737	0.8124
Opt (AK-MCS)	1	Linear	Gaussian	H_c	0.5255	0.6169	0.8982	0.6451
	2	Linear	Spline	REIF	0.4655	0.5312	0.8982	0.7124
	3	Linear	Linear	$KO_{05(2)}$	0.5117	0.5224	0.8982	0.6433
	4	Linear	Exponential	REIF	0.4606	0.4827	0.8982	0.6903
	5	Linear	Spherical	U	0.4393	0.4833	0.8982	0.6903

Table 22 shows a similar pattern to that of the girder findings, linear regression is optimal when considering all four parameters, the REIF learning function reoccurs the most frequently, however there is no clear optimal correlation function. It could be argued that the Gaussian correlation and the $KO_{05(2)}$ and H learning functions reoccur the most frequently, but this is not indicative of a preferred AK configuration.

The pier analysis had a larger number of random variables compared to the girders; this addition was simply the treatment of the area of the steel bars as a random variable in each layer of rebar. Comparing the resistance models of the girder and pier it is clear that both are computationally

demanding, however the girder took significantly longer to run then that of the pier. This could indicate that the pier resistance model is further optimized than the girder model. This significant difference in analysis run time is characterised by the two factors, the number of random variables and the complexity of the resistance model.

5.4.4 Parametric Analysis of Multiple Column Design Configurations

Six additional geometric configurations where considered, as shown in Table 23 including PIER ID 3, 4, 7, 8, 11, and 12. The additional configurations are the geometric complements of the initial six geometries considered in Chapter 4. This means that they share the same variation in height and bar size, however they have significantly higher reinforcement ratios around 3 and 4 % versus the 1 and 2% from Chapter 4. All geometric configurations where subjected to the analysis based on the five optimal AK configurations, including those from Chapter 4 but excluding PIER ID 5 as it was the geometric case considered in the metric application and could skew the results.

Table 23. Additional pier geometric cases considered.

Section ID	H (mm)	ρ (%)	Bar Size	A_s (mm^2)	A_{si} (mm^2)	d_i (mm)	ρ_{act} (%)
PIER 01	500	1	6-25M	3000	25M*[2,2,2]	[50,250,450]	1.20
PIER 02	500	2	10-25M	5000	25M*[4,2,4]	[50,250,450]	2.00
PIER 03	500	3	15-25M	8000	25M*[5,2,2,2,5]	[50,150,250,350,450]	3.20
PIER 04	500	4	20-25M	10000	25M*[7,2,2,2,7]	[50,150,250,350,450]	4.00
PIER 06	750	2	12-30M	8400	30M*[5,2,5]	[50,375,700]	2.24
PIER 07	750	3	18-30M	12600	30M*[6,2,2,2,6]	[50,212.5,375,537.5,700]	3.36
PIER 08	750	4	22-30M	15400	30M*[8,2,2,2,8]	[50,212.5,375,537.5,700]	4.10
PIER 09	1000	1	6-35M	6000	35M*[2,2,2]	[50,500,950]	1.20
PIER 10	1000	2	10-35M	10000	35M*[4,2,4]	[50,500,950]	2.00
PIER 11	1000	3	15-35M	16000	35M*[5,2,2,2,5]	[50,275,500,725,950]	3.20
PIER 12	1000	4	20-35M	20000	35M*[7,2,2,2,7]	[50,275,500,725,950]	4.00

Table 24 summarizes the outputs for all geometries when the top five optimal AK configurations are applied, and the error associated with each. Two error calculations were considered, the error as per Equation (66) and the AAE as per Equation (56), where negative

indicates underprediction and positive is over prediction. The AAE identifies the consistency of the AK configuration based on the absolute differences in the results, which results in a larger error value.

When utilizing the top 5 optimum AK configurations on the assorted geometric configurations, the number of initial points was 19 or 23 and the number of added points ranged from 0 to 36, with a mean value of 8.25 and a mode value of 7. The difference in the number of initial points was caused by the number of rebar layers in the sections despite the fact that all used a linear regression function. This range is small in comparison to the results from the Chapter 4 analysis that had a range of initial points between 6 and 125, and the number of added points between 0 and 246, with a mean value of 13.19 and a mode value of 0. The reason of the zero mode is due to the use of the quadratic regression function as explained in Section 5.3.4.

Table 24. Optimum AK-MCS configuration for alternate pier configurations.

PIER ID	β_{MCS}	β_{AK-MCS} Values for Optimum AK Configurations					Error	AAE
		1	2	3	4	5		
01	4.5658	4.4652	4.3776	4.5264	4.7564	4.4172	-0.0125	0.0292
02	4.6667	4.6114	4.5264	4.7534	4.4652	4.4652	-0.0219	0.0294
03	4.6922	4.7534	4.5264	4.7534	4.4652	4.7534	-0.0089	0.0246
04	4.7150	4.4652	4.7534	4.6114	4.6114	4.5264	-0.0258	0.0290
05*	-	-	-	-	-	-	-	-
06	4.6351	4.7534	4.5264	4.7534	4.5264	4.6114	-0.0002	0.0206
07	4.7045	4.7534	4.7534	4.4172	4.3776	4.7534	-0.0199	0.0323
08	4.7358	4.6114	4.5264	4.5264	4.6114	4.6114	-0.0334	0.0334
09	4.5758	4.5264	4.7534	4.7534	4.4172	4.7534	0.0142	0.0324
10	4.6404	4.3145	4.6114	4.4652	4.6114	4.5264	-0.0290	0.0290
11	4.7144	4.6114	4.6114	4.7534	4.5264	4.7534	-0.0134	0.0200
12	4.7380	4.7534	4.7534	4.6114	4.5264	4.7534	-0.0123	0.0162

* was considered in Section 4.4.3.

5.5 CHAPTER SUMMARY

The AK-MCS analysis of bridge girders and piers were optimized in this chapter by utilizing a newly introduced metric for AK-MCS analysis in literature called the CMS. CMS is used to train

the performance of the AK analysis (accuracy and efficiency) by considering four parameters including the RSME, AAE, DOC, and the TTP. Two sensitivity analyses were performed: the first was performed by determining the reliability index for a singular girder and pier geometric configurations but with a multiple number of AK configurations, while the second was performed by determining the reliability index of multiple girder and pier geometric configurations but with the top five AK configurations determined in the first sensitivity analysis.

Analyses results indicated the accuracy and efficiency of the determined top five AK configurations in assessing the reliability of the select girder and pier geometric cases. The sensitivity analysis showed promising results, indicating the benefit of using an optimum configuration through the decrease in error and decrease in the number of required training points. The determined AK configurations are recommended for the general analysis of similar girder and pier configurations.

CHAPTER 6 CONCLUSIONS AND RECOMMENDATIONS

6.1 SUMMARY

Bridge assist management requires developing tools to evaluate the performance of structures to allow direct comparison to priorities repairs and replacements. Reliability-based frameworks of analysis facilitate the evaluation and comparison of bridge systems and/or elements by quantifying the structural safety (i.e., determining the reliability index, β). The β is a measurement of safety of a given structure based on the inherent randomness of the system. Sources of uncertainties include the natural variability of physical properties, operating conditions, and the lack of knowledge or mathematical representation.

There were numerous methods of analysis available to evaluate the LSF including approximate methods, simulation techniques, surrogate models, and surrogate model aided methods. A *generic*, *efficient*, and *accurate* framework of analysis was needed to assess and evaluate multiple types and configurations of bridges. The selection of the AK-MCS method in this research was due to its applicability in estimating the reliability for simple LSF and efficiency in simulating complex and nonlinear LSF, where other methods may not be as versatile. The objective of this research was to develop a functional framework and a computer code that evaluates the reliability of bridge components using AK-MCS as the method of analysis

The framework of AK-MCS was reviewed and coded in MATLAB. AK-MCS uses a Kriging predictor trained in a stage-wise manner, along with a learning function to further optimize the training of the surrogate model. This is completed through the conditional selection of additional training points. AK-MCS methodology is comprised of four main sections, the initial and updated DoE, Kriging, active learning, and reliability assessment. Within the initial DoE, the random variables are generated and evaluated by the LSF, where the DoE is comprised of the inputs and

outputs. The DoE is then fed into the Kriging section. Kriging used stochastic regression and correlation functions to generate a surrogate predictor. The predictor is used to evaluate the predefined number of trials and the mean and variance of the surrogate model. The learning function is used to evaluate the stopping criteria and the selection of the additional training point. The final stage is the reliability assessment where the probability of failure equal to the number of failed trials over the total number trials.

The developed AK-MCS framework was validated by analyzing select girder and pier configurations designed according to the Canadian Highway Bridge Design Code (CHBDC) and the Concrete handbook (CSA S6, 2019; CSA A23.3, 2014). The load model was developed based on the CHBDC and included a singular load combination, as define in Equation (28). 54 unique AK configurations were considered in the verification stage for nine girder geometries and 54 AK configurations were considered for the six pier configurations.

The AK-MCS was further optimized in this research by recommending AK configurations (set of correlation, regression, and learning functions) that reduce the reliability prediction error and the number of training points. This was accomplished by utilizing a newly developed metric system, the CMS, in literature used to rank the performance of AK-MCS analysis as a function of the AK configuration. CMS formulation is described in Equations (55) to (63). Top performing AK configurations were determined based on select girder and pier configurations and then utilized to perform a larger sensitivity analysis to evaluate the performance of the determined AK configurations for assessing multiple configurations of bridge girders (12 geometries) and piers (6 geometries).

6.2 CONCLUSION

The conclusion and framework recommendations are presented in three sections: Chapter 4 verification results, Chapter 5 sensitivity and optimization results, and lastly general remarks.

6.2.1 Verification of AK-MCS

The accuracy and efficiency of the sensitivity analysis in Chapter 4, where the analysis results are discussed based on measuring the error of AK-MCS as compared with crude MCS.

- AK-MCS was validated for the considered geometric cases of girders and piers.
- The mean error of the AK-MCS of all 54 AK configurations is 0.0225 ± 0.0307 as compared to the crude MCS.
- The results show that AK configuration 32, which has a linear regression function, a linear correlation function and U learning function was the optimum configuration with a RMSE of 1.98E-4.
- The results suggest that AK-MCS is sensitive to the choice of the optimal AK configuration may be influenced by the complexity of the considered limit state and the number of considered random variables.
- As the ρ increase so does the β_{MCS}, both of which are directly related to the variability seen in the spread of the β_{AK-MCS} around the β_{MCS}, as see in Figure 8.
- The mean error of the AK configuration of the pier configurations with ρ of 1% (Pier 1, Pier 5, and Pier 9) and 2% (Pier 2, Pier 6, and Pier 10) were 0.0792 ± 0.02636 and 0.0453 ± 0.0258, respectively, where positive indicates overprediction and negative indicates underprediction.
- The pier results suggest that AK-MCS for ρ of 1% is more accurate than 2% based on the mean value of β although the former is more dispersed than the latter. The mean error of the

AK configuration of the pier configurations with H of 500 mm (Pier 1 and Pier 2), H of 750 mm (Pier 3 and Pier 4), H of 1000 mm (Pier 5 and Pier 6) are 0.0985 ± 0.0274 and 0.0686 ± 0.0263, 0.0196 ± 0.0284 respectively.

- The results suggest that AK-MCS for H of 750 mm (height-to-width ratio of 1.5) is most accurate based on the mean and the standard deviation. Also, it is observed that the mean value tends to shift from underprediction to overprediction as the section depth increases.
- It was also observed that while the quadratic regression function worked well, the number of initial design points required was very high, resulting in high computational burden and in most times, resulting in the non use of the learning function. This was because the stopping criterion was met and there was no optimization of the surrogate model through the selection of added points. It could be argued that in the case of the quadratic regression function, Kriging suffices (no nee for active learning).
- It was evident that the input data generated varies and this indicates that the fit of the analysis can vary as one data set might preform better then another. It was recommended this be investigated through running identical analyses multiple times to see the effects of this inherent bias. This was the focus of Chapter 5.
- The computational limits defined based on computer processor and memory are still of concern when conducting a sensitivity analysis. It was determined in the cases of quadratic or constant regression functions, the number of required training points (sum of initial and added points) are large and unrealistic when considering more complex load and resistance models.

6.2.2 Optimization of AK-MCS

The accuracy and efficiency of the sensitivity analysis in Chapter 5, where the analysis results are discussed based on measuring the error of AK-MCS as compared with crude MCS. This is for the sensitivity analysis and the application of the optimum configuration to additional geometries.

- **Accuracy:** The error associated with the girder configurations with f_c' of 45 MPa and 55 MPa were 0.0076 ± 0.0119 and 0.0076 ± 0.0142. The error associated with the pier configurations with ρ of 1% (PIER ID 1 and 9), ρ of 2% (PIER ID 2, 6, and 10), ρ of 3% (PIER ID 3, 7, and 11), and ρ of 4% (PIER ID 4, 8, and 12) were 0.0008 ± 0.0189, - 0.0236 ± 0.0150, - 0.0141 ± 0.0055 and - 0.0238 ± 0.0107. The error is low which indicates accurate representation of the results compared to the MCS.
- **Efficiency:** The total number of initial training pints ($N_{initial}$) was 18 as all optimum configurations had a linear regression function and the lower and upper bound of the added training points (N_{added}) were 1 and 38, respectively. This shows a significant decrease in the number of total required training points and could indicate significant computational savings if the load or resistance models in question are complex. The total number of initial training points for PIER ID 1, 2, 6, 9, and 10 were 19 and for PIER ID 2, 4, 7, 8, 11, and 12 were 23, respectively. This is due to an increase in the number of bar layers which in turn increased the number of random variables. The lower and upper bounds of the added points are 4 and 16, respectively. The optimum configurations took approximately 10 minutes to run, seeing a reduction in computational time by 97.9%, with respects to the duration of the MCS run time.
- **Regression Function**: It is evident that the linear regression function relates the data more accurately when considering all four parameters in the CMS compared to constant function.

Table 22 shows that linear regression was optimal when considering all four parameters and constant was optimal when considering singular components (i.e., RMSE, AAE, TTP and DOC).

- **Correlation Function**: There is no clear optimal correlation function indicated based on Chapter 5 results. The two functions that reoccur the most frequently are Gaussian and cubic as displayed in Table 17. However, when considering all four parameters simultaneously the most frequent reoccur function is the spherical correlation function.
- **Learning Function**: The REIF learning function only occur when the four parameters are considered, however in general the function that reoccur the most frequently is the H_c learning function. There was no clear optimal learning function. It could be argued that the REIF and H_c learning functions reoccur the most frequently, but this was not indicative of a preferred AK configuration.
- **Length of Computational Time**: 18 of the 108 AK configurations (37, 39, 40, 41, 55, 56, 57, 58, 59, 73, 74, 75, 76, 77, 78, 79, and 80) took approximately 5-8 hours each to run, with more then 200 added points required. The 18 cases did not provide any time savings as the MCS with $5x10^7$ trials took roughly 8 hours. The remaining AK configurations had a reduction in computational time of approximately 93.75%. Using the SAR research groups server, the 108 AK configurations took about 24 hours each run averaging between 10-15 minutes, while the MCS only took six hours each. It is clear that the computational savings reduces the analysis run time by approximately 95.8%, as compared with crude MCS.

6.2.3 General Remarks

The duration of time required to run an AK-MCS analysis, arguably the training of the surrogate model, will become more costly as the complexity of the original model of the LSF increases. The difference in analysis run time savings between a simplified model and a complex model will be amplified, relative to the number of training points. It was clear that the recommended regression function is linear, the distinction of the optimal correlation and learning functions were not as clear in the sensitivity analysis findings. Based on the CMS the correlation function, has little effect on the results outcome. The two most frequent learning functions were RIEF and H_c are recommended for girder and pier with configurations, and reinforcement ratios similar to what was presented in the scope of this work.

6.3 Recommended Future Research

Theoretically, this framework of analysis is generic in nature and can be used with a variety or resistance and load models to train the surrogate model. Recommended future research includes the following:

- To expand upon the AK-MCS framework application, it should be applied to reliability problems where the resistance model is solved using numerical simulation. This is important because such method will be most beneficial in cases where the computational cost of the resistance model is high.
- To ensure the methodology functions for time-dependant reliability analysis, recommended future work includes a sensitivity analysis using a series of degradation models augmented within the resistance model.
- Consider that an optimal AK configuration may not be possible and approach the problems with the mindset that different analysis types (i.e., components, analysis configuration, load

case etc.) will determine the AK configuration selection. A larger sensitivity analysis is required as current examples and applications are limited within literature.

- Further studies are required to recommend a generalized AK-MCS analysis configurations for a wide range of bridge configurations and analysis types. The preliminary research findings indicate the efficiency of the proposed AK-MCS method for software programing applications.
- There are many forms of analysis that couple the Kriging method with learning functions and reliability assessment tools. This include but are not limited to AK-MCS, AK-IS, and AK-FORM. Literature indicates that AK-IS could preform better then that of AK-MCS, since the probability of failure of the considered bridge pier and girder configurations is low. The comparison will determine if the accuracy of the AK-MCS can be further improved upon.

REFERENCES

AASHTO. (2004). “LRFD bridge design specifications” American Association of State Highway and Transportation Officials, Washington, DC.

Al-Bittar, T., Soubra, A. H., and Thajeel, J. (2018). Kriging-Based Reliability Analysis of Strip Footings. *Journal of Geotechnical and Gioenviromental Engineering, 144*(10).

Allen, D. (1991). Canadian highway bridge evaluation: reliability index. *Canadian Journal of Civil Engineering*, *19*(6), 987-991.

Assad, A. A., and Gass, S. I. (2005). Model World: Tales from the Time Line - The Definition of OR and the Origings of Monte Carlo Simulation. *Interfaces, 32*(5), 429-435.

Bichon, B., Eldred, M., Swiler, L., Mahadevan, S., and McFarland, J. (2008). Efficient Global Reliability Analysis for Nonlinear Implicit Preformance Functions. *AIAA Journal*, 135(1), 2459-2468.

Brooks, S., Gelman, A., Jones, G., and Meng, X. L. (2011). *Handbook of Markov Chain Monte Carlo* (1st ed.). New York: Chapman and Hall.

Brzev, S., and Pao, J. (2016a). Reinforced Concrete Design: A Practical Approach. In *Chapter Three Flexure: Behaviour of Beams and one-way slabs* (Third ed., pp. 72-133). New York, New York, USA: Pearson Education Inc.

Brzev, S., and Pao, J. (2016b). Reiforced Concrete Design: A Practical Approach. In *Chapter Eight Columns* (Third ed., pp. 347-415). New York, New York, USA: Pearson Education Inc.

Buckley, E., Khorramian, K., and Oudah, F. (2021). Application of Adaptive Kriging Method is Bridge Girder Reliability Analysis. *Structural Reliability and Risk Assessment.*

Buckley, E., Khorramian, K., and Oudah, F. (2022). Optimal Active Learning Kriging Predictor Configuration for Calculating the Reliability Index of Bridge Piers. *11th International Conference on Short and Medium Span Bridges*. Toronto.

Canadian Precast/Prestressed Concrete Institute. (2017). *CPCI Design Manual* (5 ed.).

Chiles, J. P., and Chauvet, P. (1997). Kriging: A method for cartography of the sea floor. *International Hydrographic Review, 52*(1).

Cressie, N. (1990). The Origins og Kriging. *Mathematical Geology. 22*, 239-251.

CSA A23.3. (2014). *Concrete Design Handbook.* Toronto, ON: Cement Association of Canada.

CSA S6. (2019). *Canadian Highway Bridge Design Code* Toronto, ON: Canadian Standards Association.

CSA S6.1. (2019). *Commentary on the Canadian Highway Bridge Design Code.* Toronto: Canadian Standards Association.

Dey, A., Miyani, G., and and Sil, A. (2019). Reliability assessment of reinforced concrete (RC) bridges due to service loading. *Innovative Infrastructure Solutions, 4*(1).

Echard, B., Gayton, N., and Lemaire, M. (2011). AK-MCS: An active learnin reliability method combining Kriging and Monte Carlo Simulation. *Structural Safety, 33*(2), 145-154.

Estes, A. C., and Frangopol, D. M. (2001). Bridge Lifetime System Reliability Under Multiple Limit States. *Journal of Bridge Engineering, 6*(6), 523-528.

Ghorbanpoor, A., and Dudek, J. (2007). *Bridge Intergrated Analysis and Decision Support: Case Histories.* Wisconsin Department of Transportation.

Ghosn, M., Moses, F., and Frangopol, D. M. (2010, February - April). Redundancy and robustness of highway bridge superstructures and substructures. *Structure and Infrastructure Engineering, 6*(1-2), 257-278.

Hu, Z., and Mahadevan, S. (2016). A Single-loop Kriging Surrogate Modeling for Time-Dependant Reliability Analysis. *Journal of Mechanical Design, 138*(6).

Huang, J., Fenton, G. A., and Griffiths, D. V. (2012). *Risk Assessment in Geotechnical Engineering,* (Vol. 461). New York: John Wiley and Sons.

Jiang, Y., Saito, M., and Sinha, K. C. (1988). Bridge Preformance Prediction Model Using the Markov Chain. *Transportation Research Record*, 25-32.

Journel, A. G. (1977). Kriging in Terms of Projections. *Mathematical Geology, 9*(6).

Kaymaz, I. (2005). Application of Kriging method to structural reliability problems. *Structural Safety*, *27*(2) 133-151.

Kennedy, L., Gagnon, D., Allen, D., and MacGregor, J. (1992). Canadian highway bridge evaluation: load and resistance factors. *Canadian Journal of Civil Engineering, 19*(6), 992-1006.

Khanzada, K. M. (2012). State of Bridge Management in Canada. [Master's thesis, North Dakota State University].

Khorramian, K., and Oudah, F. (2022a). Reliability Analysis of Structural Elements with Active Learning Kriging using a New Learning Function: KO Function. *CSCE 2022 Annual Conference.* Whistler.

Khorramian, K., and Oudah, F. (2022b). Active Learning Kriging-Based Reliability for Assessing the Safety of Structures: Theory and Application. *Leveraging Artificial intelligence into Engineering, Management, and Safety of Infrastructure*, *Taylor and Francis* (CRC).

Khorramian, K., and Oudah, F. (2022c). Metric Systems for Performance Evaluation of Active Learning Kriging Configurations for Reliability Analysis. *ASCE-ASME Journal of Risk and Uncertainty in Engineering Systems, Part A: Civil Engineering* (under review).

Khorramian, K., Alhashmi, A. E., and Oudah, F. (2022a). Effect of Random Fields in Stochastic FEM on the Structural Reliability Assessment of Pile Groups in Soil. *CSCS 2022 Annual Conference.* Whistler.

Khorramian, K., Alhashmi, A. E., and Oudah, F. (2022b). Optimized Active Learning Kriging Reliability Based Assessment of Laterally Loaded Pile Groups Modeled Using Random Finte Element. *Computers and Geotechnics*, *146*(1).

Lophaven, S., Nielsen, H., and Sondergaard, J. (2002). *DACE A MATLAB Kriging Toolbox. Technical Report IMM-TR-2002-1.*

Lounis, Z. (2000). Reliability-based life prediction of aging concrete bridge decks. In Z. Lounis, *International RILEM Workshop on Life Prediction and Aging Management of Concrete Structures,* 229-238.

MacGregor, J., Kennedy, F., Bartlett, D., Maes, M., and Dunaszegi, L. (1997). Design criteria and load resistance factors for the Confederation Bridge. *Canadian journal of Civil Engineering, 24*(6), 882-897.

Melchers, R. (2006). Structural reliability theroy in the context of structural safety. *Civiel Engineering and Enviromental Systems, 24*(1), 55-69.

Moustapha, M., Marelli, S., and Sudret, a. B. (2022). Active learning for structural reliability: Survey, general framwork and benchmark. *Structural Safety, 96*(2).

Nowak, A. S., and Collins, K. R. (2013). *Reliability of Structures.* Boca Raton: Taylor and Francis Group.

Nowak, A., and Szerzen, M. (2003). Calibration of design code for buildings: Part 1 Statistical models for resistance. *ACI Structural Journal, 100*(3), 377-382.

Oudah, F., and Alhshmi, A. E. (2022). Time-Dependanet Reliability Analysis of Degrading Structural Elements using Stochastic FE and LSTM Learning. *CSCE 2022 Annual Conference.* Whistler.

Peijuan, Z., Ming, W. C., Zhouhong, Z., and Liqi, W. (2017). A new active learning method based on the learning function U of the. *Engineering Structures, 148*, 185-194.

Petrie, C. (2022). *Reliability Analysis of Externally Bonded FRP Strengthened Beams Considering Existing Conditions: Applications of Stochastic FE and Conditional Probability.* [Master's thesis, Dalhousie University]. http://hdl.handle.net/10222/81910

Public Works. (2019a). Standard Specification: Highway Construction and Maintenance. Retrieved from The Province of NS: https://novascotia.ca/tran/publications/standard.pdf

Public Works. (2022b). Five Year Highway Improvement Plan 2022-2023 Edition. Retrieved from The Province of NS: https://novascotia.ca/tran/highways/5yearplan/5-year-Highway-Capital-Plan-2022-2023.pdf

Puppo, L., Pedroni, N., Bersano, A., Di Maio, F., Bertani, C., and Zio, E. (2021). Failure identification in a nuclear passive safety system by Monte Carlo. Nuclear Engineering and Design, 380.

Rajashekhar, M., and Ellingwood, B. (1993). A new look at the response surface approach for reliability analysis. *Structural Safety*, *12*(3), 205-220.

Rakoczy, A., and Nowak, A. (2013). Reliability-based sensitivity analysis for prestress concrete girder bridges. *PCI Journal*, *58*(2), 81-92.

Razaaly, N., and Congedo, P. M. (2020). Extension of AK-MCS for the efficient computation of very small failure. *Reliability Engineering and System Safety. 203*.

Shi, Y., Lu, Z., Xu, L., and Chen, S. (2019). An adaptive multiple-Kriging-surrogate method for time-dependant reliability analysis. *Applied Mathematical Modeling, 70*, 545-571.

Shi, Y., Lu, Z., Xu, L., and Chen, S. (2020). A novel learning function based on Kriging for reliability analysis. *Reliability Engineering and System Safety,* 198.

Teixeria, R., Nogal, M., and O'Connor, A. (2021). Adaptive approaches in metamodel-based reliability analysis: a review. *Structural Safety*, 89.

Thompson, P. D., Merlo, T., Kerr, B., Cheetham, A., and Ellis, R. (1999). The New Ontario Bridge Management System. *8th International Bridge Management Conference*, *153*.

Watson, G. (1970). Quantification of Geological Variables.

Whiten, T. (1977). Stochastic Models in Geology. *The Journal of Geology*, *85*(3), 321-330.

Zhang, X., Wang, L., and Sorens, J. D. (2019, January 10). REIF: A novel active-learning function toward adaptive Kriging Surrogate models for structural reliability analysis. *Reliability Engineering and System Safety*, *185*, 440-454.

Zhang, X., Wang, L., and Sorensen, J. (2020). AKOIS: An adaptive Kriging oriented importance sampling method for structural system reliability analysis. *Structural Safety, 82*.

Zhaoyan, L., Zhenzhou, L., and Wang, P. (2013). A new learning function of Kriging and its applications to solve reliability problems in engineering. *Computers and Mathematics with Applications, 70*(5), 1182-1197.

APPENDIX A: GIRDER SECTION IDEALIZATION

As indicated in Section 4.5.1, four girder sections were considered and idealized as I-shaped girders with the objective of simplifying the resistance model to reduce computational demand. A summary of the simplified geometries is detailed in Table A.1 Table A.2 details the actual cross-sectional area (A_{actual}), second moment of inertia (I_{actual}) and depth to neutral axis (Y_{actual}), compared to the idealized sections area (A_{ideal}), moment of inertia (I_{ideal}) and depth to neutral axis (Y_{ideal}) and the error of the idealization.

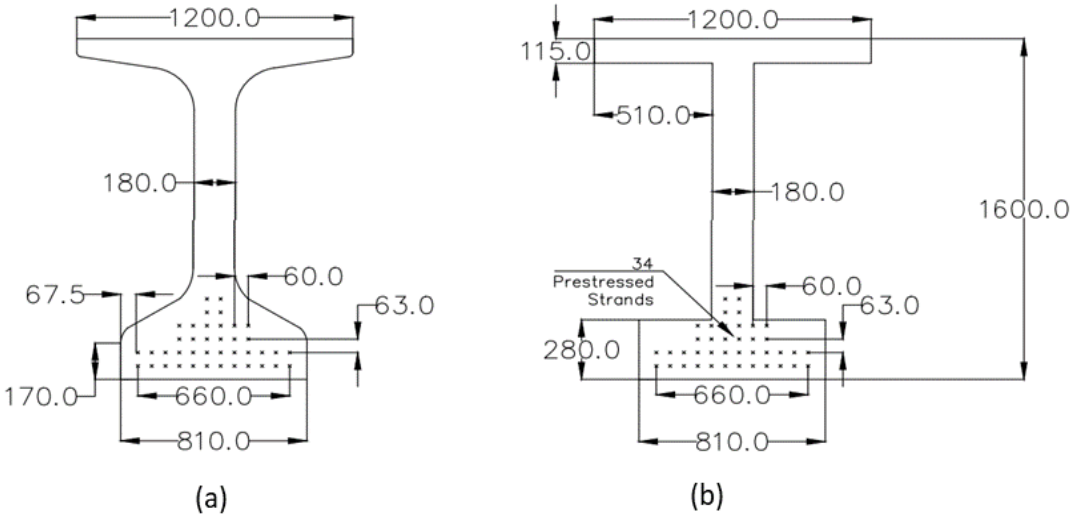

Figure A.1 Girder cross-sectional geometry in mm: (a) standard NEBT 1600 girder, and (b) idealized NEBT 1600 girder.

Table A.1 Idealized girder cross-sectional dimensions considered in the analysis.

NEBT ID	H (mm)	H_1 (mm)	H_2 (mm)	H_3 (mm)	B_1 (mm)	B_2 (mm)	B_3 (mm)	A_c (mm^2)
NEBT 1	1200	130	270	805	1200	810	180	518,700
NEBT 2	1400	130	270	1005	1200	810	180	554,700
NEBT 3	1600	130	270	1205	1200	810	180	589,000
NEBT 4	1800	130	270	1405	1200	810	180	626,700

The idealization was achieved by maintaining the overall section height (H), and width (B) and ensuring the second moment of inertia (I), the gross cross-sectional area (A_g) and the geometric centroid ($\bar{Y}$), are approximately the same, Equations (72) to (74) were used respectively.

$$A_g\ (mm^2) = \sum_{i=1}^{n} H_i B_i \tag{72}$$

$$I_x(mm^4) = \frac{BH^3}{12} + Ad^2 \tag{73}$$

$$Y_{centriod}(mm) = \frac{\sum H_i B_i \bar{Y}}{\sum H_i B_i} \tag{74}$$

Table A.2 Idealized girder cross-sectional parameters: idealized and original.

NEBT ID	A_{actual}	A_{ideal}	E_A	I_{actual}	I_{ideal}	E_I	Y_{actual}	Y_{ideal}	E_Y
	$(x10^3 mm^2)$		(%)	$(x10^8 mm^4)$		(%)	(mm)		(%)
NEBT 1	517	509.7	1.41	99.1	114.0	-6.19	574.8	496.4	13.64
NEBT 2	553	545.7	1.32	146.5	152.0	-9.36	667.3	617.4	7.48
NEBT 3	589	581.7	1.24	204.8	199.0	-8.70	760.9	750.7	1.34
NEBT 4	625	617.7	1.17	274.9	256.0	-8.32	855.1	896.5	-4.84

APPENDIX B: AK CONFIGURATIONS

Table B.1 AK configuration master list for girder analysis in Chapter 4.

AK Config. ID	Regression Function	Correlation Function	Learning Function
1	Constant	Gaussian	EFF
2	Constant	Gaussian	U
3	Constant	Gaussian	H
4	Linear	Gaussian	EFF
5	Linear	Gaussian	U
6	Linear	Gaussian	H
7	Quadratic	Gaussian	EFF
8	Quadratic	Gaussian	U
9	Quadratic	Gaussian	H
10	Constant	Cubic	EFF
11	Constant	Cubic	U
12	Constant	Cubic	H
13	Linear	Cubic	EFF
14	Linear	Cubic	U
15	Linear	Cubic	H
16	Quadratic	Cubic	EFF
17	Quadratic	Cubic	U
18	Quadratic	Cubic	H
19	Constant	Exponential	EFF
20	Constant	Exponential	U
21	Constant	Exponential	H
22	Linear	Exponential	EFF
23	Linear	Exponential	U
24	Linear	Exponential	H
25	Quadratic	Exponential	EFF
26	Quadratic	Exponential	U
27	Quadratic	Exponential	H
28	Constant	Linear	EFF
29	Constant	Linear	U
30	Constant	Linear	H
31	Linear	Linear	EFF
32	Linear	Linear	U
33	Linear	Linear	H
34	Quadratic	Linear	EFF
35	Quadratic	Linear	U
36	Quadratic	Linear	H
37	Constant	Spherical	EFF
38	Constant	Spherical	U
39	Constant	Spherical	H
40	Linear	Spherical	EFF
41	Linear	Spherical	U
42	Linear	Spherical	H
43	Quadratic	Spherical	EFF
44	Quadratic	Spherical	U
45	Quadratic	Spherical	H
46	Constant	Spline	EFF
47	Constant	Spline	U
48	Constant	Spline	H

AK Config. ID	Regression Function	Correlation Function	Learning Function
49	Linear	Spline	EFF
50	Linear	Spline	U
51	Linear	Spline	H
52	Quadratic	Spline	EFF
53	Quadratic	Spline	U
54	Quadratic	Spline	H

Table B.2 AK configuration master list for pier analysis in Chapter 4.

AK Config. ID	Regression Function	Correlation Function	Learning Function
1	Constant	Gaussian	EFF
2	Constant	Gaussian	U
3	Constant	Gaussian	REIF
4	Linear	Gaussian	EFF
5	Linear	Gaussian	U
6	Linear	Gaussian	REIF
7	Quadratic	Gaussian	EFF
8	Quadratic	Gaussian	U
9	Quadratic	Gaussian	REIF
10	Constant	Cubic	EFF
11	Constant	Cubic	U
12	Constant	Cubic	REIF
13	Linear	Cubic	EFF
14	Linear	Cubic	U
15	Linear	Cubic	REIF
16	Quadratic	Cubic	EFF
17	Quadratic	Cubic	U
18	Quadratic	Cubic	REIF
19	Constant	Exponential	EFF
20	Constant	Exponential	U
21	Constant	Exponential	REIF
22	Linear	Exponential	EFF
23	Linear	Exponential	U
24	Linear	Exponential	REIF
25	Quadratic	Exponential	EFF
26	Quadratic	Exponential	U
27	Quadratic	Exponential	REIF
28	Constant	Linear	EFF
29	Constant	Linear	U
30	Constant	Linear	REIF
31	Linear	Linear	EFF
32	Linear	Linear	U
33	Linear	Linear	REIF
34	Quadratic	Linear	EFF
35	Quadratic	Linear	U
36	Quadratic	Linear	REIF
37	Constant	Spherical	EFF

AK Config. ID	Regression Function	Correlation Function	Learning Function
38	Constant	Spherical	U
39	Constant	Spherical	REIF
40	Linear	Spherical	EFF
41	Linear	Spherical	U
42	Linear	Spherical	REIF
43	Quadratic	Spherical	EFF
44	Quadratic	Spherical	U
45	Quadratic	Spherical	REIF
46	Constant	Spline	EFF
47	Constant	Spline	U
48	Constant	Spline	REIF
49	Linear	Spline	EFF
50	Linear	Spline	U
51	Linear	Spline	REIF
52	Quadratic	Spline	EFF
53	Quadratic	Spline	U
54	Quadratic	Spline	REIF

Table B.3 AK configuration master list for both girder and pier analyses in Chapter 5.

AK Config. ID	Regression Function	Correlation Function	Learning Function
1	Constant	Gaussian	$KO_{05(2)}$
2	Constant	Gaussian	$KO_{005(2)}$
3	Constant	Gaussian	$KO_{05(5)}$
4	Constant	Gaussian	$KO_{005(5)}$
5	Constant	Gaussian	EFF
6	Constant	Gaussian	U
7	Constant	Gaussian	H
8	Constant	Gaussian	H_c
9	Constant	Gaussian	REIF
10	Linear	Gaussian	$KO_{05(2)}$
11	Linear	Gaussian	$KO_{005(2)}$
12	Linear	Gaussian	$KO_{05(5)}$
13	Linear	Gaussian	$KO_{005(5)}$
14	Linear	Gaussian	EFF
15	Linear	Gaussian	U
16	Linear	Gaussian	H
17	Linear	Gaussian	H_c
18	Linear	Gaussian	REIF
19	Constant	Cubic	$KO_{05(2)}$
20	Constant	Cubic	$KO_{005(2)}$
21	Constant	Cubic	$KO_{05(5)}$
22	Constant	Cubic	$KO_{005(5)}$
23	Constant	Cubic	EFF
24	Constant	Cubic	U
25	Constant	Cubic	H

AK Config. ID	Regression Function	Correlation Function	Learning Function
26	Constant	Cubic	H_c
27	Constant	Cubic	REIF
28	Linear	Cubic	$KO_{05(2)}$
29	Linear	Cubic	$KO_{005(2)}$
30	Linear	Cubic	$KO_{05(5)}$
31	Linear	Cubic	$KO_{005(5)}$
32	Linear	Cubic	EFF
33	Linear	Cubic	U
34	Linear	Cubic	H
35	Linear	Cubic	H_c
36	Linear	Cubic	REIF
37	Constant	Exponential	$KO_{05(2)}$
38	Constant	Exponential	$KO_{005(2)}$
39	Constant	Exponential	$KO_{05(5)}$
40	Constant	Exponential	$KO_{005(5)}$
41	Constant	Exponential	EFF
42	Constant	Exponential	U
43	Constant	Exponential	H
44	Constant	Exponential	H_c
45	Constant	Exponential	REIF
46	Linear	Exponential	$KO_{05(2)}$
47	Linear	Exponential	$KO_{005(2)}$
48	Linear	Exponential	$KO_{05(5)}$
49	Linear	Exponential	$KO_{005(5)}$
50	Linear	Exponential	EFF
51	Linear	Exponential	U
52	Linear	Exponential	H
53	Linear	Exponential	H_c
54	Linear	Exponential	REIF
55	Constant	Linear	$KO_{05(2)}$
56	Constant	Linear	$KO_{005(2)}$
57	Constant	Linear	$KO_{05(5)}$
58	Constant	Linear	$KO_{005(5)}$
59	Constant	Linear	EFF
60	Constant	Linear	U
61	Constant	Linear	H
62	Constant	Linear	H_c
63	Constant	Linear	REIF
64	Linear	Linear	$KO_{05(2)}$
65	Linear	Linear	$KO_{005(2)}$
66	Linear	Linear	$KO_{05(5)}$
67	Linear	Linear	$KO_{005(5)}$
68	Linear	Linear	EFF
69	Linear	Linear	U
70	Linear	Linear	H
71	Linear	Linear	H_c
72	Linear	Linear	REIF
73	Constant	Spherical	$KO_{05(2)}$

AK Config. ID	Regression Function	Correlation Function	Learning Function
74	Constant	Spherical	$KO_{005(2)}$
75	Constant	Spherical	$KO_{05(5)}$
76	Constant	Spherical	$KO_{005(5)}$
77	Constant	Spherical	EFF
78	Constant	Spherical	U
79	Constant	Spherical	H
80	Constant	Spherical	H_c
81	Constant	Spherical	REIF
82	Linear	Spherical	$KO_{05(2)}$
83	Linear	Spherical	$KO_{005(2)}$
84	Linear	Spherical	$KO_{05(5)}$
85	Linear	Spherical	$KO_{005(5)}$
86	Linear	Spherical	EFF
87	Linear	Spherical	U
88	Linear	Spherical	H
89	Linear	Spherical	H_c
90	Linear	Spherical	REIF
91	Constant	Spline	$KO_{05(2)}$
92	Constant	Spline	$KO_{005(2)}$
93	Constant	Spline	$KO_{05(5)}$
94	Constant	Spline	$KO_{005(5)}$
95	Constant	Spline	EFF
96	Constant	Spline	U
97	Constant	Spline	H
98	Constant	Spline	H_c
99	Constant	Spline	REIF
100	Linear	Spline	$KO_{05(2)}$
101	Linear	Spline	$KO_{005(2)}$
102	Linear	Spline	$KO_{05(5)}$
103	Linear	Spline	$KO_{005(5)}$
104	Linear	Spline	EFF
105	Linear	Spline	U
106	Linear	Spline	H
107	Linear	Spline	H_c
108	Linear	Spline	REIF

APPENDIX C: RELIABILITY INDEXES CHAPTER 4

Table C.1 Comparison of reliability indexes for MCS versus AK-MCS for all girders – Analysis results ranked based on accuracy.

Analysis Type	AK ID	Average Error	GIRD ID								
			1	2	3	4	5	6	7	8	9
Crude MCS	-	-	4.1700	4.2073	4.1897	4.4627	4.4790	4.4920	4.2276	4.2609	4.3197
AK-MCS	32	4.01E-04	4.1318	4.1449	4.2059	4.5264	4.5264	4.4652	4.1892	4.2649	4.3439
AK-MCS	54	4.15E-04	4.1735	4.1193	4.2436	4.4652	4.4652	4.5264	4.2436	4.3145	4.2436
AK-MCS	53	4.24E-04	4.1449	4.1449	4.1892	4.3776	4.5264	4.5264	4.1892	4.3776	4.3439
AK-MCS	36	4.36E-04	4.1587	4.2649	4.2436	4.5264	4.4172	4.4172	4.1449	4.3439	4.2884
AK-MCS	46	4.42E-04	4.2649	4.2059	4.1587	4.3776	4.3776	4.4652	4.1735	4.3439	4.3145
AK-MCS	42	4.61E-04	4.2240	4.3439	4.2240	4.5264	4.5264	4.5264	4.2649	4.2436	4.3439
AK-MCS	18	4.69E-04	4.0962	4.2436	4.3145	4.3439	4.4652	4.5264	4.2059	4.3145	4.3439
AK-MCS	45	4.84E-04	4.1587	4.2059	4.1892	4.6114	4.4172	4.4172	4.2059	4.2240	4.3145
AK-MCS	24	5.08E-04	4.1735	4.2240	4.1587	4.4652	4.4652	4.3439	4.1449	4.2240	4.3145
AK-MCS	43	5.82E-04	4.1193	4.1735	4.2059	4.4652	4.6114	4.4172	4.3439	4.2649	4.3439
AK-MCS	49	6.19E-04	4.2059	4.0652	4.2649	4.4172	4.4652	4.3776	4.1892	4.3776	4.3145
AK-MCS	16	6.36E-04	4.1892	4.1587	4.2240	4.4652	4.3439	4.4652	4.2240	4.4652	4.4172
AK-MCS	44	6.42E-04	4.2884	4.1449	4.2240	4.5264	4.5264	4.5264	4.2649	4.2059	4.4652
AK-MCS	4	6.48E-04	4.0854	4.1892	4.2240	4.2649	4.5264	4.5264	4.1587	4.3145	4.4172
AK-MCS	17	6.66E-04	4.2059	4.2436	4.2649	4.6114	4.6114	4.4652	4.1587	4.2240	4.3776
AK-MCS	33	6.78E-04	4.0962	4.2884	4.1892	4.3776	4.6114	4.5264	4.3439	4.2059	4.3776
AK-MCS	6	6.91E-04	4.2059	4.2059	4.3776	4.3439	4.4652	4.4652	4.1587	4.2059	4.3439
AK-MCS	27	6.93E-04	4.1892	4.2436	4.2436	4.3776	4.4172	4.3145	4.1318	4.3776	4.4172
AK-MCS	22	7.11E-04	4.2436	4.2649	4.1449	4.7534	4.4652	4.4652	4.2240	4.3145	4.3145
AK-MCS	26	7.31E-04	4.1075	4.2240	4.1587	4.4652	4.7534	4.6114	4.2436	4.3145	4.3145
AK-MCS	35	7.43E-04	4.1892	4.2649	4.2649	4.4652	4.4172	4.7534	4.3145	4.3145	4.3776
AK-MCS	40	7.50E-04	4.2240	4.2059	4.1892	4.7534	4.4172	4.3776	4.2059	4.3776	4.2436
AK-MCS	7	7.54E-04	4.2436	4.2436	4.3145	4.3776	4.7534	4.4652	4.2884	4.2884	4.2649
AK-MCS	34	7.63E-04	4.1193	4.1735	4.2649	4.6114	4.6114	4.6114	4.4652	4.2649	4.3776
AK-MCS	23	8.04E-04	4.1587	4.2059	4.2884	4.6114	4.7534	4.6114	4.2059	4.3145	4.3145
AK-MCS	25	8.30E-04	4.2059	4.0962	4.1735	4.7534	4.6114	4.7534	4.3439	4.2884	4.5264
AK-MCS	5	7.55E-03	4.2240	4.2649	4.1587	4.7534	4.5264	4.7534	4.6114	4.3776	4.3145
AK-MCS	12	7.57E-03	>4.753	4.2059	4.1318	4.7534	4.3439	4.4172	4.3776	4.1892	4.3145
AK-MCS	13	7.73E-03	4.1193	4.2240	4.2884	4.4652	4.6114	4.4652	4.3145	4.3776	>4.753
AK-MCS	9	7.73E-03	4.2884	4.2240	4.2884	4.3145	4.4652	4.5264	4.1587	4.1735	>4.753
AK-MCS	14	7.74E-03	4.2436	4.0751	4.2059	4.4652	4.7534	4.6114	4.2649	4.6114	>4.753
AK-MCS	50	7.85E-03	4.1735	4.1193	4.1892	>4.753	4.6114	4.7534	4.3776	4.3439	4.2436
AK-MCS	52	7.86E-03	4.1587	4.1587	4.2240	4.4652	>4.753	4.6114	4.1892	4.2884	4.2884
AK-MCS	37	1.03E-02	4.2059	4.2059	4.1735	4.5264	>4.753	4.6114	4.2884	4.2649	4.2884
AK-MCS	31	1.08E-02	4.1449	4.2240	4.3776	4.6114	>4.753	4.4652	4.4172	4.4172	4.2649
AK-MCS	51	1.09E-02	4.1587	4.1449	4.1587	4.5264	4.4172	>4.753	4.2884	4.3145	4.3145
AK-MCS	1	1.10E-02	4.1587	4.1735	4.0962	4.4172	4.4172	>4.753	4.2059	4.2649	4.3439
AK-MCS	15	1.10E-02	4.2649	4.1892	4.2240	4.3145	4.6114	>4.753	4.0962	4.2649	4.3776
AK-MCS	41	1.33E-02	4.1449	4.2240	4.3145	4.4172	4.6114	>4.753	4.6114	4.3439	4.2649
AK-MCS	28	1.33E-02	4.2240	>4.753	4.2884	4.4172	4.6114	4.7534	4.2884	>4.753	4.1892
AK-MCS	8	1.35E-02	4.2436	4.2240	4.2649	4.3145	4.6114	4.3439	4.2059	>4.753	>4.753
AK-MCS	30	1.53E-02	4.1735	4.1735	4.2436	4.3776	>4.753	4.4172	4.3776	4.2649	>4.753
AK-MCS	19	1.70E-02	4.1587	4.1075	>4.753	4.4172	4.5264	>4.753	4.2240	4.2240	4.4172

Analysis Type	AK ID	Average Error	GIRD ID								
			1	2	3	4	5	6	7	8	9
Crude MCS	-	-	4.1700	4.2073	4.1897	4.4627	4.4790	4.4920	4.2276	4.2609	4.3197
AK-MCS	10	1.86E-02	4.2240	4.0652	>4.753	4.3439	4.3776	>4.753	4.1587	4.4172	4.2436
AK-MCS	39	1.86E-02	4.2059	4.4172	4.4652	4.6114	>4.753	>4.753	4.3145	4.4652	4.4652
AK-MCS	21	1.86E-02	>4.753	4.1892	4.4172	4.4652	4.6114	>4.753	>4.753	4.2436	4.2884
AK-MCS	48	1.86E-02	4.2240	4.2059	4.2240	4.4652	>4.753	>4.753	>4.753	4.2059	4.3776
AK-MCS	3	1.86E-02	>4.753	4.2436	4.2059	>4.753	4.3776	>4.753	>4.753	4.2649	4.3439
AK-MCS	11	1.86E-02	>4.753	>4.753	>4.753	>4.753	>4.753	>4.753	>4.753	4.4172	4.6114
AK-MCS	2	1.86E-02	>4.753	>4.753	>4.753	>4.753	>4.753	>4.753	>4.753	>4.753	>4.753
AK-MCS	20	1.86E-02	>4.753	>4.753	>4.753	>4.753	>4.753	>4.753	>4.753	>4.753	>4.753
AK-MCS	29	1.86E-02	>4.753	>4.753	>4.753	>4.753	>4.753	>4.753	>4.753	>4.753	>4.753
AK-MCS	38	1.86E-02	>4.753	>4.753	>4.753	>4.753	>4.753	>4.753	>4.753	>4.753	>4.753
AK-MCS	47	1.86E-02	>4.753	>4.753	>4.753	>4.753	>4.753	>4.753	>4.753	>4.753	>4.753

Table C.2 Comparison of reliability indexes for MCS versus AK-MCS for piers – Analysis results ranked based on accuracy.

Analysis Type	AK ID	Average Error	PIER ID					
			1	2	5	6	9	10
Crude MCS	-		4.5658	4.6667	4.5714	4.6351	4.5758	4.6404
AK-MCS	36	4.01E-04	4.5264	4.6114	4.6114	4.5264	4.7534	4.5264
AK-MCS	9	4.15E-04	4.4652	4.4652	4.6114	4.6114	4.4652	4.6114
AK-MCS	22	4.24E-04	4.6114	4.4652	4.6114	4.6114	4.4652	4.7534
AK-MCS	54	4.36E-04	4.6114	4.6114	4.4652	4.4652	4.4652	4.5264
AK-MCS	43	4.42E-04	4.5264	4.6114	4.6114	4.4652	4.3776	4.6114
AK-MCS	32	4.61E-04	4.4652	4.6114	4.6114	4.5264	4.5264	4.4172
AK-MCS	44	4.69E-04	4.5264	4.7534	4.4172	4.5264	4.4172	4.5264
AK-MCS	13	4.84E-04	4.4652	4.6114	4.5264	4.4652	4.7534	4.7534
AK-MCS	34	5.08E-04	4.5264	4.4172	4.5264	4.6114	4.5264	4.4652
AK-MCS	42	5.82E-04	4.4652	4.4172	4.6114	4.4652	4.4652	4.5264
AK-MCS	35	6.19E-04	4.7534	4.6114	4.3776	4.4652	4.6114	4.4652
AK-MCS	26	6.36E-04	4.7534	4.4172	4.3776	4.6114	4.4652	4.6114
AK-MCS	8	6.42E-04	4.4652	4.4172	4.5264	4.4652	4.5264	4.4172
AK-MCS	18	6.48E-04	4.6114	4.4172	4.7534	4.6114	4.7534	4.4652
AK-MCS	41	6.66E-04	4.6114	4.5264	4.7534	4.4652	4.4652	4.3776
AK-MCS	27	6.78E-04	4.5264	4.4172	4.5264	4.4172	4.7534	4.4652
AK-MCS	25	6.91E-04	4.3776	4.7534	4.2884	4.7534	4.5264	4.4652
AK-MCS	16	6.93E-04	4.6114	4.3439	4.4172	4.6114	4.5264	4.4172
AK-MCS	5	7.11E-04	4.7534	4.4652	4.4652	4.4652	4.6114	4.3776
AK-MCS	4	7.31E-04	4.6114	4.4172	4.5264	4.5264	4.6114	4.2884
AK-MCS	23	7.43E-04	4.4172	4.6114	4.5264	4.4172	4.4172	4.3145
AK-MCS	33	7.50E-04	4.7534	4.6114	4.6114	4.3145	4.4652	4.4172
AK-MCS	51	7.54E-04	4.7534	4.5264	4.4172	4.3439	4.7534	4.5264
AK-MCS	45	7.63E-04	4.4652	4.4172	4.7534	4.7534	4.7534	4.3776
AK-MCS	53	8.04E-04	4.3776	4.4652	4.7534	4.4172	4.4652	4.3776
AK-MCS	24	8.30E-04	4.6114	4.4652	4.7534	4.7534	4.4652	4.2436
AK-MCS	17	7.55E-03	4.4652	4.3776	4.6114	4.6114	4.4652	>4.753
AK-MCS	50	7.57E-03	4.7534	4.3439	4.7534	4.5264	4.3776	>4.753
AK-MCS	40	7.73E-03	4.5264	4.6114	4.6114	>4.753	4.4652	4.5264

Analysis Type	AK ID	Average Error	PIER ID					
			1	2	5	6	9	10
Crude MCS	-		4.5658	4.6667	4.5714	4.6351	4.5758	4.6404
AK-MCS	15	7.73E-03	4.6114	4.6114	>4.753	4.6114	4.5264	4.5264
AK-MCS	14	7.74E-03	4.5264	4.4652	4.4652	>4.753	4.4172	4.4652
AK-MCS	7	7.85E-03	>4.753	4.7534	4.4172	4.5264	4.3439	4.4172
AK-MCS	49	7.86E-03	>4.753	4.4652	4.3776	4.7534	4.3439	4.5264
AK-MCS	6	1.03E-02	4.5264	>4.753	4.6114	4.7534	>4.753	4.7534
AK-MCS	52	1.08E-02	4.3776	4.3439	>4.753	4.7534	4.6114	>4.753
AK-MCS	10	1.09E-02	4.6114	4.5264	>4.753	>4.753	4.7534	4.4172
AK-MCS	46	1.10E-02	>4.753	4.5264	4.5264	>4.753	4.4172	4.4652
AK-MCS	37	1.10E-02	>4.753	4.4172	>4.753	4.5264	4.5264	4.3439
AK-MCS	19	1.33E-02	>4.753	>4.753	>4.753	4.3776	4.5264	4.6114
AK-MCS	31	1.33E-02	>4.753	>4.753	>4.753	4.3776	4.7534	4.4172
AK-MCS	1	1.35E-02	>4.753	4.3145	>4.753	>4.753	4.3439	4.6114
AK-MCS	28	1.53E-02	>4.753	>4.753	4.6114	>4.753	4.4172	>4.753
AK-MCS	47	1.70E-02	>4.753	4.3145	>4.753	>4.753	>4.753	>4.753
AK-MCS	2	1.86E-02	>4.753	>4.753	>4.753	>4.753	>4.753	>4.753
AK-MCS	3	1.86E-02	>4.753	>4.753	>4.753	>4.753	>4.753	>4.753
AK-MCS	11	1.86E-02	>4.753	>4.753	>4.753	>4.753	>4.753	>4.753
AK-MCS	12	1.86E-02	>4.753	>4.753	>4.753	>4.753	>4.753	>4.753
AK-MCS	20	1.86E-02	>4.753	>4.753	>4.753	>4.753	>4.753	>4.753
AK-MCS	21	1.86E-02	>4.753	>4.753	>4.753	>4.753	>4.753	>4.753
AK-MCS	29	1.86E-02	>4.753	>4.753	>4.753	>4.753	>4.753	>4.753
AK-MCS	30	1.86E-02	>4.753	>4.753	>4.753	>4.753	>4.753	>4.753
AK-MCS	38	1.86E-02	>4.753	>4.753	>4.753	>4.753	>4.753	>4.753
AK-MCS	39	1.86E-02	>4.753	>4.753	>4.753	>4.753	>4.753	>4.753
AK-MCS	48	1.86E-02	>4.753	>4.753	>4.753	>4.753	>4.753	>4.753

APPENDIX D: RELIABILITY INDEXES CHAPTER 5

Table D.1 Optimum AK-MCS configuration for alternate girder configurations at 45 MPa.

GIRD ID	β_{MCS}	β_{AK-MCS} Values for Optimum AK-MCS Config.					Average Error	AAE
		1	2	3	4	5		
01	-	-	-	-	-	-	-	-
02	4.2073	4.1318	4.224	4.224	4.2649	4.1449	-0.0022	0.01088
03	4.1897	4.3145	4.2884	4.2059	4.1193	4.2059	0.0089	0.01558
04	4.4627	4.3439	4.2884	4.4172	4.4172	4.4172	-0.0193	0.01925
05	4.4790	4.4652	4.4652	4.7534	4.7534	4.2436	0.0128	0.03625
06	4.4920	4.5264	4.6114	4.7534	4.7534	4.3439	0.0235	0.03672
07	4.2276	4.1735	4.2436	4.3439	4.2884	4.2649	0.0083	0.01346
08	4.2609	4.3145	4.2059	4.2884	4.3776	4.5264	0.0192	0.02433
09	4.3197	4.3439	4.4172	4.3439	4.3776	4.224	0.0050	0.01387
10	4.2092	4.2059	4.2059	4.1587	4.1735	4.3439	0.0020	0.01081
11	4.2079	4.224	4.2884	4.4172	4.2059	4.1449	0.0114	0.01763
12	4.1699	4.1735	4.224	4.1449	4.2436	4.1449	0.0039	0.0087
13	4.1658	4.1892	4.1193	4.224	4.4172	4.2884	0.0196	0.02411
14	4.5184	4.4652	4.5264	4.4172	4.4652	4.4652	-0.0112	0.0119
15	4.4766	4.7534	4.4172	4.7534	4.4172	4.5264	0.0217	0.03227
16	4.4434	4.3145	4.4652	4.4172	4.4652	4.3439	-0.0095	0.01342
17	4.4255	4.3439	4.5264	4.4652	4.5264	4.4652	0.0090	0.0164
18	4.3248	4.3439	4.5264	4.3439	4.5264	4.3439	0.0213	0.0213
19	4.2898	4.2884	4.4172	4.1075	4.4172	4.6114	0.0183	0.03544
20	4.2251	4.2649	4.2884	4.2436	4.3439	4.224	0.0113	0.01143
21	4.2361	4.2649	4.1892	4.2436	4.2059	4.224	-0.0025	0.00593

Table D.2 Optimum AK-MCS configuration for alternate girder configurations at 55 MPa.

GIRD ID	β_{MCS}	β_{AK-MCS} Values for Optimum AK-MCS Config.					Average Error	AAE
		1	2	3	4	5		
01	-	-	-	-	-	-	-	-
02	4.1844	4.1735	4.1587	4.1318	4.1318	4.2436	-0.0039	0.0096
03	4.1788	4.3439	4.1587	4.1449	4.2059	4.2649	0.0107	0.0159
04	4.4128	4.7534	4.3145	4.3439	4.4172	4.4652	0.0104	0.0256
05	4.4230	4.4172	4.4652	4.3776	4.2884	4.4652	-0.0046	0.0122
06	4.4213	4.4172	4.6114	4.4172	4.4652	4.4652	0.0122	0.0129
07	4.1960	4.2649	4.1193	4.1193	4.1587	4.2649	-0.0025	0.0157
08	4.2303	4.3145	4.2884	4.4652	4.2436	4.2884	0.0212	0.0212
09	4.2622	4.4172	4.2884	4.1735	4.3145	4.3439	0.0106	0.0190
10	4.1784	4.1587	4.1075	4.1892	4.224	4.1587	-0.0026	0.0080
11	4.1685	4.2884	4.1587	4.2240	4.1318	4.1318	0.0044	0.0124
12	4.1620	4.0291	4.1193	4.1193	4.2649	4.1735	-0.0050	0.0160
13	4.1947	4.1587	4.1193	4.1449	4.2240	4.0854	-0.0115	0.0143
14	4.4485	4.4652	4.4652	4.6114	4.6114	4.4652	0.0169	0.0169

GIRD ID	β_{MCS}	β_{AK-MCS} Values for Optimum AK-MCS Config.					Average Error	AAE
		1	2	3	4	5		
15	4.4299	4.3776	4.4652	4.4172	4.6114	4.5264	0.0112	0.0171
16	4.3947	4.4652	4.7534	4.7534	4.3145	4.7534	0.0485	0.0558
17	4.3810	4.6114	4.3776	4.3439	4.2884	4.3146	0.0014	0.0196
18	4.2657	4.4172	4.4652	4.2649	4.4172	4.3145	0.0258	0.0259
19	4.2415	4.2436	4.1449	4.224	4.2649	4.2436	-0.0041	0.0067
20	4.2128	4.1735	4.224	4.2059	4.1735	4.1735	-0.0054	0.0065
21	4.1705	4.2059	4.3439	4.2436	4.2240	4.2059	0.0178	0.0178